Chapter

2 BASIC THEORY AND APPLICATIONS OF SYMMETRY REPRESENTATIONS (ABELIAN SYMMETRY GROUPS)

2.1 Symmetry Groups / 60
2.2 Representing Symmetry and Symmetry Groups / 62
2.3 Solving a Problem with Symmetry Analysis (C_2) / 69
2.4 Irreducible Representations / 79
2.5 Partially Solving a Problem with Symmetry Analysis (C_2) / 82
2.6 An Example with Slightly Higher Symmetry (C_3) / 84
2.7 More Examples with C_n Symmetry: One-Dimensional Lattices / 91
A. Symmetry Breaking / 97
B. Galloping Waves / 100
C. Comparison with Fourier Analysis / 104
2.8 Other Types of Abelian Symmetry / 104
2.9 Theory of Commuting Idempotents / 109
2.10 General Theory of Abelian Groups / 110
2.11 Some Abelian Point Symmetries / 111
2.12 Symmetry Analysis for Quantum Mechanics / 115
A. Bohr Levels and Bloch Waves: C_{12} Clocktane Orbitals / 115
B. C_2 Symmetry and the Two-Level System / 129
C. C_2 Symmetry Analysis and Scattering Theory / 132
D. Crossing Matrices and One-Dimensional Tunneling / 137
Additional Reading / 141
Problems / 143

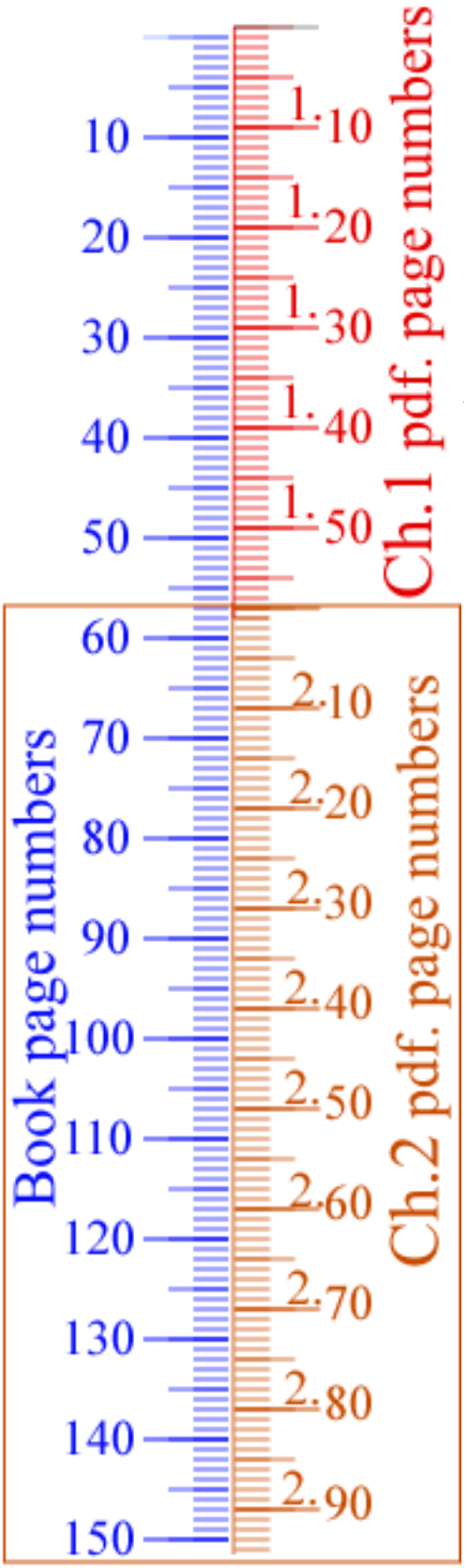

CHAPTER 2

BASIC THEORY AND APPLICATIONS OF SYMMETRY REPRESENTATIONS (ABELIAN SYMMETRY GROUPS)

In the preceding review of matrices the ideas of projection operators and spectral decompositions were introduced. In this chapter we shall see how frequency spectra of physical systems are analyzed in terms of mathematical spectral decompositions. Mathematical concepts will be introduced in this and following chapters by analyzing the simplest physical models which exhibit them. In this way the mathematical and physical ideas can be closely related. It is hoped that this particular pedagogical approach to the theory of spectra will be easy to understand.

Symmetry is a key mathematical and physical concept in the classical and quantum theory of spectra. Symmetry analysis and group theory were first applied by Eugene Wigner and Herman Weyl shortly after the invention of quantum mechanics. Since then applications of symmetry analysis have been made to virtually all types of spectroscopy. Spectra, ranging in energy from radio frequency ($\sim 10^3$ Hz) to x ray ($\sim 10^{18}$ Hz), have given information about atoms, molecules, and solids. Higher-frequency γ radiation ($> 10^{20}$ Hz) has been used to study nuclear spectra. A most widely publicized application of symmetry principles concerns very high energy "elementary particle" spectra where researchers are thinking about energies in excess of 10^{12} eV or 10^{26} Hz. (1 eV is equivalent to 2.42×10^{14} Hz.)

Meanwhile the application of laser devices has reopened atomic and molecular spectroscopy. Instead of obtaining higher and higher frequency, laser spectroscopists are obtaining ever-increasing frequency *resolution*. This means finer spectral details are seen and more detailed models of atomic and molecular processes are needed. This has stimulated the development of new

symmetry analysis techniques, some of which are discussed in later chapters of this book.

However, the fundamental ideas of symmetry analysis are simple and basic to all present theories. The beginnings of most symmetry mathematics involves several mutually commuting operators. We have seen in the preceding chapter that the eigenvalue spectrum of one of several commuting operators may help to solve the others. This is the main mathematical idea which will be developed in this chapter.

2.1 SYMMETRY GROUPS

First we shall explain how a physicist can say "symmetry" precisely. Consider a simple fan blade such as you might see on the ceilings of bar and hotel rooms in the tropical areas. This is shown in Figure 2.1.1. Everybody would probably agree that this blade has some symmetry, but the question is: How much?

To answer this we ask, "In how many positions could the fan blade be put so that it would still look the same in a drawing like Figure 2.1.1?" We list these below and draw them in Figure 2.1.2. (In the latter figure some markings "left" and "right" have been added. They spoil the symmetry but allow you to distinguish the different positions.)

1 : THE ORIGINAL POSITION	Don't touch the fan blade.
R_z: THE HALF-TURN POSITION	Rotate it by 180° around its axle or the z axis.
R_y: THE OVERTURNED POSITION	Overturn it 180° around the y axis.
R_x: THE FLIPPED POSITION	Flip it 180° around the x axis.

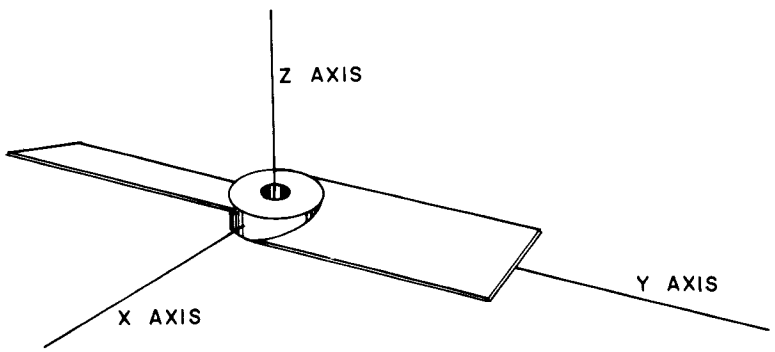

Figure 2.1.1 Fan blade. This is an example of an object which has an Abelian symmetry D_2.

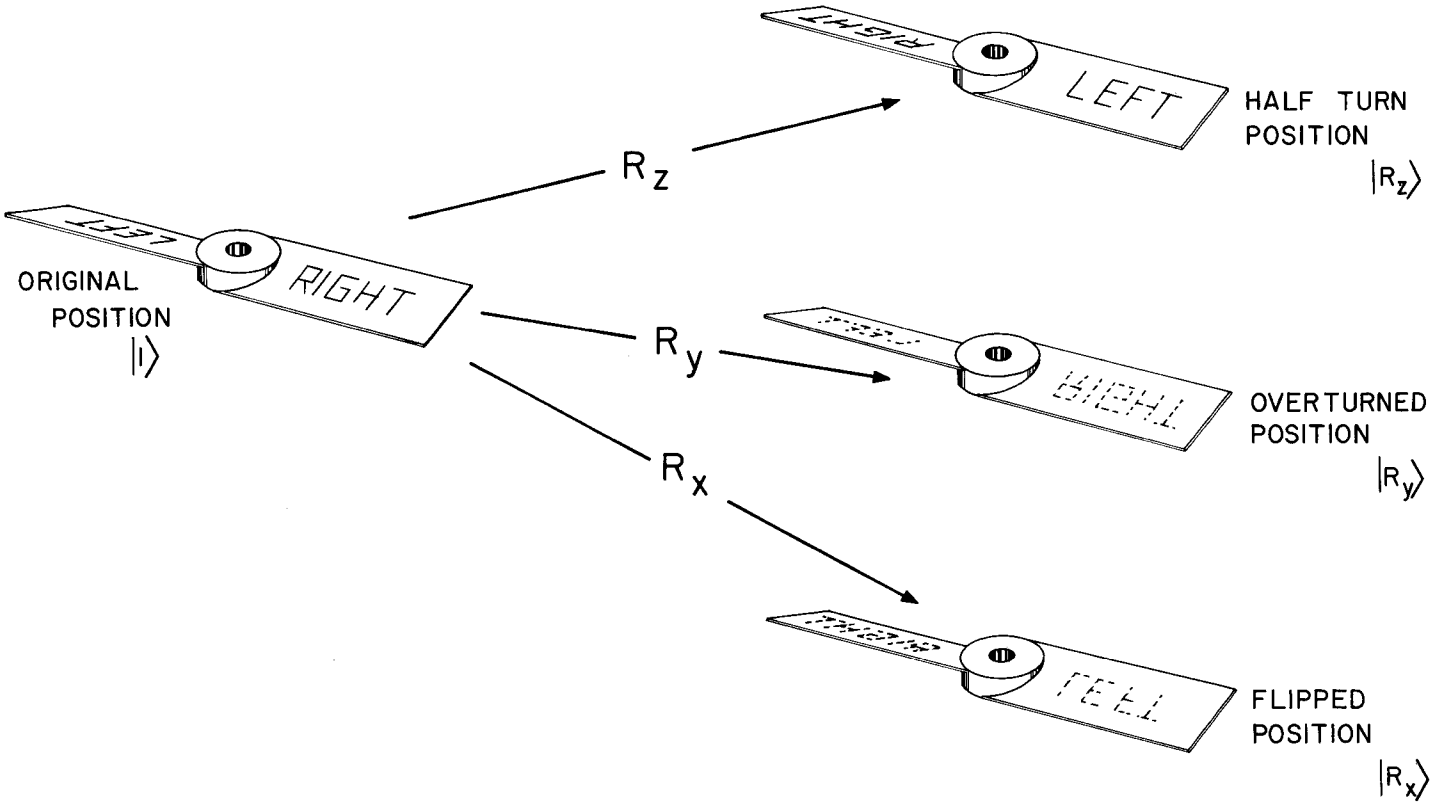

Figure 2.1.2 Symmetry operations. The 180° rotations R_x, R_y, and R_z around the x, y, and z axes, respectively, all leave the fan blade in similar positions.

The first two possibilities are obvious enough; however, the third (R_y) and the fourth (R_x) might be a little surprising at first. Note that a fan blade like this one works just as well when it is installed "backwards."

Now we see there are basically two ways to keep track of this symmetry. According to one we can tally up the allowed positions or position states $|1\rangle$, $|R_x\rangle$, $|R_y\rangle$, and $|R_z\rangle$ that look the same. According to the other, we tally up the operations (turn, flip, etc.) or OPERATORS $\{\mathbf{1}, R_x, R_y, R_z\}$ that change one allowed position state to another. These operations have a number of mathematical properties which we shall study shortly. Most important is the idea of combination or GROUP MULTIPLICATION.

For example, if we do an R_y (overturn) followed by a R_z (half turn), all with respect to fixed spatial axes x, y, and z, then what do we get? Examination of Figure 2.1.2 shows that the same position state shows up which would have been obtained by just doing R_x (flip) by itself. Let us express these observations by the following operator and position state equation:

$$R_z R_y|1\rangle = R_z|R_y\rangle = |R_x\rangle = R_x|1\rangle. \tag{2.1.1}$$

Now Eq. (2.1.1) is true no matter whether you start with $|1\rangle$ or the other states, and so we may write it abstractly as Eq. (2.1.2):

$$R_z R_y = R_x. \tag{2.1.2}$$

In this way we make a multiplication table or GROUP TABLE such as is shown below. Here all possible products are accounted for:

	$\mathbf{1}$	R_x	R_y	R_z
$\mathbf{1}$	$\mathbf{1}$	R_x	R_y	R_z
R_x	R_x	$\mathbf{1}$	R_z	R_y
R_y	R_y	R_z	$\mathbf{1}$	R_x
R_z	R_z	R_y	R_x	$\mathbf{1}$

(2.1.3)

This is ultimately how symmetry is coded, through abstract mathematical properties of symmetry operators. Now we shall see how this type of mathematics enters a physical problem.

2.2 REPRESENTING SYMMETRY AND SYMMETRY GROUPS

We start by analyzing in detail one of the simplest examples of a physical system having one of the simplest symmetries. Consider the two identical and

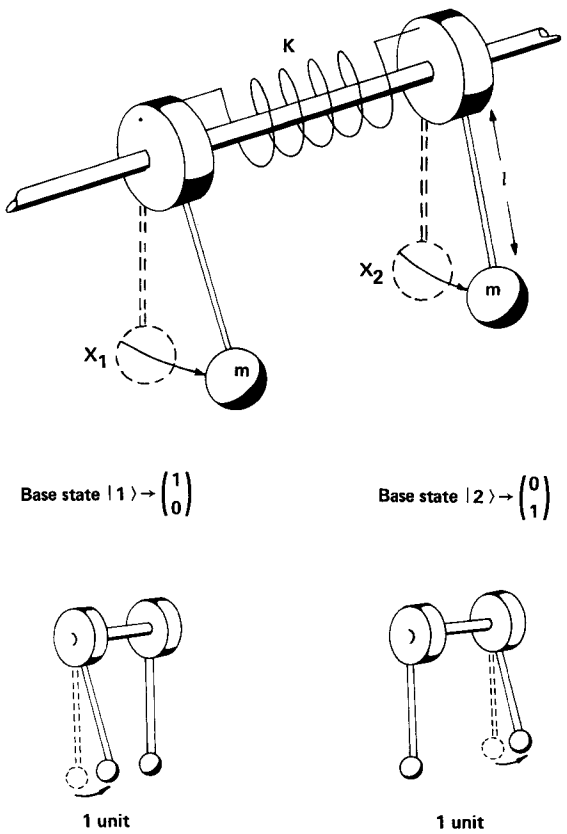

Figure 2.2.1 Coupled pendulums. This is an example of a mechanical system having one of the simplest Abelian symmetries $C_2 = \{1, R\}$. The base states are related by the symmetry operation R of reversal or reflection according to $|2\rangle = R|1\rangle$.

coupled torsion pendulums in Figure 2.2.1. Their motion will be described by the classical matrix equations if the coordinates ($\chi_1 = \langle 1|x\rangle$, $\chi_2 = \langle 2|x\rangle$) are not too great, as was explained in Chapter 1. The unit position base states $|1\rangle$ and $|2\rangle$ are indicated on the right-hand side of Figure 2.2.1. Newton's equation of motion is given abstractly by

$$|\ddot{x}(t)\rangle = -\mathbf{a}|x(t)\rangle. \tag{2.2.1a}$$

It is represented in the $\{|1\rangle, |2\rangle\}$ basis by the following matrix equation of motion:

$$\begin{pmatrix}\langle 1|\ddot{x}(t)\rangle\\ \langle 2|\ddot{x}(t)\rangle\end{pmatrix} = -\begin{pmatrix}\langle 1|\mathbf{a}|1\rangle & \langle 1|\mathbf{a}|2\rangle\\ \langle 2|\mathbf{a}|1\rangle & \langle 2|\mathbf{a}|2\rangle\end{pmatrix}\begin{pmatrix}\langle 1|x(t)\rangle\\ \langle 2|x(t)\rangle\end{pmatrix} \tag{2.2.1b}$$

or

$$\begin{pmatrix} \ddot{x}_1 \\ \ddot{x}_2 \end{pmatrix} = -\begin{pmatrix} a+b & -a \\ -a & a+b \end{pmatrix}\begin{pmatrix} x_1 \\ x_2 \end{pmatrix}. \tag{2.2.1c}$$

where $a \equiv 2k/ml^2$, and $b \equiv g/l$.

The constants are gravity (g), coupling spring constant (k), pendulum length (l), and mass (m). The classical position state vector $|x\rangle$ is represented in the $\{|1\rangle, |2\rangle\}$ basis by the ket

$$\begin{aligned} |x\rangle &= |1\rangle\langle 1|x\rangle + |2\rangle\langle 2|x\rangle \\ &= |1\rangle x_1 \quad + |2\rangle x_2, \end{aligned}$$

or by the two-component column vector in Eq. (2.2.1). This classical application of Dirac notation for vectors and operators ($\langle i|\mathbf{a}|j\rangle$) was introduced in Section 1.4.A.

The symmetry of this device is fairly obvious. The pendulums are identical, and if someone switches them in the middle of the night no one should be able to tell the difference. The problem is to formulate this fact in a mathematical description.

This may be done by defining a symmetry operator R that reflects or switches the pendulum states according to the following equations (see also Figure 2.2.1):

$$\begin{aligned} R|1\rangle &= |2\rangle, \\ R|2\rangle &= |1\rangle. \end{aligned} \tag{2.2.2a}$$

This allows R to be represented in the $\{|1\rangle, |2\rangle\}$ basis by the following matrix:

$$\begin{pmatrix} \langle 1|R|1\rangle & \langle 1|R|2\rangle \\ \langle 2|R|1\rangle & \langle 2|R|2\rangle \end{pmatrix} = \begin{pmatrix} 0 & 1 \\ 1 & 0 \end{pmatrix}. \tag{2.2.2b}$$

Then for every state $|x\rangle$ of the system, there is a reflected state $R|x\rangle$ which is represented as follows:

$$R|x\rangle \leftrightarrow \begin{pmatrix} \langle 1|R|1\rangle & \langle 1|R|2\rangle \\ \langle 2|R|1\rangle & \langle 2|R|2\rangle \end{pmatrix}\begin{pmatrix} \langle 1|x\rangle \\ \langle 2|x\rangle \end{pmatrix} = \begin{pmatrix} 0 & 1 \\ 1 & 0 \end{pmatrix}\begin{pmatrix} x_1 \\ x_2 \end{pmatrix} = \begin{pmatrix} x_2 \\ x_1 \end{pmatrix}. \tag{2.2.3}$$

Now the mathematical statement of the physical symmetry is: THE EQUATION FOR A REFLECTED STATE $R|x\rangle$ IS THE SAME AS IT WAS FOR THE ORIGINAL STATE $|x\rangle$. This is written as follows:

$$R|\ddot{x}\rangle = -\mathbf{a} \cdot R|x\rangle, \tag{2.2.4a}$$

$$\begin{pmatrix} \ddot{x}_2 \\ \ddot{x}_1 \end{pmatrix} = -\begin{pmatrix} \langle 1|\mathbf{a}|1\rangle & \langle 1|\mathbf{a}|2\rangle \\ \langle 2|\mathbf{a}|1\rangle & \langle 2|\mathbf{a}|2\rangle \end{pmatrix}\begin{pmatrix} x_2 \\ x_1 \end{pmatrix}. \tag{2.2.4b}$$

Note that Eq. (2.2.4b) does not agree with Eq. (2.2.1b) for arbitrary choice of $\langle i|\mathbf{a}|j\rangle$, but that it does agree for the constants we have chosen. In fact we can now deduce the constraints that operator $\langle \mathbf{a} \rangle$ must satisfy when reflection symmetry is present.

First, Eq. (2.2.5) below follows directly from the equation of motion $|\ddot{x}\rangle = -\mathbf{a}|x\rangle$ no matter whether R symmetry is present or not:

$$R|\ddot{x}\rangle = -R \cdot \mathbf{a}|x\rangle, \tag{2.2.5a}$$

$$\begin{pmatrix} 0 & 1 \\ 1 & 0 \end{pmatrix}\begin{pmatrix} \ddot{x}_1 \\ \ddot{x}_2 \end{pmatrix} = \begin{pmatrix} \ddot{x}_2 \\ \ddot{x}_1 \end{pmatrix} = -\begin{pmatrix} 0 & 1 \\ 1 & 0 \end{pmatrix}\begin{pmatrix} \langle 1|\mathbf{a}|1\rangle & \langle 1|\mathbf{a}|2\rangle \\ \langle 2|\mathbf{a}|1\rangle & \langle 2|\mathbf{a}|2\rangle \end{pmatrix}\begin{pmatrix} x_1 \\ x_2 \end{pmatrix}$$

$$= -\begin{pmatrix} \langle 2|\mathbf{a}|1\rangle & \langle 2|\mathbf{a}|2\rangle \\ \langle 1|\mathbf{a}|1\rangle & \langle 1|\mathbf{a}|2\rangle \end{pmatrix}\begin{pmatrix} x_1 \\ x_2 \end{pmatrix}. \tag{2.2.5b}$$

But the presence of R symmetry gives Eq. (2.2.4), which together with Eq. (2.2.5) gives the following:

$$\mathbf{a} \cdot R = R \cdot \mathbf{a}, \tag{2.2.6a}$$

$$\begin{pmatrix} \langle 1|\mathbf{a}|1\rangle & \langle 1|\mathbf{a}|2\rangle \\ \langle 2|\mathbf{a}|1\rangle & \langle 2|\mathbf{a}|2\rangle \end{pmatrix}\begin{pmatrix} 0 & 1 \\ 1 & 0 \end{pmatrix} = \begin{pmatrix} 0 & 1 \\ 1 & 0 \end{pmatrix}\begin{pmatrix} \langle 1|\mathbf{a}|1\rangle & \langle 1|\mathbf{a}|2\rangle \\ \langle 2|\mathbf{a}|1\rangle & \langle 2|\mathbf{a}|2\rangle \end{pmatrix}, \tag{2.2.6b}$$

$$\begin{pmatrix} \langle 1|\mathbf{a}|2\rangle & \langle 1|\mathbf{a}|1\rangle \\ \langle 2|\mathbf{a}|2\rangle & \langle 2|\mathbf{a}|1\rangle \end{pmatrix} = \begin{pmatrix} \langle 2|\mathbf{a}|1\rangle & \langle 2|\mathbf{a}|2\rangle \\ \langle 1|\mathbf{a}|1\rangle & \langle 1|\mathbf{a}|2\rangle \end{pmatrix}. \tag{2.2.6c}$$

The last equation shows that R symmetry of a requires that $\langle 1|\mathbf{a}|1\rangle = \langle 2|\mathbf{a}|2\rangle$ and $\langle 1|\mathbf{a}|2\rangle = \langle 2|\mathbf{a}|1\rangle$. However, the first equation (2.2.6a) is a general abstract definition of a physical symmetry.

Definition 1 A symmetry operator commutes with any operator that is part of an equation of motion for a physical system having that symmetry.

In quantum mechanics, all symmetry operators commute with the Hamiltonian according to this definition.

A second definition of symmetry operators involves the state vectors or basis of a physical system. We shall require that the inner product $\langle x|y\rangle$ of

any two vectors $|x\rangle$ and $|y\rangle$ shall be equal to that of the transformed vectors $R|x\rangle$ and $R|y\rangle$ as given in Eq. (2.2.7):

$$\langle x|y\rangle = \langle x|R^\dagger R|y\rangle. \tag{2.2.7}$$

We demand this for quantum and classical descriptions, alike. As explained in Chapter 1 [see, for example, Eqs. (1.1.8)], these last requirements imply that a linear symmetry operator R and its representations $\mathscr{R}_{ij} = \langle i|r|j\rangle$ will be unitary.

Definition 2 Symmetry operators and their representations are unitary.

$$RR^\dagger = 1 = R^\dagger R, \tag{2.2.8a}$$

$$(\mathscr{R}_{ij})^\dagger = \mathscr{R}^*_{ji} = (\mathscr{R}_{ij})^{-1}. \tag{2.2.8b}$$

In fact, the matrices $\langle i|R|j\rangle \equiv \langle i|j'\rangle$ will be seen to have the properties of the transformation matrix defined in Chapter 1.

Combining Eq. (2.2.8a) with Eq. (2.2.6b) gives the most commonly written expression for symmetry:

$$\mathbf{a} = R \cdot \mathbf{a} \cdot R^\dagger. \tag{2.2.9}$$

In other words, the operator **a** which has R symmetry is invariant or unchanged when transformed by R. [Recall the form of matrix operator transformations in Eq. (1.1.23c).] The set of all symmetry operators R satisfying Eq. (2.2.9) for a given **a** is called a GROUP by mathematicians or the SYMMETRY GROUP of **a** by physicists. The mathematical axioms for a group, which are shown on the left of Table 2.2.1, were introduced abstractly by a mathematician named Galois long before matrix applications like quantum mechanics came along. One may see by examining the right side of Table 2.2.1 that the mathematical axioms are closely related to the physical axioms 1–4 for transformation matrices given in Chapter 1.

A lot of mathematical work has involved the determination of all possible abstract groups with a given order or number of elements. It is not so easy to come up with a multiplication table which satisfies all four group definitions. For example, Eq. (2.2.10) is a multiplication table of a group of order 6, but Eq. (2.2.11) is a multiplication table of something that is not a group (possibly, this set should be called a "heap" instead), since $(ab)c = a \neq$

TABLE 2.2.1 Demonstrating that the Set of All Symmetry Transformation Operators Is a Group

Group Definitions	Testing the Symmetry Operators
1. If Q and R are in a group then so is their product $P = QR$ (called CLOSURE rule).	1. If $R\mathbf{a} = \mathbf{a}R$ and $Q\mathbf{a} = \mathbf{a}Q$ then $RQ\mathbf{a} = \mathbf{a}RQ$, so RQ is a symmetry operator, too. (Recall Axiom 4.)
2. If Q, R, and S are in a group, then $Q(RS) = (QR)S$ (called ASSOCIATIVITY rule).	2. The operators we discuss satisfy associativity since they are defined by matrices.
3. There exists an IDENTITY element 1 such that $R1 = R = 1R$ for all R in the group.	3. The unit operator commutes with any operator, including $\mathbf{a}$, so it is a symmetry operator. (Recall Axiom 3.)
4. For each R in the group there is an INVERSE R^{-1} such that $RR^{-1} = R^{-1}R = 1$.	4. If $R\mathbf{a} = \mathbf{a}R$, then $R^\dagger = R^{-1}$, which exists by Axioms 2–4, is a symmetry operation, too, because $R^\dagger R\mathbf{a}R^\dagger = R^\dagger \mathbf{a}RR^\dagger$ or $\mathbf{a}R^\dagger = R^\dagger\mathbf{a}$.

$a(bc) = c$ breaks rule 2. *Associativity* is a very restrictive property which one tends to take for granted.

Group

	1	A	B	C	D	F
1	1	A	B	C	D	F
A	A	B	C	D	F	1
B	B	C	D	F	1	A
C	C	D	F	1	A	B
D	D	F	1	A	B	C
F	F	1	A	B	C	D

(2.2.10)

Not a group

	1	a	b	c	d	f
1	1	a	b	c	d	f
a	a	1	d	b	f	c
b	b	d	1	f	c	a
c	c	b	f	1	a	d
d	d	f	c	a	1	b
f	f	c	a	d	b	1

(2.2.11)

However, the determination of all possible groups will not concern us at first, since the elementary symmetry groups such as $C_2 = \{1, R\}$ for the

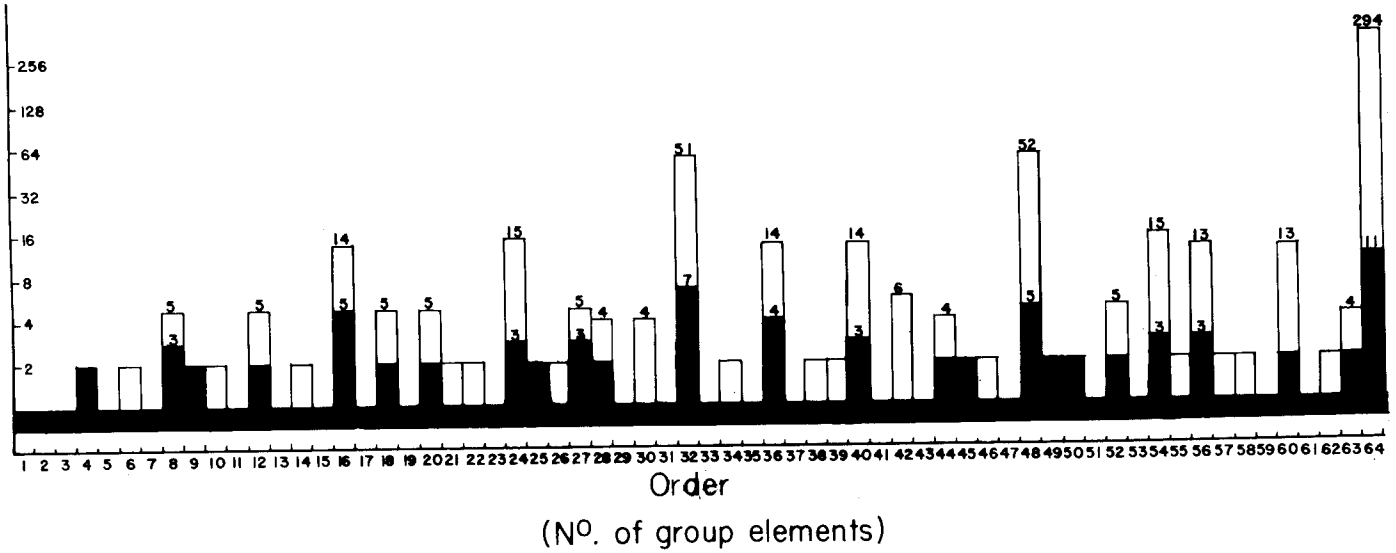

Figure 2.2.2 Plot of number of groups versus their order (^{o}G) for $^{o}G \leq 64$. The number of Abelian groups is indicated by the dark lines.

pendulums will be given by multiplication tables [viz., Eq. (2.2.12)] or by some other definition. (C_2 means "cyclic group of order 2." Actually the symmetry group we are using for the pendulums is called C_h or C_v, as will be explained in Section 2.11.)

	1	R
1	**1**	R
R	R	**1**

Pendulum symmetry group C_2. (2.2.12)

Nevertheless, it is instructive to see the plot in Figure 2.2.2 of the number of different groups that exist for order less than 65. Physicists have only applied a fraction of these finite groups so far. Nobody knows yet what all the rest can mean.

The following introduction to the uses of group theory begins with the application of some ABELIAN GROUPS including C_2. Abelian simply means commutative; that is, $ab = ba$ for all a, b in the Abelian group. (The name itself is in memory of the mathematician Abel.) Following this, the next three chapters contain theory and applications of the more general non-Abelian finite groups. This is followed by theory and applications of continuous symmetry groups of infinite order. However, the basic structure which we are about to derive in this chapter for some simple examples is basic to all symmetry theory.

2.3 SOLVING A PROBLEM WITH SYMMETRY ANALYSIS (C_2)

In order to use symmetry to simplify any physical problem, it is necessary to express the symmetry information, i.e., the group of symmetry operators, in a more digestible form. Let us now introduce the mechanics of this form using our simple example of two pendulums, Figure 2.2.1, which has the symmetry group $C_2 = \{\mathbf{1}, R\}$.

First we observe that the operator R and any representation thereof must satisfy an equation of the form $R^2 = \mathbf{1}$, which can be rewritten as

$$R^2 - \mathbf{1} = 0. \tag{2.3.1}$$

This has two roots: $r_+ = 1$ and $r_- = -1$.

Now, whenever you see an operator or matrix satisfying an nth-degree polynomial equation, you should remember what to do. Following Chapter 1, you use the roots $r_1 r_2 \cdots r_n$ to construct a set of idempotent projection operators using the following equation, which comes from Eq. (1.2.15):

$$P^{r_j} = \prod_{r_l \neq r_j} (R - r_l \mathbf{1}) \Big/ \prod_{r_l \neq r_j} (r_j - r_l). \tag{2.3.2}$$

For this example we have $r_+ = 1$ and $r_- = -1$, whence Eq. (2.3.2) gives the following:

$$P^+ = (\mathbf{1} + R)/2, \qquad P^- = (\mathbf{1} - R)/2. \tag{2.3.2}_x$$

Such operators must be orthogonal idempotents for the same reasons that their matrix counterparts were orthogonal in Chapter 1 [recall Eq. (1.2.17)]:

$$P^{r_j} P^{r_k} = \delta_{r_j r_k} P^{r_j}. \tag{2.3.3}$$

This is easily verified for the example being treated:

$$P^+P^+ = P^+, \qquad P^+P^- = 0 = P^-P^+, \qquad P^-P^- = P^-. \tag{2.3.3}_x$$

Now the representation $\langle i|P^r|j\rangle$ of P^r in the basis $\{|1\rangle, |2\rangle\}$ will help us reduce the equation of motion. From Eq. (2.2.2) the following representations result:

$$\begin{pmatrix} \langle 1|P^+|1\rangle & \langle 1|P^+|2\rangle \\ \langle 2|P^+|1\rangle & \langle 2|P^+|2\rangle \end{pmatrix} = \begin{pmatrix} \frac{1}{2} & \frac{1}{2} \\ \frac{1}{2} & \frac{1}{2} \end{pmatrix},$$

$$\begin{pmatrix} \langle 1|P^-|1\rangle & \langle 1|P^-|2\rangle \\ \langle 2|P^-|1\rangle & \langle 2|P^-|2\rangle \end{pmatrix} = \begin{pmatrix} \frac{1}{2} & -\frac{1}{2} \\ -\frac{1}{2} & \frac{1}{2} \end{pmatrix}.$$

By taking the first column of each of these matrices one obtains representations of the eigenkets $|e_+\rangle = P^+|1\rangle\sqrt{2}$, and $|e_-\rangle = P^-|1\rangle\sqrt{2}$:

$$\begin{pmatrix} \langle 1|e_+\rangle \\ \langle 2|e_+\rangle \end{pmatrix} = \begin{pmatrix} 1/\sqrt{2} \\ 1/\sqrt{2} \end{pmatrix}, \qquad \begin{pmatrix} \langle 1|e_-\rangle \\ \langle 2|e_-\rangle \end{pmatrix} = \begin{pmatrix} 1/\sqrt{2} \\ -1/\sqrt{2} \end{pmatrix}. \tag{2.3.4}$$

Here the normalization coefficient is the inverse square root of the diagonal component $[(\langle 1|P^\pm|1\rangle)^{-1/2} = \sqrt{2}]$ in each case. The vectors $|e_\pm\rangle$ are orthonormal eigenvectors of the symmetry operator:

$$R|e_+\rangle = |e_+\rangle, \qquad R|e_-\rangle = -|e_-\rangle.$$

They are also the eigenvectors of the acceleration matrix $\langle \mathbf{a} \rangle$ in Eq. (2.2.1):

$$\begin{pmatrix} a+b & -a \\ -a & a+b \end{pmatrix} \begin{pmatrix} 1/\sqrt{2} \\ 1/\sqrt{2} \end{pmatrix} = b \begin{pmatrix} 1/\sqrt{2} \\ 1/\sqrt{2} \end{pmatrix},$$

$$\begin{pmatrix} a+b & -a \\ -a & a+b \end{pmatrix} \begin{pmatrix} 1/\sqrt{2} \\ -1/\sqrt{2} \end{pmatrix} = (2a+b) \begin{pmatrix} 1/\sqrt{2} \\ -1/\sqrt{2} \end{pmatrix}.$$

This may be written abstractly as

$$\mathbf{a}|e_+\rangle = \alpha_+|e_+\rangle, \qquad \mathbf{a}|e_-\rangle = \alpha_-|e_-\rangle,$$

where the eigenvalues are

$$\alpha_+ = b, \qquad \alpha_- = 2a + b,$$
$$= g/l, \qquad = 2k/ml^2 + g/l.$$

The eigenvalues may change if the parameters k, m, or l vary, but the eigenvectors are fixed by the symmetry.

This shows one of the main ideas of symmetry analysis. Easily reducible symmetry operators will help reduce more complicated operators which commute with the symmetry operators. One starts with base states

$$|1\rangle = \mathbf{1}|1\rangle, \qquad |2\rangle = R|1\rangle$$

defined by the action of C_2 group operators $\mathbf{1}$ and R on the first state $|1\rangle$. This basis is convenient for deriving the equation of motion ($|\ddot{x}\rangle = -\mathbf{a}|x\rangle$). Then the idempotents [$P^+ = (\mathbf{1} + R)/2$] and [$P^- = (\mathbf{1} - R)/2$] are applied to the first state to give new base states

$$|e_+\rangle = P^+|1\rangle\sqrt{2} = (\mathbf{1} + R)|1\rangle/\sqrt{2}, \qquad |e_-\rangle = P^-|1\rangle\sqrt{2} = (\mathbf{1} - R)|1\rangle/\sqrt{2}$$
$$= (|1\rangle + |2\rangle)/\sqrt{2} \qquad = (|1\rangle - |2\rangle)/\sqrt{2}.$$

This basis is convenient for *solving* the equation of motion because off-diagonal components vanish:

$$\langle e_+|\mathbf{a}|e_-\rangle = \langle 1|P^+\mathbf{a}P^-|1\rangle$$
$$= \langle 1|\mathbf{a}P^+P^-|1\rangle = 0. \tag{2.3.5}$$

Here the first definition of symmetry is used ($R\mathbf{a} = \mathbf{a}R$ implies $P^+\mathbf{a} = \mathbf{a}P^+$) along with orthogonality ($P^+P^- = 0$). Hence $|e_+\rangle$ and $|e_-\rangle$ must be eigenvectors of $\mathbf{a}$ as indeed they are according to the representation in Eqs. (2.3.5). This is the main idea behind the applications of group theory.

However, one should note that this whole theory beginning with Eq. (2.3.1) is really outside of the area known by mathematicians as group theory. As soon as linear combinations of group operators, viz., ($\frac{1}{2}\mathbf{1} - \frac{1}{2}R$), $17R$, or 0 are considered one obtains a group ALGEBRA or RING. Elements of a group algebra satisfy the rules for a vector space (see Appendix A) whose dimension is the order of the group.

To complete the problem one writes the equations of motion in the $\{|e_+\rangle, |e_-\rangle\}$ basis. The $\langle e_+|$ component of the motion is determined by

$$\begin{aligned}\langle e_+|\ddot{x}\rangle &= -\langle e_+|\mathbf{a}|x\rangle \\ &= -\langle e_+|\mathbf{a}|e_+\rangle\langle e_+|x\rangle - \langle e_+|\mathbf{a}|e_-\rangle\langle e_-|x\rangle, \\ \langle e_+|\ddot{x}\rangle &= -\alpha_+\langle e_+|x\rangle. \end{aligned} \tag{2.3.6}$$

This is an equation for an amplitude oscillating with angular frequency $\omega_+ = \sqrt{\alpha_+}$. The solution is

$$\langle e_+|x(t)\rangle = A_+ \cos(\omega_+ t + B_+), \tag{2.3.7a}$$

where the constants A_+ and B_+ depend on initial conditions. Similarly, the $\langle e_-|$ amplitude oscillates according to

$$\langle e_-|x(t)\rangle = A_- \cos(\omega_- t + B_-), \tag{2.3.7b}$$

with generally higher frequency $\omega_- = \sqrt{\alpha_-}$. The general solution is a combination of these obtained by using completeness:

$$\begin{aligned}|x(t)\rangle &= |e_+\rangle\langle e_+|x(t)\rangle + |e_-\rangle\langle e_-|x(t)\rangle, \\ \begin{pmatrix}\chi_1(t)\\ \chi_2(t)\end{pmatrix} &= \begin{pmatrix}1/\sqrt{2}\\ 1/\sqrt{2}\end{pmatrix} A_+ \cos(\omega_+ t + B_+) + \begin{pmatrix}1/\sqrt{2}\\ -1/\sqrt{2}\end{pmatrix} A_- \cos(\omega_- t + B_-). \end{aligned} \tag{2.3.8}$$

The two terms $|e_+\rangle$ and $|e_-\rangle$ denote the familiar ELEMENTARY RESONANCES or NORMAL MODES of the system pictured in Figure 2.3.1. The figure also shows elementary examples of SPECTRA with two "lines." Two peaks or lines appear in plots of the response of the system to a harmonic driving force of frequency ω for three different values of the coupling constant k. A particular resonance $|e_j\rangle$ will be excited whenever ω^2 comes close to its eigenvalue α_j. (See Problem 2.3.1.)

These double pendulums have been sold in novelty shops from time to time. They are capable of performing a "beat trading" motion that can be quite slow for low values of k. By setting initial conditions $\dot{\chi}_1(0) = 0 = \dot{\chi}_2(0) = \chi_2(0)$ and $\chi_1(0) = 1$ (i.e., by selecting equal amounts of modes $|e_+\rangle$ and $|e_-\rangle$; $A^+ = 1/\sqrt{2} = A^-$ and $B^+ = 0 = B^-$), we get the alternating suppression or "beats" of activity for one pendulum and then the other, as depicted in Figure 2.3.2(a). The pendulums trade beats at a frequency equal to the difference between the eigenfrequencies [$\omega(\text{beat}) = \sqrt{\alpha_-} - \sqrt{\alpha_+}$].

A perfect beating is only possible if C_2 symmetry is present. The last point we would like to make here is that plain physical appearance does not always indicate the physical symmetry. For example, the Wilberforce pendulum in

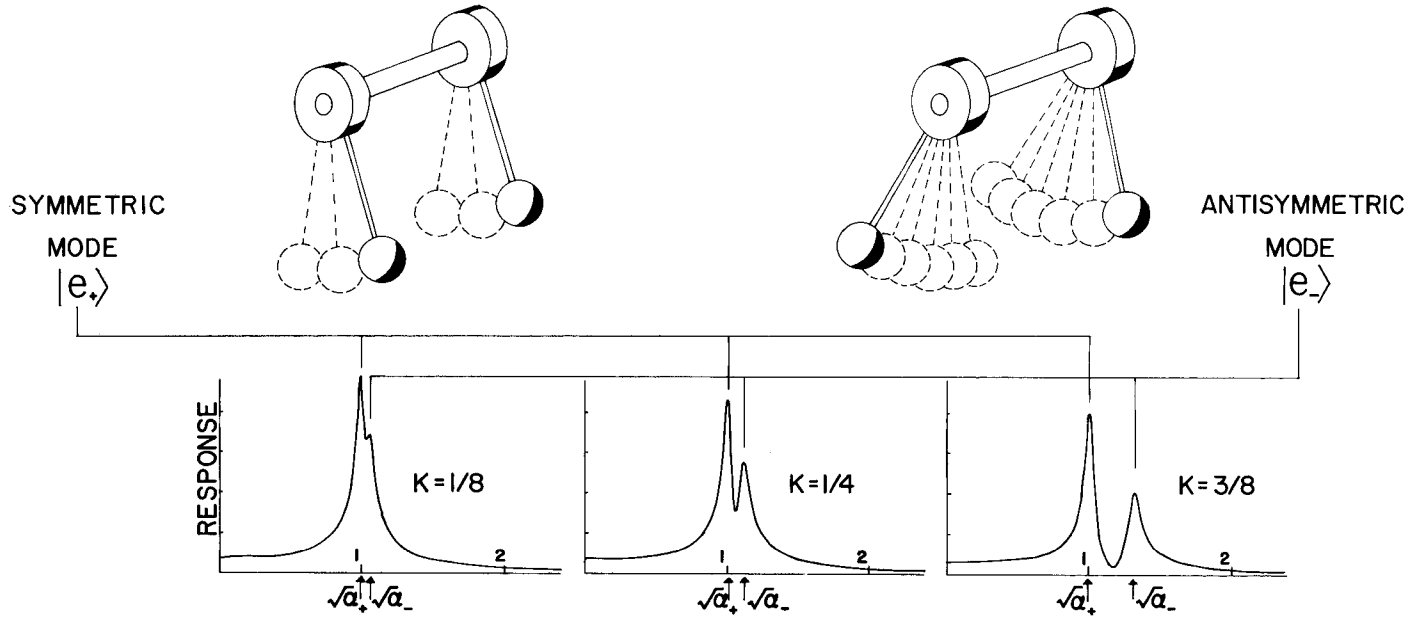

Figure 2.3.1 Normal modes and spectra of C_2 symmetrically coupled pendulums.

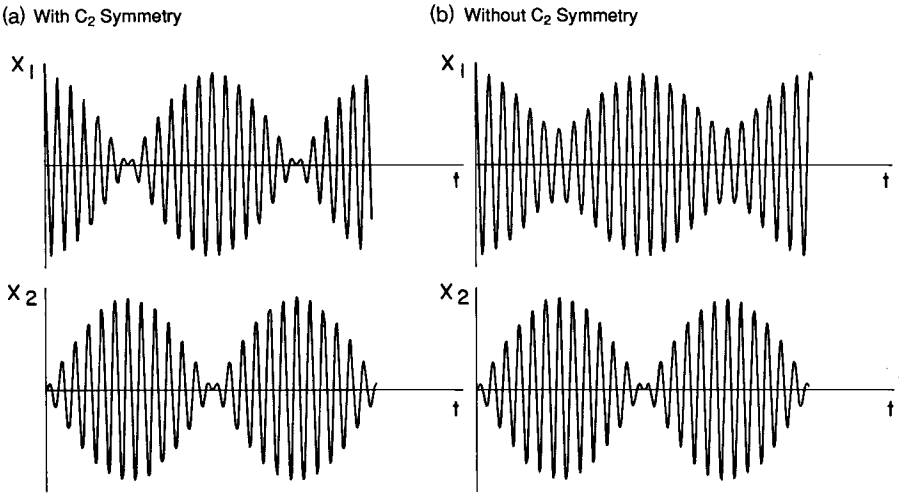

Figure 2.3.2 Beating results when two eigenmodes are excited simultaneously. Perfect transfer of motion between coordinates x_1 and x_2 occurs only if C_2 symmetry is present. Transfer occurs with a beat frequency equal to the difference of the eigenfrequencies.

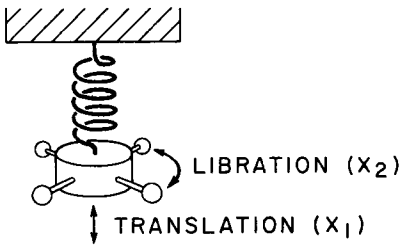

Figure 2.3.3 Wilberforce pendulum. A system can have a C_2 physical symmetry even if its geometrical form is asymmetrical.

Figure 2.3.3 certainly does not "look" C_2 symmetric, but it will execute its perfect trade of beats only if its parameters are adjusted so that it has C_2 physical symmetry.

Having used symmetry projection to help solve coupled oscillator problems, one should compare other methods for studying such problems. Throughout this book we will try to show the advantages of using a variety of approaches to help one gain a solid physical picture of the systems being studied. Also, since the coupled oscillator is such an important paradigm for many physical systems, we should pause here to consider some alternative views of it.

(a) The Configuration Space View: Lissajous Figures One may recast the problem of two equivalent one-dimensional oscillators into the identical problem of a single two-dimensional oscillator. If one plots one oscillator

coordinate versus the other (i.e., x_1 versus x_2) the resulting two-dimensional space is called configuration space. However, x_1 and x_2 could just as well be coordinates x and y, respectively, of a single oscillating mass in ordinary space.

As explained in Section 1.4.B forces are obtained from the derivatives of the potential function of the form

$$V(x_1, x_2) = \tfrac{1}{2}(\mathscr{F}_{11}x_1^2 + 2\mathscr{F}_{12}x_1x_2 + \mathscr{F}_{22}x_2^2). \tag{2.3.9}$$

The curves $V(x_1, x_2)$ = constant are tipped ellipses, and some examples are drawn next to the potential surface in Figure 2.3.4. They are the equipotential or level lines for the two-dimensional valley. One can imagine that they are the topography lines for the "Bare Valley" ski resort which has the most gentle beginner slope running NE to SW along the long axes of the ellipses, and the steepest path running NW to SE along the short axes. If the potential has C_2 symmetry then these axes are exactly at $+45°$ and $-45°$, respectively, to the x_1 axis.

Using the potential map one can see that a particle starting out on one or the other of the elliptical axes will oscillate back and forth on that axis forever. This motion is indicated in the right-hand and left-hand parts of Figure 2.3.5. The major and minor axes correspond to the symmetric low-frequency (+) mode and the antisymmetric high-frequency (−) mode, respectively, in Figure 2.3.1. If a particle starts out in between these eigenaxes, say on the x_1 axis as shown in the central figure, then its trajectory will be a curve which is called a Lissajous figure. Some examples of Lissajous curves are given in Figure 2.3.6. Let us consider first the case in Figure 2.3.6a for which the equipotential lines would be nearly circular, and the coupling constant (a) in Eq. (2.2.1c) or force $\mathscr{F}_{12}$ in (2.3.9) is very small. This will

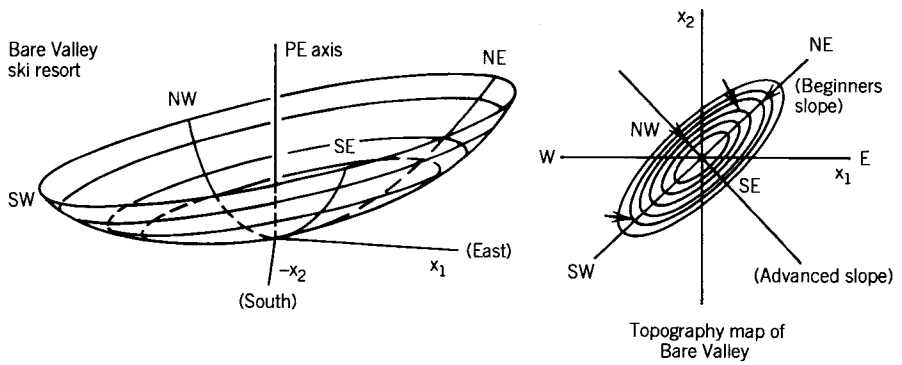

Figure 2.3.4 Topography plot of two-dimensional oscillator potential with C_2 symmetry.

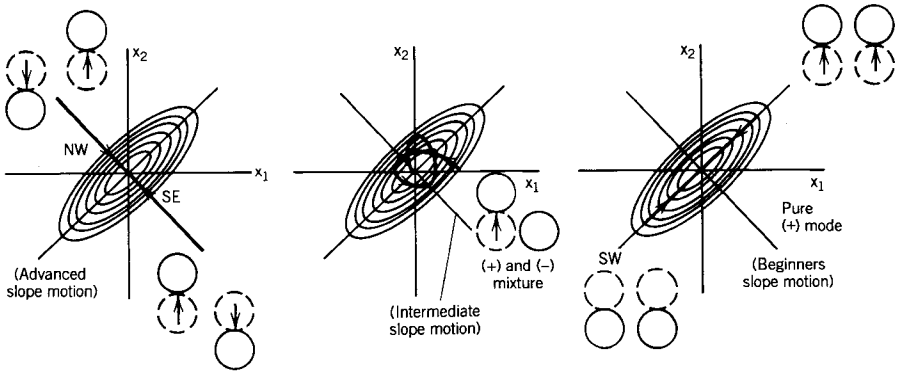

Figure 2.3.5 Motions corresponding to pure and mixed models.

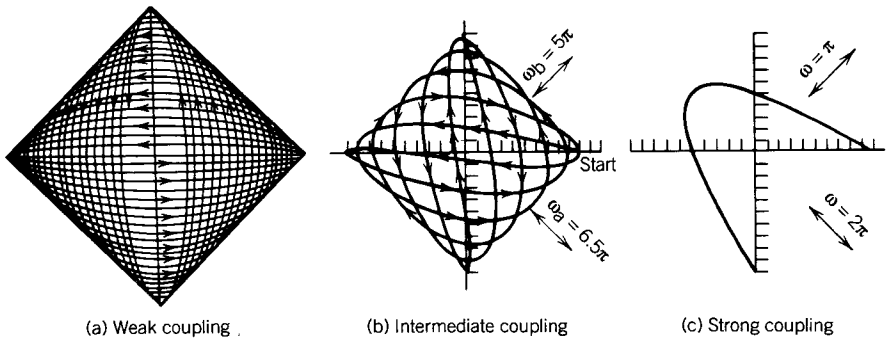

Figure 2.3.6 Lissajous plots of mixed mode motions.

provide an example of the very important phenomenon of *resonance*, whereby the effects of small forces can be greatly amplified.

A particle which starts at rest on the x_1 axis is deflected slightly upward toward the positive x_2 axis by the gradient as it falls from the right to the left. It subsequently follows a counterclockwise path which resembles an ellipse whose x_2 amplitude or minor axis increases slightly each period. Meanwhile, the major axis or x_1 amplitude decreases until the two are about the same and the trajectory encloses a maximum area which is nearly circular. From the equation of motion it follows that the x_2 oscillation is experiencing a coupling force which equals ax_1. One may consider the quantities x_2 and x_1 as distance and applied force, respectively, for the x_2 oscillator, and vice versa for x_1. Hence, the area enclosed by the Lissajous curve is a direct measure of the work done on the x_2 coordinate by the x_1 motion, where the

work is

$$\int F_2(\text{by } 1)\, dx_2 = a \int x_1\, dx_2. \tag{2.3.10}$$

The rate of energy transfer is greatest when the Lissajous curve is most nearly a circle and the phase of the driven oscillator is nearly 90° behind the driver. This is a resonance condition, and is discussed at length in Section 6.5.

Eventually x_1 becomes exhausted while x_2 reaches its maximum amplitude. At this point x_1 falls behind x_2 in phase by nearly 90°, so that x_2 becomes the driver and x_1 the driven. The Lissajous curve now is orbiting around in a clockwise or negative sense until x_2 becomes exhausted and the curve passes near its starting point on the x_1 axis. This marks the end of one beat period in Figure 2.3.2(a).

Beat periods become shorter for stronger coupling, and the difference between eigenfrequencies becomes greater. An example of larger coupling is shown in Figure 2.3.6(b), and a more extreme example is shown in Figure 2.3.6(c) (for which $\omega_+ = 2\pi$ and $\omega_- = \pi$) and there a complete beating takes place in exactly two seconds. In each of the latter two examples the ratio of the two eigenfrequencies is exactly a ratio of two integers. When the ratio of eigenfrequencies is a rational number, i.e., a ratio of relatively prime integers,

$$\omega_+/\omega_- = n_+/n_-, \tag{2.3.11}$$

then the Lissajous trajectory will be closed and must repeat perfectly after a period of time

$$\begin{aligned} t_{\text{LJ}} &= 2\pi n_+/\omega_+ = 2\pi n_-/\omega_- \\ &= n_+ t_+ \qquad = n_- t_-. \end{aligned} \tag{2.3.12}$$

Since the beat period is given by

$$\begin{aligned} t_{\text{BEAT}} &= 1/((1/t_+) - (1/t_-)) \\ &= t_+ t_-/(t_- - t_+), \end{aligned}$$

it then follows that the Lissajous period is

$$t_{\text{LJ}} = (n_+ - n_-) t_{\text{BEAT}}. \tag{2.3.13}$$

If the frequency ratio is irrational then t_{LJ} is infinite. For the example in Figure 2.3.6(b) the ratio is $(n_+/n_- = \frac{13}{10})$, and so a complete Lissajous cycle takes three beats. The arrows in the figure represent direction of the path for the first $1(\frac{1}{2})$ beats. You should trace the motion from the extreme right-hand

point on the x_1 axis to the top of the x_2 axis. After this the trajectory simply retraces its way back to the starting point. For the "most rational" example in Figure 2.3.6 the two kinds of periods are equal. In nonlinear or anharmonic vibrational problems the idea of proximity to rationality is an important one. (See Problem 2.3.3.)

(b) The Phase Space View: Phasors One may think of a harmonic oscillator as a clock and let its sweep second hand be a complex vector which represents the oscillator phase. If the complex number

$$\mathscr{C} = Ce^{-i\omega t} = C\cos(\omega t) - iC\sin(\omega t)$$

is used to represent an oscillator, then the real and imaginary parts correspond to the position and the frequency-scaled velocity ($\text{Im}\,\mathscr{C} = -C\sin(\omega t) = v/\omega$) of the oscillator. A vector whose abscissa and ordinate are the real and imaginary part, respectively, of $\mathscr{C}$ is called a PHASOR. As time advances the phasor rotates clockwise like a second hand, and traces a circular trajectory in a rescaled phase space of the oscillator.

To use the phasor picture for the two coupled pendulums we let each coordinate x_1 and x_2 be represented by a separate phasor clock. This is one way to represent the four-dimensional phase space of the two coupled oscillators. However, one first needs to find ways to set the clocks so that they run like clocks and maintain constant frequency and amplitude. The normal modes $|e_+\rangle$ and $|e_-\rangle$ each correspond to such a setting. If the clocks are set with equal phase and amplitude this corresponds to the $|e_+\rangle$ mode in which the clocks run synchronously at frequency $\omega_+/(2\pi)$. For the $|e_-\rangle$ mode the clocks are set with opposite ($\pm 180°$) phase and they both run at frequency $\omega_-/(2\pi)$.

An arbitrary clock setting corresponds to a combination of the $|e_+\rangle$ and $|e_-\rangle$ modes. The first frame on the left-hand side of Figure 2.3.7 shows a sum of equal amounts of $|e_+\rangle$ and $|e_-\rangle$ settings at $t = 0$. As time advances the (+) and (−) components each turn synchronously at their respective rates, which are taken to be 0.5 and 1.0 Hz, respectively. The phasor vector sums of the (+) and (−) clocks are shown at $\frac{1}{4}$-second intervals at the bottom of each frame. One can see that the x_1 phasor is roughly 90° ahead of the x_2 phasor until the former vanishes at $t = 1$ sec, and this corresponds to resonant transfer of energy from x_1 to x_2. By $t = 2$ sec the x_1 coordinate will have recovered all the energy it had at the beginning of the beat period as shown in the Lissajous plot of this example, which is Figure 2.3.6(c).

The example just treated is one of very strong coupling. The energy transfer is accomplished in one or two oscillations of the coordinates. The process is more like a series of jarring collisions than a gentle but persistent persuasion of resonance. Nevertheless, in the harmonic limit for which the equations of motion are linear the description of strong coupling is the same as that of weak coupling for which the beats take a long time.

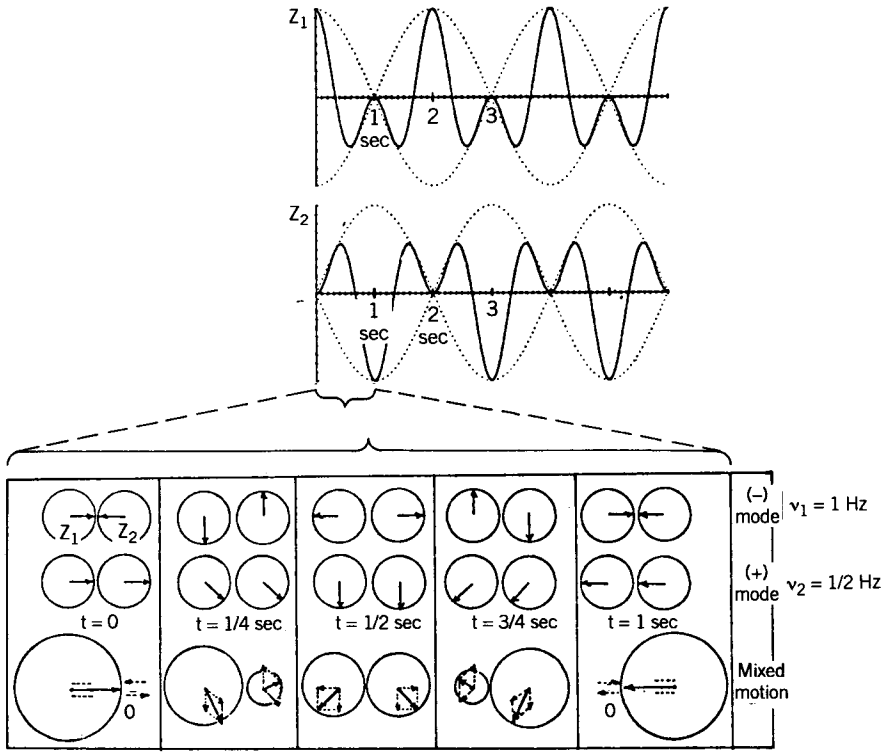

Figure 2.3.7 Phasor diagram of strongly coupled oscillation.

We shall use phasors to describe resonance and wave phenomena throughout this book. They are convenient for displaying the motions of three or more oscillators while the configuration space view can be rather limiting as the number of dimensions goes up. When discussing any pair of directly coupled phasors one should always remember that the one which is behind in phase by some amount between 0° and 180° is receiving energy on the average from the one which is ahead.

2.4 IRREDUCIBLE REPRESENTATIONS

The orthonormality of P^+ and P^- has just been used to solve an equation of motion. Now we study some of the mathematics associated with the completeness relation [Eq. (2.4.1)] and spectral decomposition [Eq. (2.4.2)], which will later help us to do more complicated problems:

$$\mathbf{1} = P^+ + P^-, \tag{2.4.1}$$

$$R = P^+ - P^-. \tag{2.4.2}$$

TABLE 2.4.1

	$g =$	$\mathbf{1}$	R
$\mathbf{1} = D^+(1)P^+ + D^-(1)P^-$	$D^+(g) =$	1	1
$R = D^+(R)P^+ + D^-(R)P^-$	$D^-(g) =$	1	−1

These equations are analogous to the matrix equations (1.2.18) and (1.2.21), respectively, which were derived in the preceding review chapter. The coefficients or eigenvalues in these equations are called IRREDUCIBLE REPRESENTATIONS or CHARACTERS of the Abelian group $C_2 = \{1, R\}$. Table 2.4.1 is called a CHARACTER TABLE. Equations (2.4.1) and (2.4.2) have been rewritten just to show the notation.

In Chapter 3 we shall distinguish between irreducible representations and characters. In general the latter are the traces of the former, but for 1×1 matrices the trace of the matrix is the same as the matrix itself. Since all the elements of an Abelian group are mutually commuting unitary operators it will always be possible to simultaneously reduce the entire group to combinations of projectors multiplied by eigenvalues using the procedure in Section 1.2.B(d). (see Appendix C). So each element g of Abelian group $G = \{\mathbf{1}, g, g', \ldots\}$ can therefore be spectrally decomposed into a sum of products of eigenvalues $D^\alpha(g)$ and idempotents P^α as follows:

$$\begin{aligned} \mathbf{1} &= D^\alpha(1)P^\alpha + D^{\alpha'}(1)P^{\alpha'} + \cdots = P^\alpha + P^{\alpha'} + \cdots, \\ g &= D^\alpha(g)P^\alpha + D^{\alpha'}(g)P^{\alpha'} + \cdots, \\ g' &= D^\alpha(g')P^\alpha + D^{\alpha'}(g')P^{\alpha'} + \cdots. \end{aligned} \tag{2.4.3}$$

As shown in Section 1.2.B(b) the P^α are orthonormal ($P^\alpha P^{\alpha'} = \delta^{\alpha\alpha'}P^\alpha$) and complete ($\mathbf{1} = P^\alpha + P^{\alpha'} + \cdots$). The coefficients of such decompositions must obey the following rule: The product $D^\alpha(g)D^\alpha(g')$ of an irreducible representation α of group elements must equal the same irreducible representation $D^\alpha(gg')$ of the product gg'. We see that this follows from the properties of the idempotents as follows:

$$gg' = \left(\sum_\alpha D^\alpha(g)P^\alpha\right)\left(\sum_{\alpha'} D^{\alpha'}(g')P^{\alpha'}\right) = \sum_\alpha D^\alpha(g)D^\alpha(g')P^\alpha,$$

by using the definition

$$gg' = \sum_\alpha D^\alpha(gg')P^\alpha,$$

whence

$$D^\alpha(g)D^\alpha(g') = D^\alpha(gg'). \tag{2.4.4}$$

In other words, the sets of irreducible representations will "imitate" an Abelian group with just (1×1) matrices, i.e., the numbers in a character table.

But it is more important, probably, to observe that the irreducible representations of any group are a complete set of "building blocks" for any representation of that group. Every representation has to be "made" from them and only them. Suppose somebody brings to you a representation of group C_2 without telling you where it came from. For example, let us be given a representation of C_2 by matrices $\mathscr{D}(1)$ and $\mathscr{D}(R)$ defined by

$$\left\{\mathscr{D}(1) = \begin{pmatrix} 1 & 0 & 0 \\ 0 & 1 & 0 \\ 0 & 0 & 1 \end{pmatrix} \mathscr{D}(R) = \begin{pmatrix} 0 & 0 & 1 \\ 0 & 1 & 0 \\ 1 & 0 & 0 \end{pmatrix}\right\}. \tag{2.4.5}$$

Now we check to make sure that it is a representation of our group, i.e., that $\mathscr{D}(ab) = \mathscr{D}(a)\mathscr{D}(b)$ for all a and b in the group. (Here it is enough to check that $\mathscr{D}(R^2) = \mathscr{D}(R)\mathscr{D}(R) = (1)$.) This guarantees that the completeness and orthonormality relations for the representations $\mathscr{D}(P^\alpha)$ of the idempotents must hold as well. The $\mathscr{D}(P^\alpha)$ matrices follow from Eqs. $(2.3.2)_x$ and (2.4.5):

$$\mathscr{D}(P^+) = \begin{pmatrix} \frac{1}{2} & 0 & \frac{1}{2} \\ 0 & 1 & 0 \\ \frac{1}{2} & 0 & \frac{1}{2} \end{pmatrix} \qquad \mathscr{D}(P^-) = \begin{pmatrix} \frac{1}{2} & 0 & -\frac{1}{2} \\ 0 & 0 & 0 \\ -\frac{1}{2} & 0 & \frac{1}{2} \end{pmatrix} \tag{2.4.6}$$

$$\mathscr{T} = \begin{pmatrix} \dfrac{1}{\sqrt{2}} & 0 & \dfrac{1}{\sqrt{2}} \\ 0 & 1 & 0 \\ \dfrac{1}{\sqrt{2}} & 0 & -\dfrac{1}{\sqrt{2}} \end{pmatrix}. \tag{2.4.7}$$

This implies that the transformation matrix made from orthonormal columns of $\mathscr{D}(P^\alpha)$ as just shown will diagonalize the representation as seen in Eq. (2.4.8):

$$\begin{aligned} \mathscr{T}^\dagger \mathscr{D}(1) \mathscr{T} &= \begin{pmatrix} 1 & 0 & 0 \\ 0 & 1 & 0 \\ 0 & 0 & 1 \end{pmatrix} = \begin{pmatrix} D^+(1) & 0 & 0 \\ 0 & D^+(1) & 0 \\ 0 & 0 & D^-(1) \end{pmatrix}, \\ \mathscr{T}^\dagger \mathscr{D}(R) \mathscr{T} &= \begin{pmatrix} 1 & 0 & 0 \\ 0 & 1 & 0 \\ 0 & 0 & -1 \end{pmatrix} = \begin{pmatrix} D^+(R) & 0 & 0 \\ 0 & D^+(R) & 0 \\ 0 & 0 & D^-(R) \end{pmatrix}. \end{aligned} \tag{2.4.8}$$

This is because each nonzero column of a representation of P^α must be an

eigenvector of the representation of all symmetry operators R in an Abelian group, each with eigenvalue $D^{\alpha}(R)$:

$$R \cdot P^{\alpha} = D^{\alpha}(R)P^{\alpha} \leftrightarrow \mathscr{D}(R)\mathscr{D}(P^{\alpha}) = D^{\alpha}(R)\mathscr{D}(P^{\alpha}). \qquad (2.4.9)$$

The completeness relation guarantees that one has accounted for all possibilities. So every representation $\mathscr{D}(g)$ of any Abelian group operator g must be reducible to a string of (1×1) irreducible representations $D^{\alpha}(g)$ on the diagonal. The notation for the reduction given in Eq. (2.4.8) is given in the following using the DIRECT SUM sign $\oplus$:

$$\mathscr{T}^{\dagger}\mathscr{D}(g)\mathscr{T} = D^{+}(g) \oplus D^{+}(g) \oplus D^{-}(g). \qquad (2.4.10)$$

2.5 PARTIALLY SOLVING A PROBLEM WITH SYMMETRY ANALYSIS (C_2)

It is probably a good idea now to see an "imperfect" application of symmetry analysis in order to see some of the limitations of this theory from the start. The pendulum system drawn in Figure 2.5.1 has the same symmetry $C_2 = \{1, R\}$ which we have been discussing. Operator R is defined in terms of the base kets by $R|1\rangle = |3\rangle$, $R|2\rangle = |2\rangle$, and $R|3\rangle = |1\rangle$. That is, we may

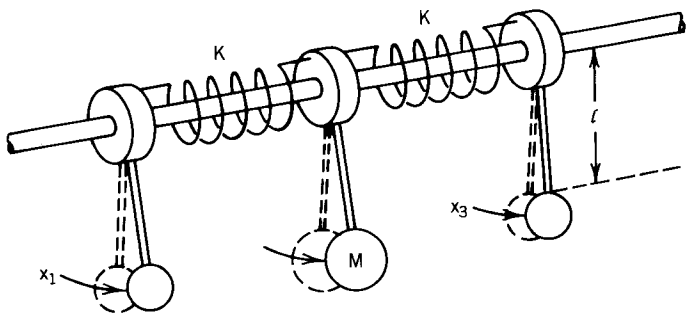

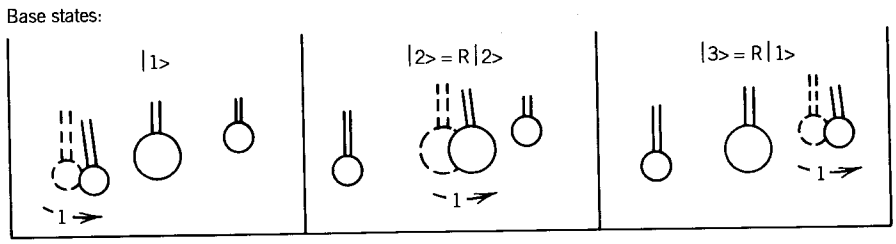

Figure 2.5.1 Coupled pendulums. This is a more complicated example of C_2 symmetry. Only two of the three bases are connected by the C_2 symmetry operator.

switch the two outside pendulums, but the middle one has to be left alone because it is different in mass and location.

The equation of motion is written out in three different forms:

$$|\ddot{x}(t)\rangle = -\mathbf{a}|x(t)\rangle, \tag{2.5.1a}$$

$$\begin{pmatrix} \langle 1|\ddot{x}(t)\rangle \\ \langle 2|\ddot{x}(t)\rangle \\ \langle 3|\ddot{x}(t)\rangle \end{pmatrix} = -\begin{pmatrix} \langle 1|\mathbf{a}|1\rangle & \langle 1|\mathbf{a}|2\rangle & \langle 1|\mathbf{a}|3\rangle \\ \langle 2|\mathbf{a}|1\rangle & \langle 2|\mathbf{a}|2\rangle & \langle 2|\mathbf{a}|3\rangle \\ \langle 3|\mathbf{a}|1\rangle & \langle 3|\mathbf{a}|2\rangle & \langle 3|\mathbf{a}|3\rangle \end{pmatrix}\begin{pmatrix} \langle 1|x(t)\rangle \\ \langle 2|x(t)\rangle \\ \langle 3|x(t)\rangle \end{pmatrix}, \tag{2.5.1b}$$

$$\begin{pmatrix} \ddot{x}_1 \\ \ddot{x}_2 \\ \ddot{x}_3 \end{pmatrix} = -\begin{pmatrix} a+b & -a & 0 \\ -A & 2A+b & -A \\ 0 & -a & a+b \end{pmatrix}\begin{pmatrix} x_1 \\ x_2 \\ x_3 \end{pmatrix}. \tag{2.5.1c}$$

The constants in the acceleration matrix are $a = k/ml^2$, $b = g/l$, and $A = k/Ml^2$.

The representation of the C_2 symmetry operator R in the $\{|1\rangle, |2\rangle, |3\rangle\}$ basis is (see Figure 2.5.1)

$$\begin{pmatrix} \langle 1|R|1\rangle & \langle 1|R|2\rangle & \langle 1|R|3\rangle \\ \langle 2|R|1\rangle & \langle 2|R|2\rangle & \langle 2|R|3\rangle \\ \langle 3|R|1\rangle & \langle 3|R|2\rangle & \langle 3|R|3\rangle \end{pmatrix} = \begin{pmatrix} 0 & 0 & 1 \\ 0 & 1 & 0 \\ 1 & 0 & 0 \end{pmatrix},$$

which is precisely the $\mathscr{C}$ representation treated in the preceding section. [Compare Eq. (2.4.5) with the preceding one.] There we found that a change of basis from $\{|1\rangle, |2\rangle, |3\rangle\}$ to $\{|e_+\rangle, |e'_+\rangle, |e_-\rangle,\}$, represented as

$$|e_+\rangle \to \begin{pmatrix} \langle 1|e_+\rangle \\ \langle 2|e_+\rangle \\ \langle 3|e_+\rangle \end{pmatrix} = \begin{pmatrix} 1/\sqrt{2} \\ 0 \\ 1/\sqrt{2} \end{pmatrix}, \qquad |e'_+\rangle \to \begin{pmatrix} \langle 1|e'_+\rangle \\ \langle 2|e'_+\rangle \\ \langle 3|e'_+\rangle \end{pmatrix} = \begin{pmatrix} 0 \\ 1 \\ 0 \end{pmatrix},$$

$$|e_-\rangle \to \begin{pmatrix} \langle 1|e_-\rangle \\ \langle 2|e_-\rangle \\ \langle 3|e_-\rangle \end{pmatrix}\begin{pmatrix} 1/\sqrt{2} \\ 0 \\ -1/\sqrt{2} \end{pmatrix}, \tag{2.5.2}$$

caused the $\mathscr{C}$ representation to assume a reduced or diagonalized form. [Recall Eq. (2.4.8).] Applying the same change of basis to the acceleration matrix in Eq. (2.5.1) we see that a partial, but not total, reduction of it occurs:

$$\mathscr{T}^{\dagger}a\mathscr{T} = \begin{pmatrix} a+b & -\sqrt{2}a & 0 \\ -\sqrt{2}A & A+b & 0 \\ 0 & 0 & a+b \end{pmatrix}. \tag{2.5.3}$$

Symmetry analysis guarantees that components like $\langle e_+|\mathbf{a}|e_-\rangle$, or $\langle e_-|\mathbf{a}|e_+\rangle$, etc., are zero, but it cannot guarantee that a coupling like $\langle e'_+|\mathbf{a}|e_+\rangle$ will go away. In fact, it does not—it equals $-\sqrt{2}a$ in Eq. (2.5.3).

So for this problem the $(-)$ eigenvector is fixed, but the $(+)$ eigenvectors still remain to be solved, and the results will depend upon the values of the constants g, k, 1, m, and M. Symmetry analysis with the group C_2 can do no more than separate the $(+)$ type modes from the $(-)$ types.

In a general symmetry analysis you will determine the REPETITION FREQUENCY f^α or the number of times each irreducible representation D^α appears in the reduction of the physical group representation. This tells you how much work is left after the symmetry analysis is completed: Each $f^\alpha \times f^\alpha$ matrix may need to be reduced. The final reduction is completed using standard techniques reviewed in Chapter 1, or may be accomplished numerically on a computer. (Or, perhaps, you may find a higher symmetry!)

2.6 AN EXAMPLE WITH SLIGHTLY HIGHER SYMMETRY (C_3)

If the three pendulums are coupled in a more symmetric way, as in Figure 2.6.1, it will be possible once again to deduce the complete solutions to the equation of motion

$$\begin{pmatrix} \ddot{x}_1 \\ \ddot{x}_2 \\ \ddot{x}_3 \end{pmatrix} = -\begin{pmatrix} 2a+b & -a & -a \\ -a & 2a+b & -a \\ -a & -a & 2a+b \end{pmatrix}\begin{pmatrix} x_1 \\ x_2 \\ x_3 \end{pmatrix} \tag{2.6.1}$$

using symmetry analysis techniques. The constants in the equation are $b = g/l$ and $a = s/ml^2$, where s is the coupling spring constant and g, l, and m are gravity, length, and mass constants, respectively. The basic coordinates x_1, x_2, and x_3 are defined by Figure 2.6.1. Symmetry operators include the cyclic exchange or 120° rotation operator labeled r which transforms base states as follows:

$$r|1\rangle = |2\rangle, \qquad r|2\rangle = |3\rangle, \qquad r|3\rangle = |1\rangle,$$

the double exchange operator r^2 which does the transformations,

$$r^2|1\rangle = |3\rangle, \qquad r^2|2\rangle = |1\rangle, \qquad r^2|3\rangle = |2\rangle,$$

and the identity **1**, which changes nothing. ($\mathbf{1}|i\rangle = |i\rangle$). There are some other symmetry operators such as "reflections" σ_{12}, σ_{23}, and σ_{31}, where, for example,

$$\sigma_{12}|1\rangle = |2\rangle, \qquad \sigma_{12}|2\rangle = |1\rangle, \qquad \sigma_{12}|3\rangle = |3\rangle.$$

However, let us put off discussing these until Chapter 3.

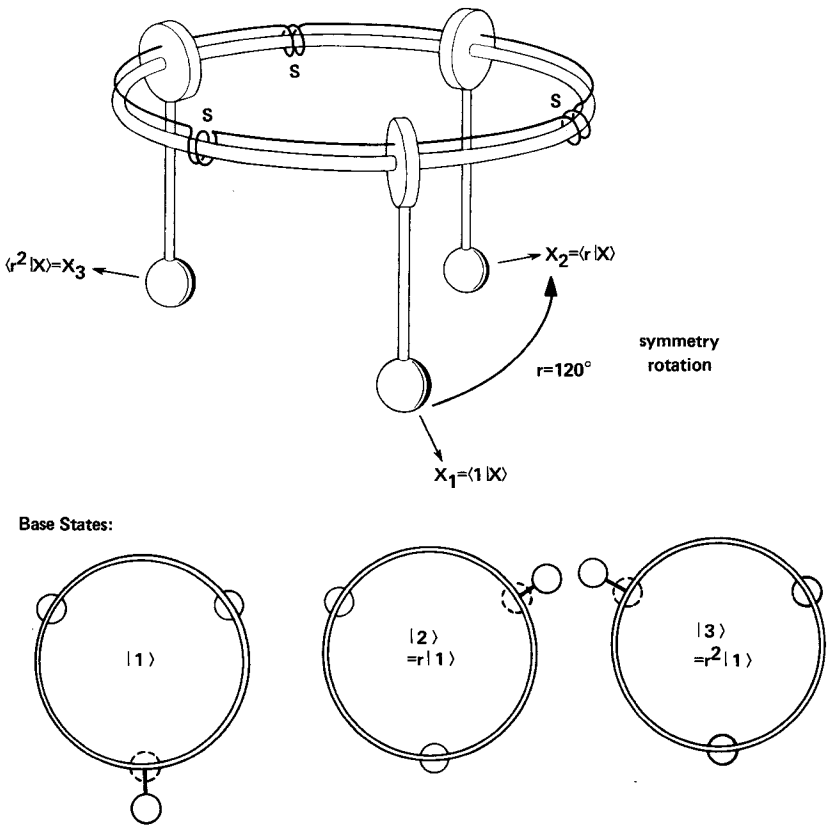

Figure 2.6.1 C_3 symmetric coupled pendulums.

The three operators $\{\mathbf{1}, r, r^2\}$ form a group called C_3. The multiplication table is

$$\begin{array}{c|ccc} & \mathbf{1} & r & r^2 \\ \hline \mathbf{1} & \mathbf{1} & r & r^2 \\ r & r & r^2 & \mathbf{1} \\ r^2 & r^2 & \mathbf{1} & r \end{array}. \tag{2.6.2}$$

Now one can use the minimal equations ($r^3 = \mathbf{1}$, or $r^3 - \mathbf{1} = 0$) to produce the idempotents associated with the group elements. The minimal equation for r is factored into the three roots of unity:

$$0 = (r^3 - \mathbf{1}) = (r - \varepsilon_1\mathbf{1})(r - \varepsilon_2\mathbf{1})(r - \varepsilon_3\mathbf{1}),$$

where

$$\varepsilon_1 \equiv 1, \qquad \varepsilon_2 \equiv e^{2\pi i/3}, \qquad \varepsilon_3 \equiv e^{-2\pi i/3}.$$

Using Eq. (2.3.2) we obtain three idempotents P^α:

$$P^1 = \frac{(r-\varepsilon_2\mathbf{1})(r-\varepsilon_3\mathbf{1})}{(\varepsilon_1-\varepsilon_2)(\varepsilon_1-\varepsilon_3)} = \frac{1}{3}(\mathbf{1}+r+r^2),$$

$$P^2 = \frac{(r-\varepsilon_1\mathbf{1})(r-\varepsilon_3\mathbf{1})}{(\varepsilon_2-\varepsilon_1)(\varepsilon_2-\varepsilon_3)} = \frac{1}{3}(\mathbf{1}+\varepsilon_3 r+\varepsilon_2 r^2),$$

$$P^3 = \frac{(r-\varepsilon_1\mathbf{1})(r-\varepsilon_2\mathbf{1})}{(\varepsilon_3-\varepsilon_1)(\varepsilon_3-\varepsilon_2)} = \frac{1}{3}(\mathbf{1}+\varepsilon_2 r+\varepsilon_3 r^2). \qquad (2.6.3)$$

The inverses of Eq. (2.6.3) are the completeness and spectral decomposition relations in the following. These follow from the theory given in Sections 1.2.B(b) and (c).

$$\mathbf{1} = P^1 + P^2 + P^3 \equiv D^1(1)P^1 + D^2(1)P^2 + D^3(1)P^3,$$

$$r = P^1 + \varepsilon_2 P^2 + \varepsilon_3 P^3 \equiv D^1(r)P^1 + D^2(r)P^2 + D^3(r)P^3,$$

$$r^2 = P^1 + \varepsilon_3 P^2 + \varepsilon_2 P^3 \equiv D^1(r^2)P^1 + D^2(r^2)P^2 + D^3(r^2)P^3. \qquad (2.6.4)$$

The eigenvalues $D^\alpha(g)$ in the decompositions above are the irreducible representations (we abbreviate this "irrep," henceforward) of C_3. There are three kinds of irreps as tabulated in the following using Eq. (2.6.4). Two other standard notations for the irreps of C_3 are shown on the left-hand side of the character table (see a "phasor" version of this table at the top of Figure 2.6.2):

$g =$	$\mathbf{1}$	r	r^2
$D^{0_3}(g) = D^A(g) = D^1(g) =$	1	1	1
$D^{1_3}(g) = D^E(g) = D^2(g) =$	1	$e^{2\pi i/3}$	$e^{-2\pi i/3}$
$D^{2_3}(g) = D^{E^*}(g) = D^3(g) =$	1	$e^{-2\pi i/3}$	$e^{2\pi i/3}$

(2.6.5)

The C_3 example shows many of the properties of general cyclic C_n groups $\{1, r, r^2, \ldots, r^{n-1}\}$. In general there will be n distinct roots to the minimal

equation $r^n = 1$ of C_n. These n roots will be labeled as in (2.6.5) by

$$\varepsilon_{k+1} = e^{i2\pi k/n} \equiv D^{k_n}(r) \qquad (k = 0, 1, 2, \ldots, n-1). \quad (2.6.6a)$$

It is easy to show that each root yields an idempotent projection operator of the form (2.6.3) or in general

$$P^{k_n} = \frac{1}{n}\sum_g D^{k_n^*}(g)\, g = \frac{1}{n}\sum_{m=0}^{n-1} e^{-i2\pi km/n} r^m, \quad (2.6.6b)$$

where the index k_n will be read as k-modulo-n in Section 2.7. One quickly verifies that (2.6.3) and (2.6.6b) satisfy the eigenequation $rP^{k_n} = D^{k_n}(r)P^{k_n}$. The spectral decomposition (2.6.3) has the general form

$$g = \sum_{k=0}^{n-1} D^{k_n}(g)\, P^{k_n}, \quad (2.6.6c)$$

where the sum is over the (n) irreps $D^{k_n}(g)$ of C_n.

The application of the C_3 idempotents proceeds in the same manner as was done before in Sections 2.3 and 2.5. We first construct a representation $\{\mathscr{R}(1), \mathscr{R}(r), \mathscr{R}(r^2)\}$ in the following of the symmetry operators $\{1, r, r^2\}$ from the definition of basic coordinates shown in Figure 2.6.1:

$$\mathscr{R}(1)\begin{pmatrix}\chi_1\\ \chi_2\\ \chi_3\end{pmatrix} = \begin{pmatrix}1&0&0\\0&1&0\\0&0&1\end{pmatrix}\begin{pmatrix}\chi_1\\ \chi_2\\ \chi_3\end{pmatrix} = \begin{pmatrix}\chi_1\\ \chi_2\\ \chi_3\end{pmatrix},$$

$$\mathscr{R}(r)\begin{pmatrix}\chi_1\\ \chi_2\\ \chi_3\end{pmatrix} = \begin{pmatrix}0&0&1\\1&0&0\\0&1&0\end{pmatrix}\begin{pmatrix}\chi_1\\ \chi_2\\ \chi_3\end{pmatrix} = \begin{pmatrix}\chi_3\\ \chi_1\\ \chi_2\end{pmatrix},$$

$$\mathscr{R}(r^2)\begin{pmatrix}\chi_1\\ \chi_2\\ \chi_3\end{pmatrix} = \begin{pmatrix}0&1&0\\0&0&1\\1&0&0\end{pmatrix}\begin{pmatrix}\chi_1\\ \chi_2\\ \chi_3\end{pmatrix} = \begin{pmatrix}\chi_2\\ \chi_3\\ \chi_1\end{pmatrix}. \quad (2.6.7)$$

Then we construct and use the representations $\mathscr{R}(P^\alpha)$ of the idempotents:

$$\mathscr{R}(P^1) = \tfrac{1}{3}\begin{pmatrix}1&1&1\\1&1&1\\1&1&1\end{pmatrix}, \qquad \mathscr{R}(P^2) = \tfrac{1}{3}\begin{pmatrix}1&\varepsilon_2&\varepsilon_3\\ \varepsilon_3&1&\varepsilon_2\\ \varepsilon_2&\varepsilon_3&1\end{pmatrix},$$

$$\mathscr{R}(P^3) = \tfrac{1}{3}\begin{pmatrix}1&\varepsilon_3&\varepsilon_2\\ \varepsilon_2&1&\varepsilon_3\\ \varepsilon_3&\varepsilon_2&1\end{pmatrix}. \quad (2.6.8)$$

From select columns and rows of (P^α), namely, the first of each in this case, we construct a matrix transformation $\mathscr{T}^\dagger$ that does the following: (a) $\mathscr{T}^\dagger$ reduces all $\mathscr{R}(g)$ to a direct sum of irreps. For example, $\mathscr{T}^\dagger\mathscr{R}(r)\mathscr{T}$ is given by

$$\begin{pmatrix} 1/\sqrt{3} & 1/\sqrt{3} & 1/\sqrt{3} \\ 1/\sqrt{3} & e^{+2\pi i/3}/\sqrt{3} & e^{-2\pi i/3}/\sqrt{3} \\ 1/\sqrt{3} & e^{-2\pi i/3}/\sqrt{3} & e^{+2\pi i/3}/\sqrt{3} \end{pmatrix} \begin{pmatrix} 0 & 0 & 1 \\ 1 & 0 & 0 \\ 0 & 1 & 0 \end{pmatrix} \begin{matrix} |e_1\rangle & |e_2\rangle & |e_3\rangle \\ \begin{pmatrix} 1/\sqrt{3} & 1/\sqrt{3} & 1/\sqrt{3} \\ 1/\sqrt{3} & e^{-2\pi i/3}/\sqrt{3} & e^{+2\pi i/3}/\sqrt{3} \\ 1/\sqrt{3} & e^{+2\pi i/3}/\sqrt{3} & e^{-2\pi i/3}/\sqrt{3} \end{pmatrix} \end{matrix} \begin{matrix} |1\rangle \\ |2\rangle \\ |3\rangle \end{matrix}$$

$$= \begin{pmatrix} 1 & 0 & 0 \\ 0 & e^{2\pi i/3} & 0 \\ 0 & 0 & e^{-2\pi i/3} \end{pmatrix} = \begin{pmatrix} D^1(r) & 0 & 0 \\ 0 & D^2(r) & 0 \\ 0 & 0 & D^3(r) \end{pmatrix}. \tag{2.6.9}$$

That is, $\mathscr{R}(g)$ is reduced or diagonalized to a direct sum $(\oplus)$

$$\mathscr{T}^\dagger\mathscr{R}(g)\mathscr{T} = D^1(g) \oplus D^2(g) \oplus D^3(g)$$

of three different irreps. [Compare the foregoing with Eqs. (2.4.8) and (2.4.10).] The $\mathscr{T}^\dagger$ matrix gives the change of basis between "old" $\{|1\rangle, |2\rangle, |3\rangle\}$ and "new" $\{|e_1\rangle, |e_2\rangle, |e_3\rangle\}$ bases. Note that the representation of the latter in terms of the former are given by the columns of $\mathscr{T}$. They are indicated in the upper right-hand side of Eq. (2.6.9).

(b) $\mathscr{T}^\dagger$ diagonalizes the acceleration matrix appearing in Eq. (2.6.1):

$$\mathscr{T}^\dagger \begin{pmatrix} 2a+b & -a & -a \\ -a & 2a+b & -a \\ -a & -a & 2a+b \end{pmatrix} \mathscr{T} = \begin{pmatrix} b & 0 & 0 \\ 0 & 3a+b & 0 \\ 0 & 0 & 3a+b \end{pmatrix}.$$

In other words, the kets $|e_1\rangle$, $|e_2\rangle$, and $|e_3\rangle$ represented by the columns of the $\mathscr{T}$ matrix are eigenvectors of the acceleration operator as well.

This is as it should be if the acceleration operator (**a**) commutes with C_3 symmetry operators. The three projected kets,

$$|e_1\rangle = P^1|1\rangle\sqrt{3}\,, \qquad |e_2\rangle = P^2|1\rangle\sqrt{3}\,, \qquad |e_3\rangle = P^3|1\rangle\sqrt{3}\,,$$

belong to three different irreps as do their companion bras,

$$\langle e_1| = \langle 1|P^1\sqrt{3}\,, \qquad \langle e_2| = \langle 1|P^2\sqrt{3}\,, \qquad \langle e_3| = \langle 1|P^3\sqrt{3}\,.$$

[Here self conjugacy $(P^{\alpha\dagger} = P^\alpha)$ of idempotents obtained from a unitary operator is used (see Appendix C).] Since the idempotents are orthogonal the

matrix $\langle e_\alpha|\mathbf{a}|e_\beta\rangle$ must be diagonal:

$$\langle e_\alpha|\mathbf{a}|e_\beta\rangle = \langle 1|P^\alpha \mathbf{a} P^\beta|1\rangle$$

$$= \langle 1|\mathbf{a}P^\alpha P^\beta|1\rangle = 0, \qquad \text{if } \alpha \neq \beta.$$

No new concepts outside of those given in Sections 2.3–2.5 are involved here, except that you might be surprised that two of the eigenvalues (for modes 2 and 3) are identical. This degeneracy is a direct consequence of that reflection symmetry, which we ignored. We will discuss this at length in Chapter 3, but for now let us examine the form of the eigenvector solutions.

One may take the liberty of combining the complex $|e_2\rangle$ and $|e_3\rangle$ eigenvectors into their real and imaginary parts since they are degenerate:

$$|e_{\mathrm{Re}}\rangle = \frac{|e_2\rangle + |e_3\rangle}{\sqrt{2}} \rightarrow \frac{1}{\sqrt{6}} \begin{pmatrix} 1 & + & 1 \\ e^{-2\pi i/3} & + & e^{2\pi i/3} \\ e^{2\pi i/3} & + & e^{-2\pi i/3} \end{pmatrix}$$

$$= \frac{1}{\sqrt{6}} \begin{pmatrix} 2 \\ 2\cos(2\pi/3) \\ 2\cos(2\pi/3) \end{pmatrix} = \frac{1}{\sqrt{6}} \begin{pmatrix} 2 \\ -1 \\ -1 \end{pmatrix},$$

$$|e_{\mathrm{Im}}\rangle = \frac{|e_2\rangle - |e_3\rangle}{i\sqrt{2}} \rightarrow \frac{-i}{\sqrt{6}} \begin{pmatrix} 1 & - & 1 \\ e^{-2\pi i/3} & - & e^{2\pi i/3} \\ e^{2\pi i/3} & - & e^{-2\pi i/3} \end{pmatrix}$$

$$= \frac{1}{\sqrt{6}} \begin{pmatrix} 0 \\ -2\sin(2\pi/3) \\ 2\sin(2\pi/3) \end{pmatrix} = \frac{1}{\sqrt{2}} \begin{pmatrix} 0 \\ -1 \\ 1 \end{pmatrix}.$$

Because of the frequency degeneracy between modes $|e_2\rangle$ and $|e_3\rangle$ the resulting real combinations are eigenvectors, too, both having eigenfrequency $\sqrt{3a + b}$. Real eigenvectors are easier to picture, as shown in Figure 2.6.2. For eigenvectors with real components, the only relative phases possible are + (in phase) and − (out of phase). Therefore real vectors correspond to so-called STANDING WAVES or modes. Complex vectors allow for arbitrary phases, so the disturbance can appear to be marching from mass to mass. Therefore, complex vectors correspond to MOVING WAVES. One way to visualize moving waves is to draw phasor clocks for each oscillator (see Figure 2.6.2) and image successive time steps. To algebraically determine time behavior of mode $|e_2\rangle$ one needs the quantity $\mathrm{Re}[e^{-i\omega_2 t}|e_2\rangle]$, where

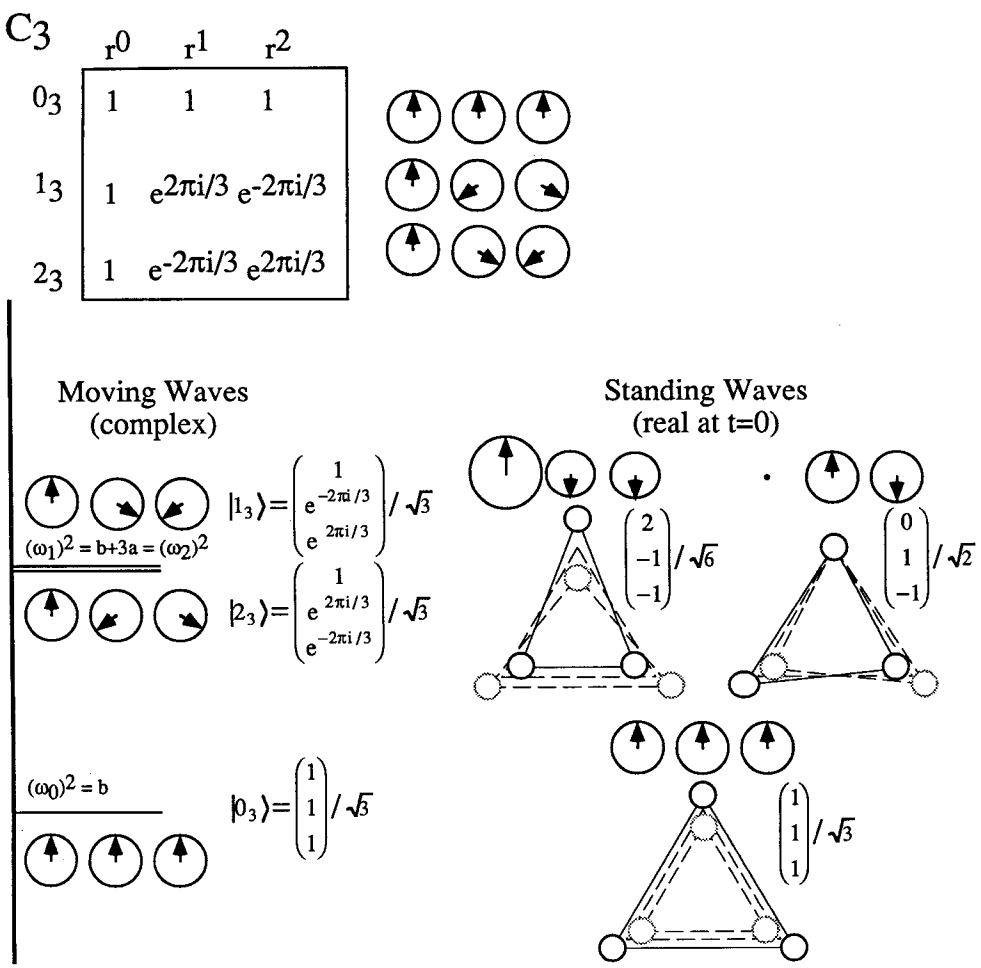

Figure 2.6.2 Normal modes or eigenwaves and spectrum of the C_3 symmetric coupled pendulums.

$\omega_2 = \omega_3 = \sqrt{3a + b}$ is the eigenfrequency. This is represented by the following:

$$\frac{1}{\sqrt{3}}\begin{pmatrix}\cos\omega_2 t\\ \cos(-2\pi/3-\omega_2 t)\\ \cos(2\pi/3-\omega_2 t)\end{pmatrix} = \frac{\cos\omega_2 t}{2\sqrt{3}}\begin{pmatrix}2\\-1\\-1\end{pmatrix} + \frac{\sin\omega_2 t}{2}\begin{pmatrix}0\\-1\\1\end{pmatrix}.$$

This may be written as

$$\mathrm{Re}\left[e^{-i\omega_2 t}|e_2\rangle\right] = (\cos\omega_2 t|e_{\mathrm{Re}}\rangle + \sin\omega_2 t|e_{\mathrm{Im}}\rangle)/\sqrt{2}\,.$$

This represents a clockwise rotation of the vibrational wave with angular eigenfrequency $\omega_2 = \sqrt{3a + b}$. Similarly the motion of the $|e_3\rangle$ mode is given by

$$\mathrm{Re}\left[e^{-i\omega_3 t}|e_3\rangle\right] = (\cos\omega_3 t|e_{\mathrm{Re}}\rangle - \sin\omega_3 t|e_{\mathrm{Im}}\rangle)/\sqrt{2},$$

which is a *counter*clockwise moving wave of the same frequency.

The low-frequency ($\omega_1 = \sqrt{b}$) modes $|e_1\rangle$ has its time behavior represented by $\mathrm{Re}[e^{-i\omega_1 t}|e_1\rangle]$ or

$$\mathrm{Re}\begin{pmatrix} e^{-i\omega_1 t} \\ e^{-i\omega_1 t} \\ e^{-i\omega_1 t} \end{pmatrix} \Big/ \sqrt{3} = \frac{\cos\omega_1 t}{\sqrt{3}} \begin{pmatrix} 1 \\ 1 \\ 1 \end{pmatrix}.$$

This is a standing wave like $|e_{\mathrm{Re}}\rangle$ and $|e_{\mathrm{Im}}\rangle$. In standing waves no energy is being transferred from one pendulum to the other, and there is no net circulation of energy or momentum around the ring. However, the *combination* of two standing waves will cause very obvious interpendulum motion. For example, the combination of $|e_1\rangle$ and $\sqrt{2}\,|e_{\mathrm{Re}}\rangle$ moves according to $\mathrm{Re}[e^{-i\omega_1 t}|e_1\rangle + e^{-i\omega_2 t}\sqrt{2}\,|e_{\mathrm{Re}}\rangle]$, which is represented by

$$\mathrm{Re}\begin{pmatrix} e^{-i\omega_1 t} + 2e^{-i\omega_2 t} \\ e^{-i\omega_1 t} - e^{-i\omega_2 t} \\ e^{-i\omega_1 t} - e^{-i\omega_2 t} \end{pmatrix} \Big/ \sqrt{3} = \begin{pmatrix} \cos\omega_1 t + 2\cos\omega_2 t \\ \cos\omega_1 t - \cos\omega_2 t \\ \cos\omega_1 t - \cos\omega_2 t \end{pmatrix} \Big/ \sqrt{3}.$$

Here the time behavior is characterized by a motion or "beating" which goes back and forth with a frequency equal to the *difference* between ω_1 and ω_2. It will be analogous to the beat trading shown in Figure 2.3.2.

2.7 MORE EXAMPLES WITH C_n SYMMETRY: ONE-DIMENSIONAL LATTICES

The graph in Figure 2.2.2 shows that there is always at least one Abelian group of any order n. This "fundamental" symmetry group is the cyclic group $C_n \equiv \{1, r, r^2, r^3, \ldots, r^{n-1}\}$. Let us now use symmetry analysis to treat examples of C_n symmetry for arbitrary n.

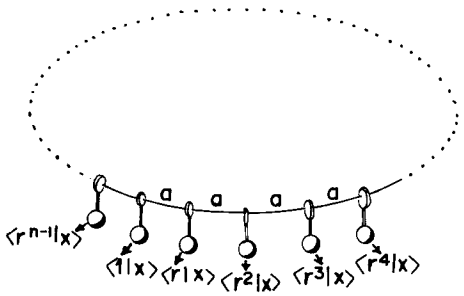

Figure 2.7.1 C_n symmetric coupled pendulums.

The first example shown in Figure 2.7.1 is a ring of n identical pendulums coupled end to end. Suppose its equation of motion is

$$
\begin{aligned}
-\begin{pmatrix} \langle 1|\ddot{x}\rangle \\ \langle r|\ddot{x}\rangle \\ \langle r^2|\ddot{x}\rangle \\ \vdots \\ \langle r^{n-1}|\ddot{x}\rangle \end{pmatrix}
&= \begin{pmatrix} \langle 1|\mathbf{a}|1\rangle & \langle 1|\mathbf{a}|r\rangle & \cdots & \langle 1|\mathbf{a}|r^{n-1}\rangle \\ \langle r|\mathbf{a}|1\rangle & \langle r|\mathbf{a}|r\rangle & \cdots & \cdot \\ \langle r^2|\mathbf{a}|1\rangle & \langle r^2|\mathbf{a}|r^2\rangle & \cdots & \cdot \\ \vdots & & & \\ \langle r^{n-1}|\mathbf{a}|1\rangle & \cdot & \cdot & \langle r^{n-1}|\mathbf{a}|r^{n-1}\rangle \end{pmatrix}
\begin{pmatrix} \langle 1|x\rangle \\ \langle r|x\rangle \\ \langle r^2|x\rangle \\ \vdots \\ \langle r^{n-1}|x\rangle \end{pmatrix} \\
&= \begin{pmatrix} 2a+b & -a & 0 & \cdots & 0 & -a \\ -a & 2a+b & -a & \cdot & & 0 \\ 0 & -a & 2a+b & & & 0 \\ \vdots & & & & & \vdots \\ -a & 0 & 0 & & & 2a+b \end{pmatrix}
\begin{pmatrix} \langle 1|x\rangle \\ \langle r|x\rangle \\ \langle r^2|x\rangle \\ \\ \langle r^{n-1}|x\rangle \end{pmatrix},
\end{aligned}
\tag{2.7.1}
$$

where the constants a and b in the acceleration matrix are defined as they were for the preceding C_3 example. Also the base states $\{|1\rangle, |r\rangle, |r^2\rangle, \ldots\}$ and coordinates $\{\langle 1|x\rangle, \langle r|x\rangle, \langle r^2|x\rangle, \ldots\}$ are labeled by C_n operators ($|r\rangle = r|1\rangle$, etc.), as indicated in the figure.

All symmetry operators are products of the rotation r by $(2\pi/n)$ radians. This operator satisfies a minimal equation ($r^n = \mathbf{1}$) or ($r^n - \mathbf{1} = 0$). The eigenvalues or roots of this equation are the n roots of unity (e^{ik_n}), where ($k_n = 2\pi k/n$). These complex numbers are therefore the irreps of C_n:

$$D^{k_n}(r) = e^{ik_n} \qquad (k_n \equiv 2\pi k/n, \qquad k = 0, 1, 2, \ldots, n-1). \tag{2.7.2}$$

One may visualize these numbers by drawing them as vectors in the complex plane. This is done for $n = 1$–6 in Figure 2.7.2. Note that the D^{k_n} and $D^{-k_n} = (D^{k_n})^*$ are usually complex-conjugate pairs. Only $k = 0$ and $k = n/2$, for even n, give real D^{k_n}. An irrep or character table is drawn using phasors to represent each $D^{k_n}(r^p)$ irrep of $C_1, C_2, \ldots,$ and C_n in Figure 2.7.2.

For each irrep D^{k_n} there is an eigenvector $|k_n\rangle$ of the acceleration operator a which we may derive by using projection operator P^{k_n} [recall (2.6.6b)]:

$$|k_n\rangle \equiv P^{k_n}|1\rangle\sqrt{n}$$

$$= \sum_{g=1,r,\ldots} D^{k_n^*}(g)|g\rangle/\sqrt{n} \rightarrow \begin{pmatrix} 1 \\ \exp(-ik_n) \\ \exp 2(-ik_n) \\ \vdots \\ \exp(n-1)(-ik_n) \end{pmatrix} \Big/ \sqrt{n}\,. \quad (2.7.3)$$

By substituting this representation of $|k_n\rangle$ into the equation (2.7.1) of motion, one obtains the eigenvalue of operator $\langle \mathbf{a} \rangle$:

$$\mathbf{a}|k_n\rangle = [2a(1 - \cos k_n) + b]|k_n\rangle = \omega^2(k_n)|k_n\rangle. \quad (2.7.4)$$

This is the square $[\omega^2(k_n)]$ of the resonant frequency. Note that the eigenvalue for $|k_n\rangle$ is the same for its complex conjugate partner $|-k_n\rangle$. Therefore different but equally valid eigenvectors can be made by combining each complex pair to form real cosine and sine standing-wave states $|c_n^k\rangle$ and $|s_n^k\rangle$:

$$|c_n^k\rangle \equiv \frac{|k_n\rangle + |k_{-n}\rangle}{\sqrt{2}} \rightarrow \begin{pmatrix} 1 \\ \cos k_n \\ \cos 2k_n \\ \vdots \\ \cos(n-1)k_n \end{pmatrix} \sqrt{2/n}\,, \quad (2.7.5a)$$

$$|s_n^k\rangle \equiv \frac{-|k_n\rangle + |k_{-n}\rangle}{i\sqrt{2}} \rightarrow \begin{pmatrix} 0 \\ \sin k_n \\ \sin 2k_n \\ \vdots \\ \sin(n-1)k_n \end{pmatrix} \sqrt{2/n}\,. \quad (2.7.5b)$$

The real cosine or sine states may be easier to picture. We see in Figure 2.7.3 that the $|c_n^k\rangle(|s_n^k\rangle)$ state is obtained if a cosine wave (sine wave) with exactly k crests is drawn to fit in the interval occupied by n connecting springs. The sine or cosine wave amplitudes oscillate with frequency $\omega(k_n)$, but the crests and nodes are fixed in standing-wave solutions. To envision the

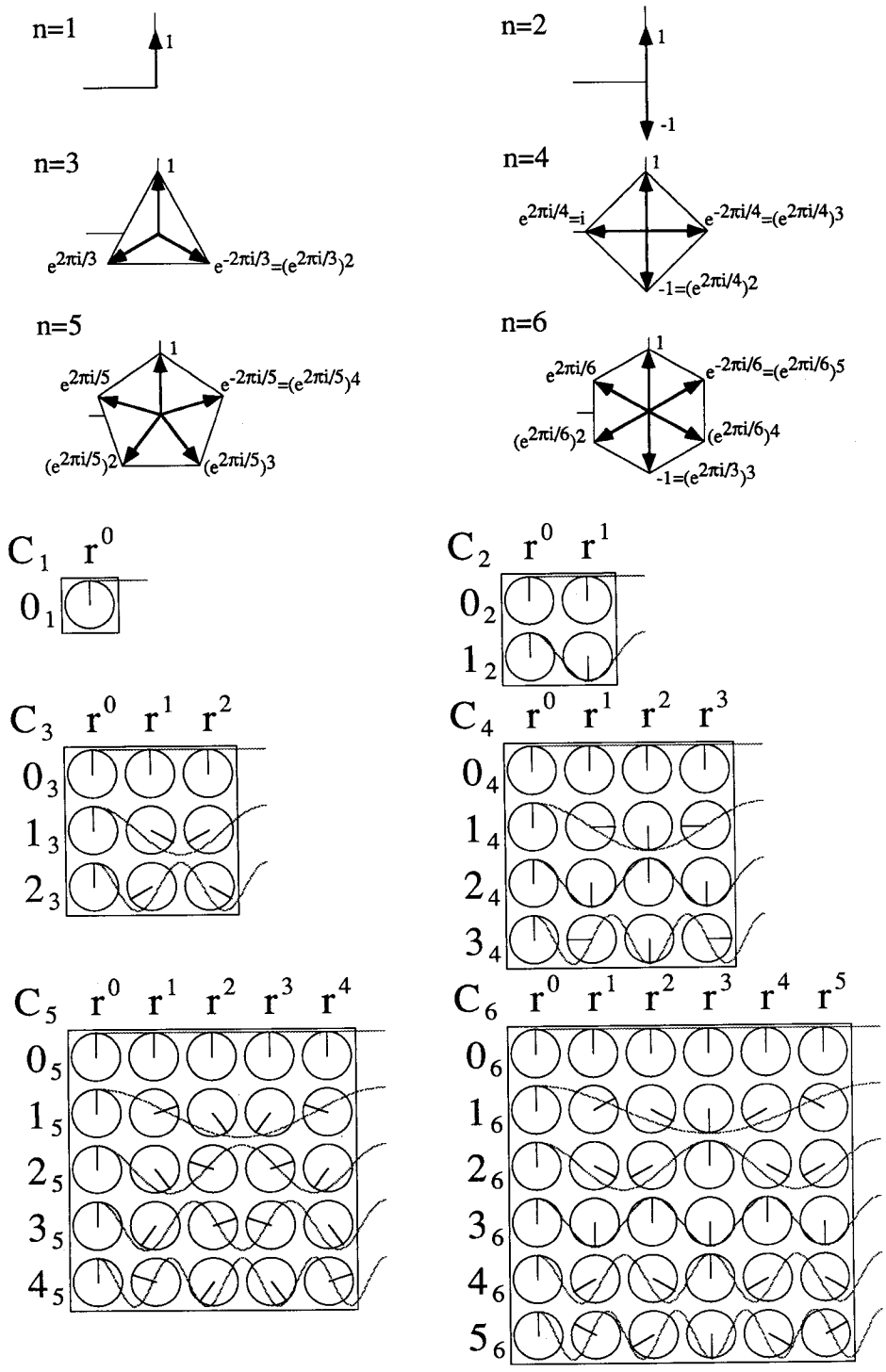

Figure 2.7.2 Representing C_n irreps by complex roots of unity ($n = 2, 3, \ldots, 6$).

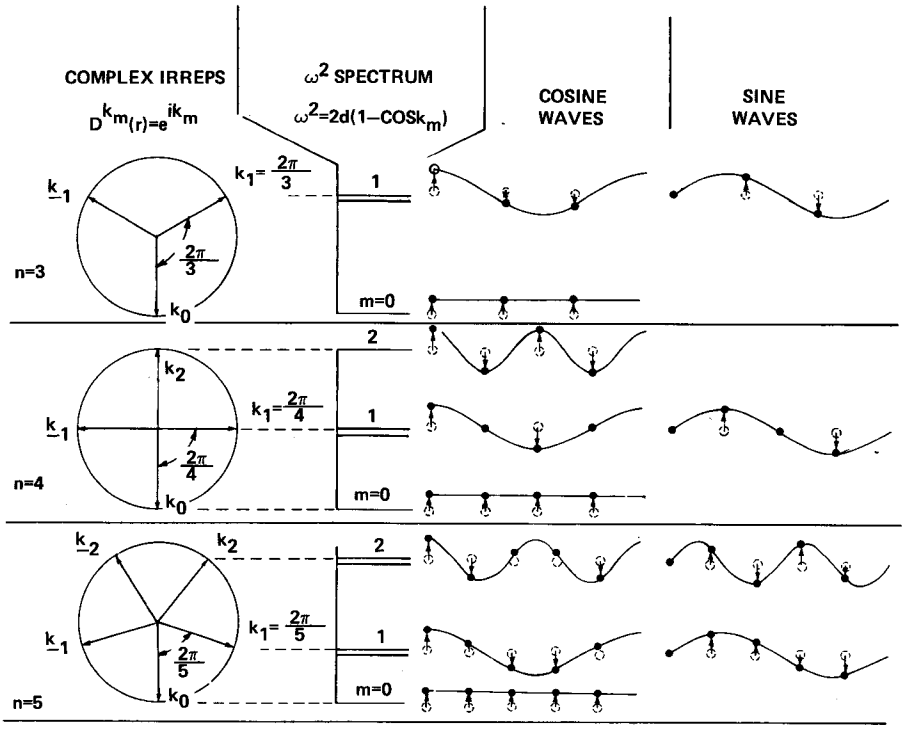

Figure 2.7.3 Standing eigenwaves and frequency spectra for C_3, C_4, C_5 symmetric coupled pendulums.

moving-wave state $|k_n\rangle$ imagine the amplitude of the cosine wave is fixed while it moves rigidly around the ring with velocity $\omega(k_n)/k_n$. (Compare Figure 2.7.3 for $n = 3$ with the C_3 solution in the preceding section.)

There is also an easy way to picture the $\omega^2(k_n)$ eigenvalue spectrum. The term $(\cos k_n)$ in Eq. (2.7.4) is the projection of kth vertex of a regular n-polygon as shown in Figure 2.7.3. (The constant term b is set equal to zero in the figure.)

As n becomes larger, the allowed points in the function $\omega^2(k_n)$ become closer together, as seen in the $n = 24$ example in Figure 2.7.4. As $n \to \infty$, the continuous band spectrum of the one-dimensional lattice is approached. Setting $b = 0$, one obtains the standard formula for angular frequency ω in terms of wave number k_n. This formula is called a lattice DISPERSION RELATION:

$$\omega(k_n) = \sqrt{2a(1 - \cos k_n)} = 2\sqrt{a}\,\sin\left(\frac{k_n}{2}\right)$$

$$= \sqrt{a}\,k_n - \frac{\sqrt{a}\,(k_n)^3}{24} + \cdots . \quad (2.7.6)$$

For small k_n this formula gives the phase velocity $c \equiv \omega/k_n = \sqrt{a}$ for long

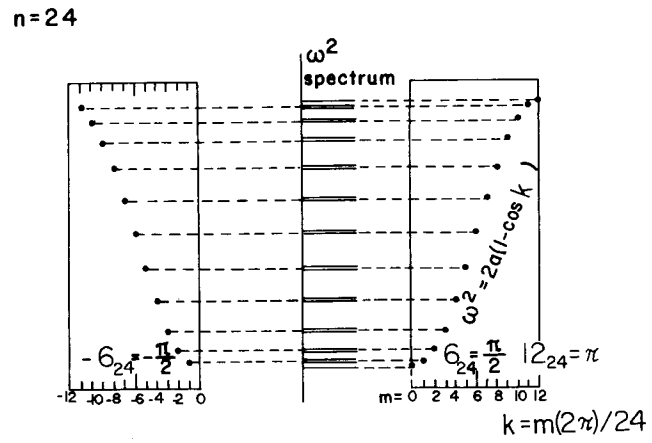

Figure 2.7.4 ω^2 spectrum of C_{24} symmetric coupled pendulums.

acoustical waves. (Here the unit of distance is the interval occupied by one connecting spring.)

Now consider waves with large k_n that lie outside the range $|k| \leq n/2$. For example, $|-3_5\rangle$ or $|7_5\rangle$ are wave states which lie outside this range for $n = 5$. However, from Figure 2.7.5 we see that $|-3_5\rangle$ and $|7_5\rangle$ waves are indistinguishable from the $|2_5\rangle$ wave as far as the five oscillating pendulums are concerned. They are also indistinguishable as far as C_n irreps are concerned. The n integers k in the range $-n/2 < k < n/2$ $[-(n-1)/2 < k < (n-1)/2]$ for n even (n odd) correspond in a one-to-one fashion with the n irreps of C_n. (The corresponding range of k_n is called the FIRST BRILLOUIN ZONE in the theory of lattice waves.) Any of the $(k \pm n)_n, (k \pm 2n)_n, \ldots$ outside this range will just duplicate a C_n irrep for a k_n which is inside:

$$D^{(k \pm Nn)_n} = e^{2i\pi(k \pm Nn)/n} = e^{2i\pi(k/n \pm N)} = e^{\pm i\pi k/n} = e^{ik_n} = D^{k_n}. \quad (2.7.7)$$

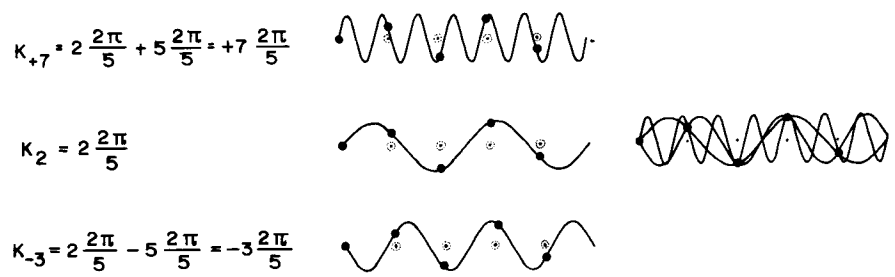

Figure 2.7.5 Higher wave-number solutions for C_5 symmetric coupled pendulums. The waves shown have all give the same motion of the pendulums.

A C_n system is like an n-nary computer register: It can only count to $n-1$ and then start over with zero. The register takes a number $m = k \pm Nn$ and reads out only m-modulo-$n = k$. A wave state $|m_n\rangle$ will have m wavelengths in the 2π interval of the full circle, but the n-pendulum system cannot distinguish this state from the state $|k_n\rangle$ with only k wavelengths where $k = m$-modulo-$n = k$-mod-n.

A. Symmetry Breaking

A physical system could tell the difference between a k_n wave and a $(k \pm n)_n$ wave if it has some kind of "detector" such as another mass between each lattice point. As an example consider the system in Figure 2.7.6. This is a copy of the one in Figure 2.7.1, except every even spring is weakened ($\underline{a} < a$) and every odd spring is made stiffer ($\bar{a} > a$). Also let there be $n = 24$ pendulums. The acceleration matrix $\langle \mathbf{a} \rangle$ now takes the following form:

$$\begin{pmatrix} \langle 1|\mathbf{a}|1\rangle & \langle 1|\mathbf{a}|r\rangle & \langle 1|\mathbf{a}|r^2\rangle & \cdots & \langle 1|\mathbf{a}|r^{23}\rangle \\ \langle r|\mathbf{a}|1\rangle & \langle r|\mathbf{a}|r\rangle & \langle r|\mathbf{a}|r^2\rangle & \cdots & \langle r|\mathbf{a}|r^{23}\rangle \\ \vdots & \vdots & \vdots & & \vdots \end{pmatrix}$$

$$= \begin{pmatrix} \bar{a} + \underline{a} + b & -\underline{a} & 0 & \cdots & -\bar{a} \\ -\underline{a} & \bar{a} + \underline{a} + b & -\bar{a} & \cdots & 0 \\ \vdots & \vdots & \vdots & & \vdots \end{pmatrix}. \quad (2.7.8)$$

Changing the springs "breaks" the symmetry from C_{24} down to C_{12}. Now only the operations $\{1, r^2, r^4, \ldots\} = C_{12}$ will commute with a if $\bar{a} \neq \underline{a}$. The operators $\{r, r^3, \ldots\}$ are no longer symmetry operations. As explained in the preceding section (recall Figure 2.7.1) the irreps of C_{12} are labeled by 12 wave numbers $6_{12}, 5_{12}, 4_{12}, \ldots, -4_{12}, -5_{12}$, which lie in the first Brillouin zone. However, now some waves outside this zone are physically very different. For example, $|-7_{12}\rangle$ is very different from $|5_{12}\rangle$ even though they both

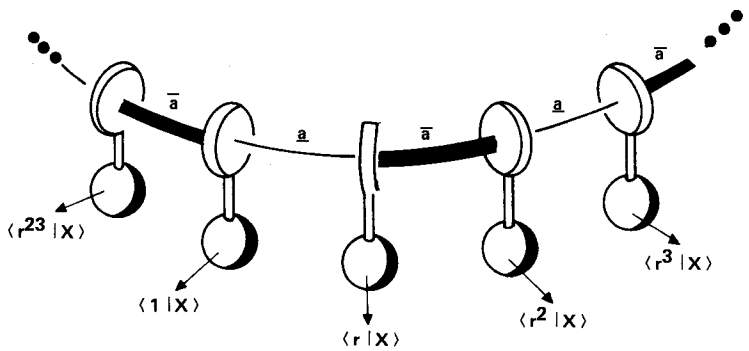

Figure 2.7.6 C_{12} symmetry breaking of C_{24} symmetric coupled pendulums.

belong to irrep $D^{5_{12}}$. The same goes for $|-8_{12}\rangle$ and $|4_{12}\rangle$, which belong to $D^{4_{12}}$, and so on. Most irreps of C_{12} appear twice in the representation of the basis. So once again (recall Section 2.5) we encounter a situation where symmetry theory does not give the complete solution immediately. We still must diagonalize a 2×2 matrix for the pairs of states which share a common irrep $D^{k_{12}}$. The resulting complete solution indicates a splitting of the C_{24} band into two separated bands as shown in Figure 2.7.7. We derive this now.

We first obtain the two independent states produced by the projector P^{k_n} of C_{12} acting first on $|1\rangle$ then on $|r\rangle$.

$$|k_n\rangle = P^{k_n}|1\rangle\sqrt{12} = (|1\rangle + e^{-ik_n}|r^2\rangle + e^{-2ik_n}|r^4\rangle + \cdots)/\sqrt{12},$$
$$|k'_n\rangle = P^{k_n}|r\rangle\sqrt{12} = (|r\rangle + e^{-ik_n}|r^3\rangle + e^{-2ik_n}|r^5\rangle + \cdots)/\sqrt{12}.$$

Then the representation of $\mathbf{a}$ in the $\{|k_n\rangle, |k_n\rangle'\}$ basis is found, using Hermiticity ($P^{k_n\dagger} = P^{k_n}$), symmetry ($P^{k_n}\mathbf{a} = \mathbf{a}P^{k_n}$), idempotency ($P^{k_n}P^{k_n} = P^{k_n}$) of P^{k_n}, and the acceleration matrix in (2.7.8):

$$\begin{aligned}\langle k_n|\mathbf{a}|k_n\rangle &= \langle 1|P^{k_n}\mathbf{a}P^{k_n}|1\rangle \cdot 12 = \langle 1|\mathbf{a}P^{k_n}|1\rangle \cdot 12 \\ &= \langle 1|\mathbf{a}|1\rangle + e^{-ik_n}\langle 1|\mathbf{a}|r^2\rangle + \cdots \\ &= \underline{a} + \bar{a} + 0 + \cdots.\end{aligned}$$

The other components are found in the same way:

$$\begin{aligned}\langle k'_n|\mathbf{a}|k_n\rangle &= \langle r|\mathbf{a}|1\rangle + e^{-ik_n}\langle r|\mathbf{a}|r^2\rangle + \cdots \\ &= -\underline{a} - e^{-ik_n}\bar{a}, \\ \langle k_n|\mathbf{a}|k'_n\rangle &= -\underline{a} - e^{ik_n}\bar{a}, \\ \langle k'_n|\mathbf{a}|k'_n\rangle &= \underline{a} + \bar{a}.\end{aligned}$$

The resulting (2×2) matrix for a given k_n is

$$\langle \mathbf{a}\rangle^{k_n} = \begin{pmatrix} \bar{a} + \underline{a} & -(\bar{a}e^{ik_n} + \underline{a}) \\ -(\bar{a}e^{-ik_n} + \underline{a}) & \bar{a} + \underline{a} \end{pmatrix} \begin{matrix} |k_n\rangle \\ |k_n\rangle' \end{matrix}. \tag{2.7.9}$$

From this the eigenvalues are easily found by a secular equation solution:

$$\omega^2 = \bar{a} + \underline{a} \pm \left(\bar{a}^2 + 2\bar{a}\underline{a}\cos k_n + \underline{a}^2\right)^{1/2}. \tag{2.7.10}$$

These eigenvalues are plotted as black dots in Figure 2.7.7(a) for $\bar{a} = 3a/2$ and $\underline{a} = a/2$ and are connected with dotted lines to the circles which represent the C_{24} symmetry case where $\bar{a} = a = \underline{a}$. When comparing the $n = 24$ case (Figure 2.7.2) with the $n = 12$ case, it must be remembered that we define $k_n = k(2\pi/n)$.

The most striking effect of the breaking of symmetry down to C_{12} is the splitting of $\{|6\rangle, |-6\rangle\}$ degeneracy in Figure 2.7.7(b). With C_{24} symmetry

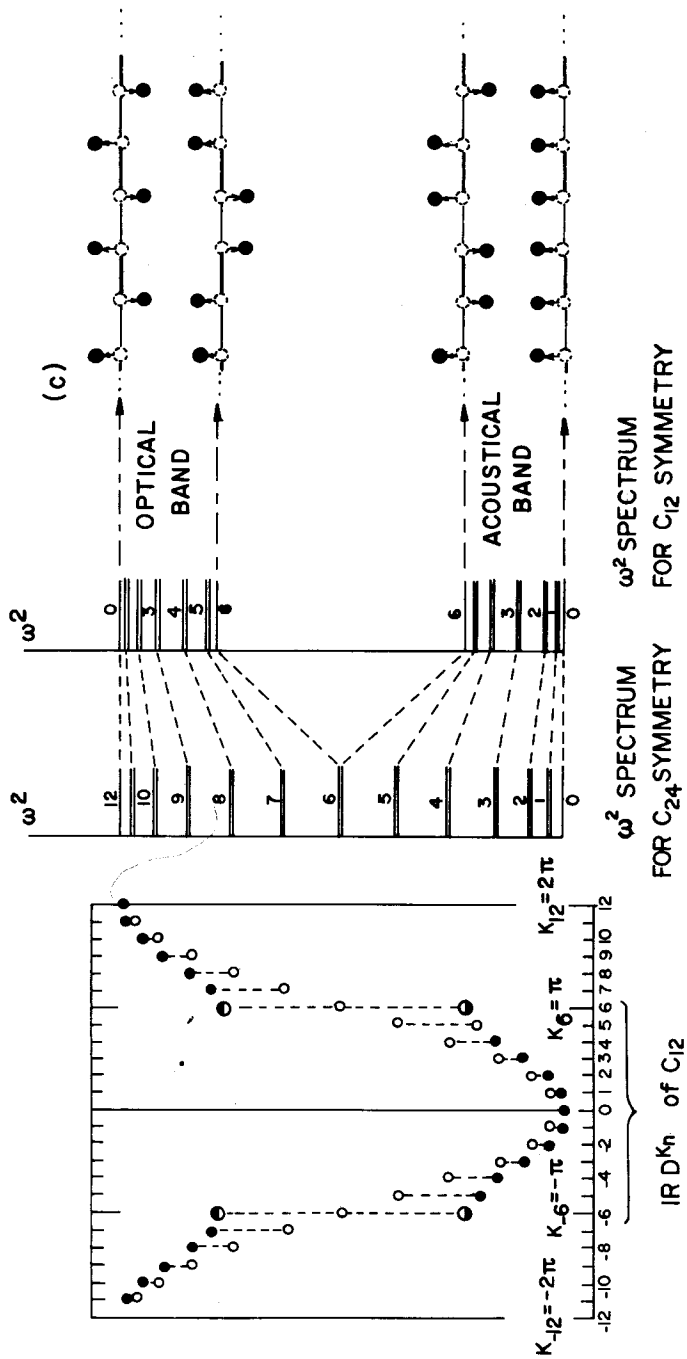

Figure 2.7.7 Band splitting due to C_{24}–C_{12} symmetry breaking.

still in effect these two wave states were degenerate. However, they belong to the same irrep $D^{6_{12}}$ of C_{12}. An acceleration matrix having only C_{12} may mix them. Indeed, equal combinations of them are needed to diagonalize the matrix

$$\langle \mathbf{a} \rangle^{6_{12}} = \begin{pmatrix} \bar{a} + \underline{a} & \bar{a} - \underline{a} \\ \bar{a} - \underline{a} & \bar{a} + \underline{a} \end{pmatrix} \begin{matrix} |6_{12}\rangle \\ |-6_{12}\rangle \end{matrix}. \tag{2.7.11a}$$

The correct combinations are the sine and cosine standing-wave states:

$$\begin{aligned} |c^6_{12}\rangle &= (|6_{12}\rangle + |-6_{12}\rangle)/\sqrt{2} \qquad (\text{eigenvalue} = 2\bar{a}), \\ |s^6_{12}\rangle &= -i(|6_{12}\rangle - |-6_{12}\rangle)/\sqrt{2} \qquad (\text{eigenvalue} = 2\underline{a}). \end{aligned} \tag{2.7.11b}$$

So if $\bar{a} > \underline{a}$ then ($k = 6$) eigenstates *must* be standing waves. This is because the standing wave which tends to twist each stiff ($\bar{a}$) spring [see Figure (2.7.7(c)] necessarily has a higher frequency than the one which tends to twist each soft ($\underline{a}$) spring. So the frequency of these modes depends on the position of the wave nodes. Note that the other states which were moving waves under C_{24} symmetry remain so under C_{12} (see Problem 2.7.3). Their frequencies are shifted in Figure 2.7.7(b) but the degeneracies are not split. The frequency of these modes does not depend on the positions of wave nodes.

B. Galloping Waves

Elementary accounts of wave mechanics are often devoted almost exclusively to either pure moving waves or else pure standing waves. In fact, there exists a doubly infinite continuum of different types of monochromatic waves which lie between these two extreme types. The general monochromatic (single-frequency) wave function has the form

$$\psi(x,t) = (Ie^{ikx} + Re^{-ikx})e^{-i\omega t}, \tag{2.7.12}$$

where the (generally complex) amplitudes for the incident (from the left) and the reflected (from the right) are I and R, respectively. If one of the amplitudes is zero, then x represents a purely moving wave, and if their magnitudes are equal ($|I| = |R|$) then it is a pure standing wave.

The waves which result for arbitrary I and R will be called GALLOPING waves here because of a peculiar motion which they exhibit. A quantity known as the STANDING-WAVE RATIO given by the definition

$$\text{SWR} = \Delta = (I - R)/(I + R). \tag{2.7.13}$$

serves as a measure of properties of the general galloping wave.

Two examples of the galloping-wave motion are shown in Figures 2.7.8(a) and 2.7.8(b) for SWR = $\frac{1}{3}$ and SWR = $\frac{1}{19}$. The upper portion of each figure contains superimposed plots or snapshots of the real part of the wave function at 10 equally spaced instants during one period. The lower portion of each figure shows over 20 instants for the same wave plotted in a space-time (x, ct) frame. The latter should be viewed as three-dimensional perspective plots with the third dimension representing wave amplitude emerging obliquely from the page.

You should notice in the upper portion of each figure that the waves all are constrained to slide through a fixed envelope given by the magnitude of

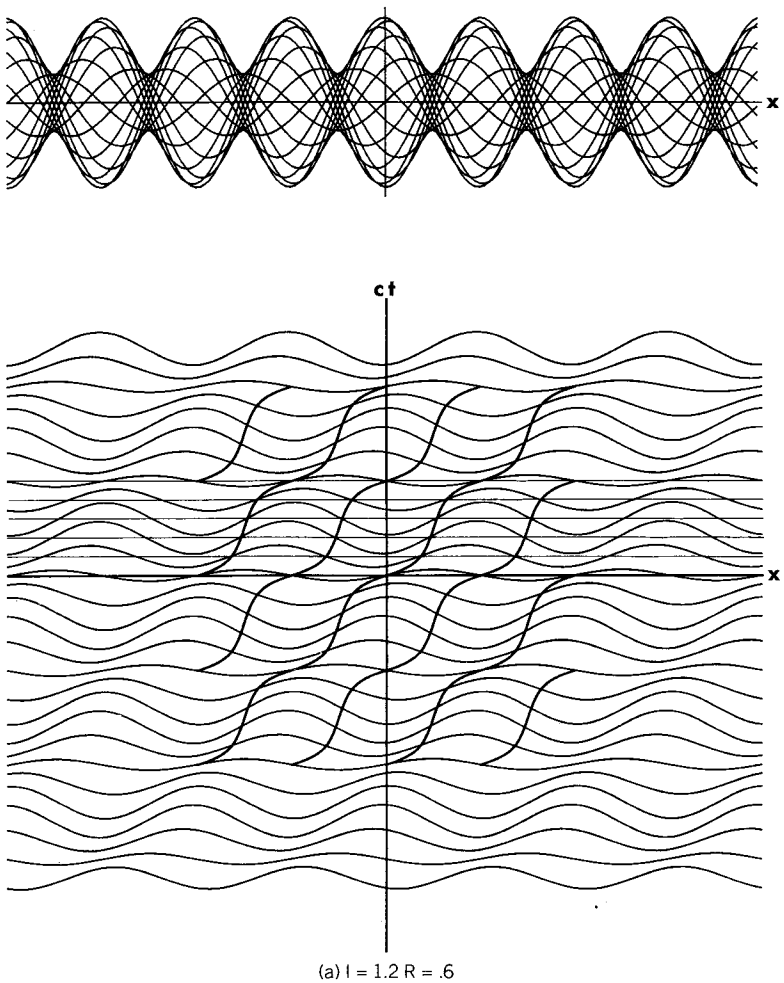

Figure 2.7.8 Space-time trajectories of the zero points of a galloping wave for two values of the standing wave ratio: (a) SWR = $\Delta = \frac{1}{3}$, (b) SWR = $\Delta = \frac{1}{19}$. Wave forms for equal space-time intervals are superimposed at the top of each figure.

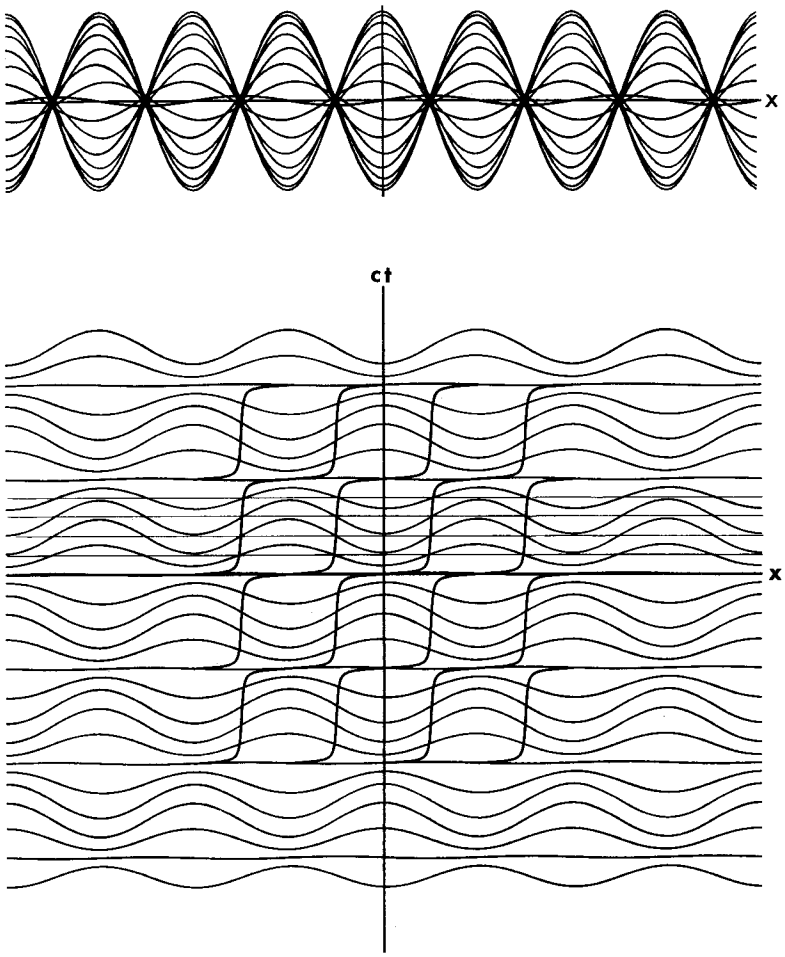

(b) I = 1 R = .9

Figure 2.7.8 (*Continued*).

the wave function (2.7.12), which is

$$|\psi(x)| = [\psi^*\psi]^{1/2} = \left[|I|^2 + |R|^2 + 2|I|\,|R|\cos(2kx)\right]^{1/2}, \quad (2.7.14)$$

where I and R are here chosen to be real. The SWR is a ratio of the maximum value of $|\psi(x)|$ to its minimum value.

It is interesting to see what the wave does when it shrinks from its maximum value and slides through the minima in the $|\psi(x)|$ envelope. It appears to speed up through the minima then slow down as though it were catching its breath while it has maximum amplitude. You can see oscillation

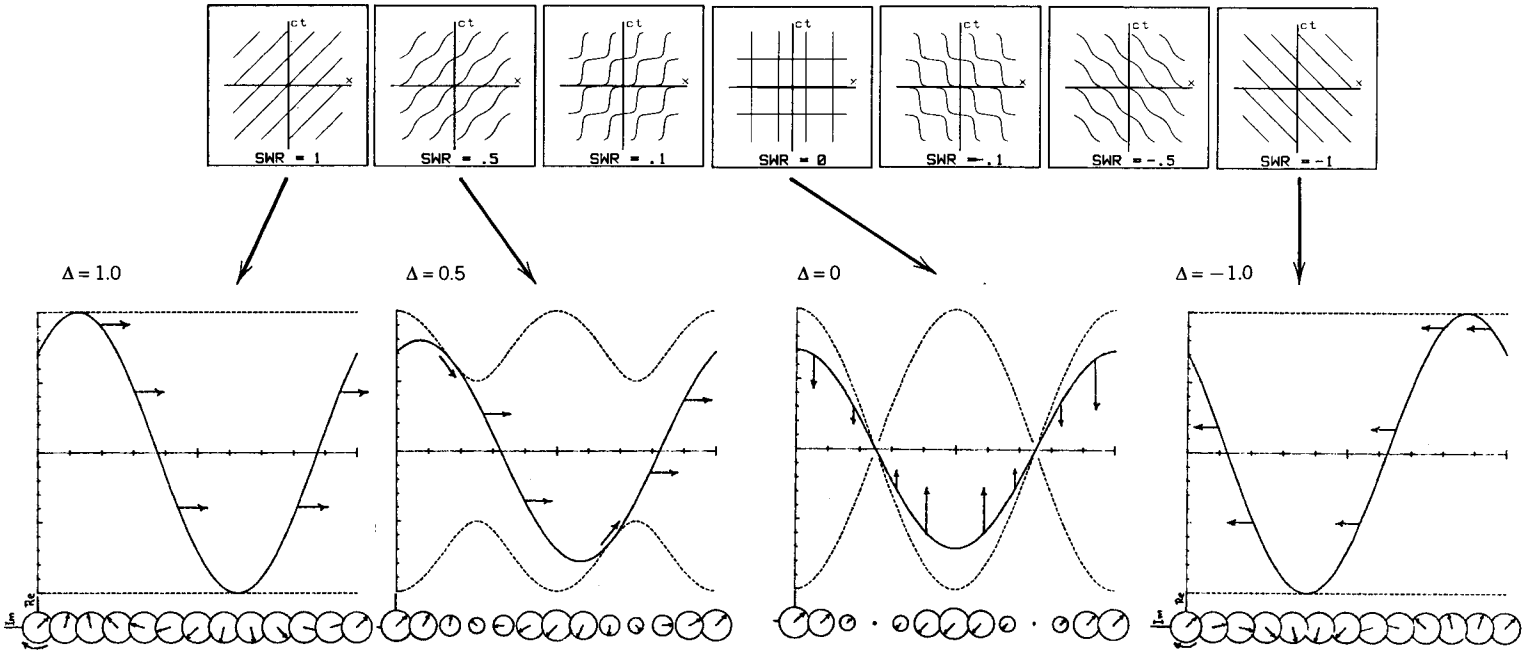

Figure 2.7.9 Varying types of monochromatic waves.

of the phase velocity defined by the space-time trajectories of the zeros in the main figures, and this provides a measure of the galloping. As the SWR deviates more from unity the galloping becomes more extreme. This is seen by comparing the zero-point motion in Figure 2.7.8(a) with those in Figure 2.7.8(b). If the latter represented a light wave then the phase velocity ranges from $c/19$ to $19c$ and back again twice in one period! You should show that, in general, the phase velocity ranges between c(SWR) and $c/$(SWR) (Problem 2.7.2).

A set of zero trajectory plots are drawn for a range of SWR values between 1 and -1 in Figure 2.7.9. Below four of the drawings are shown representative wave plots and phasor diagrams. If you are interested in working with the dynamics of waves in optics, quantum theory, or other areas of physics it probably would not hurt to familiarize yourself with these elementary pictures. Also, they provide some interesting relativistic effects if one considers the effects of Doppler shifting the R wave up and the I-wave component down in frequency.

C. Comparison with Fourier Analysis

The analysis of any system in terms of waves of varying frequency and wavelength is generally called FOURIER ANALYSIS. We have seen that representation theory of C_n is essentially Fourier analysis. A complete set of waves which one associates with irreps of C_n is used to describe a multitude of oscillator properties.

Later we shall be interested in waves of many different types traveling through more complicated spaces and topologies. It will be possible to describe these with irreps of more complicated symmetries than C_n. Ordinary Fourier analysis will not be as much help then, but it is still useful to think of representation theory of any symmetry as a generalized Fourier analysis.

2.8 OTHER TYPES OF ABELIAN SYMMETRY

Consider the example in Figure 2.8.1 of a mechanical system. Let the classical equation of motion be given by the following:

$$\begin{pmatrix} \langle 1|\ddot{x}\rangle \\ \langle 2|\ddot{x}\rangle \\ \langle 3|\ddot{x}\rangle \\ \langle 4|\ddot{x}\rangle \end{pmatrix} = \begin{pmatrix} A & a & b & c \\ a & A & c & b \\ b & c & A & a \\ c & b & a & A \end{pmatrix} \begin{pmatrix} \langle 1|x\rangle \\ \langle 2|x\rangle \\ \langle 3|x\rangle \\ \langle 4|x\rangle \end{pmatrix}. \tag{2.8.1a}$$

The components in the acceleration matrix depend upon the spring constants $\{k_a, k_b, k_c\}$ and geometry according to the theory outlined in Chapter 1

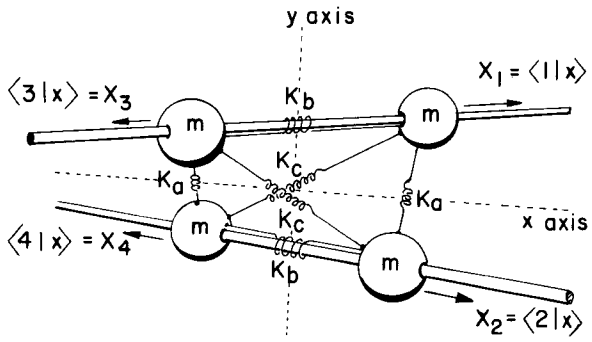

Figure 2.8.1 D_2 symmetric coupled oscillators.

(Section 1.4.B):

$$\begin{aligned} A &= -\left(k_a \cos^2(a,b) + k_b + k_c \cos^2(b,c)\right)/m, \\ a &= -k_a \cos^2(a,b)/m, \\ b &= -k_b/m, \\ c &= -k_c \cos^2(b,c)/m. \end{aligned} \tag{2.8.1b}$$

For small vibrations these components may be assumed constant.

The physical symmetry of this contraption turns out to be the same as that of the fan blade shown in Figure 2.1.1. This symmetry is called D_2 in a notation of crystallographers, which stands for "dihedral of two intersecting planes." The group D_2 is composed of 180° rotations around each of three orthogonal axes x, y, and z. The D_2 multiplication table is given by Eq. (2.1.3).

There can be no mistaking the group D_2 for the other group of order 4 (the chart in Figure 2.2.2 indicates two groups of order 4 exist), which is the cyclic group C_4. All the squares (R^2) of D_2 elements R are equal to the identity, while C_4 has elements corresponding to 90° rotations and for which the squares are not the identity.

Strictly speaking, the only way to be sure that D_2 is a physical symmetry of the model in Figure 2.8.1 is to test its representation in the assumed basis. Equations (2.8.2a) and (2.8.2b) define this representation, and you can check that it does indeed commute with the acceleration matrix. The abstract definitions obtained by inspecting Figure 2.8.1 are as follows:

$$\begin{aligned} &\mathbf{1}|1\rangle = |1\rangle, \quad R_x|1\rangle = |2\rangle, \quad R_y|1\rangle = |3\rangle, \quad R_z|1\rangle = |4\rangle, \\ &\mathbf{1}|2\rangle = |2\rangle, \quad R_x|2\rangle = |1\rangle, \quad R_y|2\rangle = |4\rangle, \quad R_z|2\rangle = |3\rangle, \\ &\mathbf{1}|3\rangle = |3\rangle, \quad R_x|3\rangle = |4\rangle, \quad R_y|3\rangle = |1\rangle, \quad R_z|3\rangle = |2\rangle, \\ &\mathbf{1}|4\rangle = |4\rangle, \quad R_x|4\rangle = |3\rangle, \quad R_y|4\rangle = |2\rangle, \quad R_z|4\rangle = |1\rangle. \end{aligned} \tag{2.8.2a}$$

The resulting matrix representation in the $\{|1\rangle|2\rangle|3\rangle|4\rangle\}$ basis is then given by

$$\mathscr{R}(1) = \begin{pmatrix} 1 & \cdot & \cdot & \cdot \\ \cdot & 1 & \cdot & \cdot \\ \cdot & \cdot & 1 & \cdot \\ \cdot & \cdot & \cdot & 1 \end{pmatrix}, \qquad \mathscr{R}(R_x) = \begin{pmatrix} \cdot & 1 & \cdot & \cdot \\ 1 & \cdot & \cdot & \cdot \\ \cdot & \cdot & \cdot & 1 \\ \cdot & \cdot & 1 & \cdot \end{pmatrix},$$

$$\mathscr{R}(R_y) = \begin{pmatrix} \cdot & \cdot & 1 & \cdot \\ \cdot & \cdot & \cdot & 1 \\ 1 & \cdot & \cdot & \cdot \\ \cdot & 1 & \cdot & \cdot \end{pmatrix}, \qquad \mathscr{R}(R_z) = \begin{pmatrix} \cdot & \cdot & \cdot & 1 \\ \cdot & \cdot & 1 & \cdot \\ \cdot & 1 & \cdot & \cdot \\ 1 & \cdot & \cdot & \cdot \end{pmatrix}. \quad (2.8.2b)$$

Now it is possible to decompose this symmetry group into sums of idempotents as was done before with the C_n groups. The minimal equations of R_x ($R_x^2 = \mathbf{1}$) and R_y ($R_y^2 = \mathbf{1}$) give two idempotents each:

$$P^{x+} = (\mathbf{1} + R_x)/2, \qquad P^{y+} = (\mathbf{1} + R_y)/2,$$
$$P^{x-} = (\mathbf{1} - R_x)/2, \qquad P^{y-} = (\mathbf{1} - R_y)/2. \quad (2.8.3)$$

Each pair satisfies a completeness relation by itself:

$$1 = P^{x+} + P^{x-}, \quad (2.8.4a)$$
$$1 = P^{y+} + P^{y-}. \quad (2.8.4b)$$

However, D_2 has four linearly independent operators, and so clearly neither pair is enough by itself to spectrally decompose the whole group. The trick is to use the two together by simply multiplying Eq. (2.8.4a) with Eq. (2.8.4b):

$$\mathbf{1} \cdot \mathbf{1} = (P^{x+} + P^{x-})(P^{y+} + P^{y-})$$
$$\mathbf{1} = P^{x+}P^{y+} + P^{x+}P^{y-} + P^{x-}P^{y+} + P^{x-}P^{y-}. \quad (2.8.5a)$$

This gives a completeness relation involving four new idempotents:

$$P^1 \equiv P^{x+}P^{y+} = (\mathbf{1} + R_x + R_y + R_z)/4,$$
$$P^2 \equiv P^{x-}P^{y+} = (\mathbf{1} - R_x + R_y - R_z)/4,$$
$$P^3 \equiv P^{x+}P^{y-} = (\mathbf{1} + R_x - R_y - R_z)/4,$$
$$P^4 \equiv P^{x-}P^{y-} = (\mathbf{1} - R_x - R_y + R_z)/4. \quad (2.8.5b)$$

The resulting four idempotents must be orthogonal as well as complete, since

their commuting factors are orthogonal. For example, the product

$$\begin{aligned} P^1P^2 &= (P^{x+}P^{y+})(P^{x-}P^{y+}) \\ &= P^{x+}P^{x-}P^{y+}P^{y+} \\ &= 0 \end{aligned}$$

is nullified by the (x) factors. Furthermore, the four idempotents are simultaneously eigenoperators of R_x, R_y, as well as $R_z = R_xR_y$. For example, we have

$$\begin{aligned} R_xP^3 &= R_xP^{x+}P^{y-}, & R_yP^3 &= R_yP^{x+}P^{y-}, & R_zP^3 &= R_zP^{x+}P^{y-} \\ &= P^3 & &= P^{x+}R_yP^{y-} & &= R_xR_yP^{x+}P^{y-} \\ & & &= -P^3 & &= R_xP^{x+}R_yP^{y-} \\ & & & & &= -P^3. \end{aligned}$$

Hence, all four D_2 operators may be simultaneously spectrally decomposed:

$$\begin{aligned} \mathbf{1} &= P^1 + P^2 + P^3 + P^4, \\ R_x &= P^1 - P^2 + P^3 - P^4, \\ R_y &= P^1 + P^2 - P^3 - P^4, \\ R_z &= P^1 - P^2 - P^3 + P^4. \end{aligned} \tag{2.8.6}$$

The coefficients in this expansion or within the parentheses of Eq. (2.8.5b) are the irreps $D^\alpha(g)$ of the group D_2. These are summarized by the equations and table that follow. The conventional (A, B) notation for the irreps is given also:

$$P^\alpha = \tfrac{1}{4}\left(\sum_g D^{\alpha *}(g)\, g\right) \qquad g = \sum_{\alpha=1}^{4} D^\alpha(g) P^\alpha$$

Conventional notation $g =$	1	R_x	R_y	R_z
$D^{A_1}(g) = D^1(g) =$	1	1	1	1
$D^{B_2}(g) = D^2(g) =$	1	−1	1	−1
$D^{B_1}(g) = D^3(g) =$	1	1	−1	−1
$D^{A_2}(g) = D^4(g) =$	1	−1	−1	1

(2.8.7)

The eigenvector solutions to the equation (2.8.1) of motion are found using the irrep idempotents as follows:

$$|e^{A_1}\rangle \equiv |e^1\rangle = P^1|1\rangle\sqrt{4} = (|1\rangle + |2\rangle + |3\rangle + |4\rangle)/2,$$

$$|e^{B_2}\rangle \equiv |e^2\rangle = P^2|1\rangle\sqrt{4} = (|1\rangle - |2\rangle + |3\rangle - |4\rangle)/2,$$

$$|e^{B_1}\rangle \equiv |e^3\rangle = P^3|1\rangle\sqrt{4} = (|1\rangle + |2\rangle - |3\rangle - |4\rangle)/2,$$

$$|e^{A_2}\rangle \equiv |e^4\rangle = P^4|1\rangle\sqrt{4} = (|1\rangle - |2\rangle - |3\rangle + |4\rangle)/2,$$

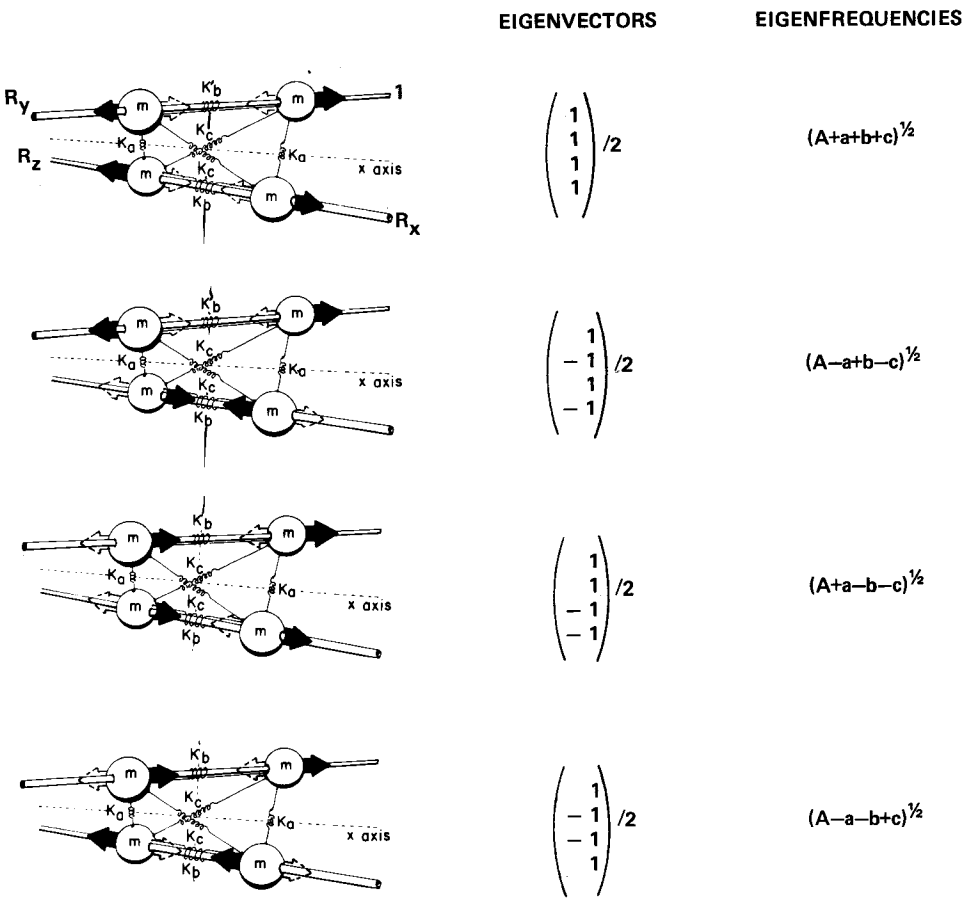

Figure 2.8.2 Normal modes, eigenvectors, and eigenfrequencies of D_2 symmetric coupled system.

where the original state definitions $|1\rangle = \mathbf{1}|1\rangle$, $|2\rangle = R_x|1\rangle$, $|3\rangle = R_y|1\rangle$, and $|4\rangle = R_z|1\rangle$ of Eq. (2.8.2a) are used. These states are pictured in Figure 2.8.2, and their eigenfrequencies from Eq. (2.8.1) are written next to each drawing.

2.9 THEORY OF COMMUTING IDEMPOTENTS

We can easily see that the trick which gave the D_2 irreps, must also work for any Abelian finite group. Suppose one element g of the Abelian group satisfies a minimal equation $g^n = \mathbf{1}$. From the theory of Section 2.6 this equation yields a set $\{p^1, p^2, \ldots, p^n\}$ of n orthogonal idempotents. Let another element h yield another set of $\{q^1, q^2, \ldots, q^m\}$. The p^j and q^k idempotents give eigenoperator expansions of g and h, respectively,

$$g = \sum_{j=1}^{n} g_j p^j, \qquad h = \sum_{k=1}^{m} h_k q^k, \tag{2.9.1}$$

while either set of idempotents satisfy the completeness relation:

$$\sum_{j=1}^{n} p^j = \mathbf{1} = \sum_{k=1}^{m} q^k. \tag{2.9.2}$$

Multiplying Eq. (2.9.2) by p^j may result in the "splitting" of p^j into a sum of operators $p^j q^k$:

$$\begin{aligned} p^j &= p^j q^1 + p^j q^2 + \cdots + p^j q^m \\ &= \cdots + P^1 + P^2 + \cdots + P^r \qquad (r \leq m). \end{aligned} \tag{2.9.3}$$

The nonzero terms $\{P^1, P^2, \ldots, P^r\}$ in these sums must satisfy orthonormality and completeness relations, too. This follows from Eqs. (2.9.1) and (2.9.2), since the p^m and q^k commute with each other ($p^m q^k = q^k p^m$) since they are polynomials of the commuting elements g and h. Furthermore, the resulting set provides a spectral decomposition of g and h simultaneously [recall Section 1.2.B(d), where matrices were treated in this way]:

$$\begin{aligned} gP^a &= D^a(g)P^a; \qquad g = D^1(g)P^1 + D^2(g)P^2 + \cdots + D^r(g)P^r, \\ hP^a &= D^a(h)P^a; \qquad h = D^1(h)P^1 + D^2(h)P^2 + \cdots + D^r(h)P^r. \end{aligned} \tag{2.9.4}$$

This splitting process can be repeated, using idempotent expansions generated by other group operators $\{k, l, \ldots\}$ which are not products of powers of g and h. Finally, this process must yield exactly as many nonzero idempotents as group elements because of linear independence. These final IRREDUCIBLE idempotents cannot split anymore because if one of them did,

there would be one more linearly independent operator than there are group elements. But this is impossible, since any operator in the group algebra is a linear combination of group operators. The number of group operators is ${}^{\circ}G$, the order of the group.

Furthermore, these irreducible or "unsplittable" idempotents are unique. Suppose two sets [Eq. (2.9.5)] have been found by using different group elements:

$$\mathbf{1} = P^1 + P^2 + \cdots + P^{{}^{\circ}G} = P^{1'} + P^{2'} + \cdots + P^{{}^{\circ}G'}. \tag{2.9.5}$$

Multiplying both sides by P^j gives

$$P^j = P^jP^{1'} + P^jP^{2'} + \cdots + P^jP^{{}^{\circ}G'}, \tag{2.9.6}$$

which can have only one nonzero term, since P^j is unsplittable. Let us say that term is $P^j = P^jP^{l'}$. Then multiplying Eq. (2.9.5) by $P^{l'}$ gives Eq. (2.9.7), which proves each idempotent set is unique no matter how you get it:

$$P^{l'} = P^jP^{l'} = P^j. \tag{2.9.7}$$

2.10 GENERAL THEORY OF ABELIAN GROUPS

There is an easy way to express the group D_2 and many others that arise in physics. D_2 is nothing but $C_2 \times C_2$. Let us now define what is meant by this "multiplication" ($\times$) of groups.

Definition A group G is said to be an OUTER PRODUCT $H \times K$ of subgroups $H = \{1, h_1, h_2, \ldots\}$ and $K = \{1, k_1, k_2, \ldots\}$ if the following holds:

(1) Every element g in G is written uniquely as a product $g = h_ik_j$ of one element from H and one element from K.
(2) Each h_i in H commutes with each k_j in $K \cdots h_ik_j = k_jh_i$.

In $D_2 = \{\mathbf{1}, R_x, R_y, R_z\}$ we find subgroups $H = \{1, R_x\} = C_2$ and $K = \{1, R_y\} = C_2$. It is easy to verify that the criteria (1) and (2) apply so that $D_2 = \{1, R_x\} \times \{1, R_y\} = C_2 \times C_2$. Of course, (2) applies automatically in Abelian groups, but the definition applies even if H and K are not Abelian.

This can be very convenient if you know the irreps of factors H and K of $G = H \times K$. Then the irreps of G can be obtained immediately, as shown for

$D_2 = C_2 \times C_2$ in the following:

$$\begin{array}{c|cc|cc|c}
 & 1 & & R_y & & \\
\hline
1 & 1 & R_x & 1 & R_x & \\
 & 1 & 1 & 1 & 1 & \\
 & 1 & -1 & 1 & -1 & 1 \\
\hline
1 & 1 & R_x & 1 & R_x & \\
 & 1 & 1 & 1 & 1 & \\
 & 1 & -1 & 1 & -1 & -1
\end{array}
=
\begin{array}{c|cccc}
1 & R_x & R_y & R_z & = R_x R_y \\
\hline
1 & 1 & 1 & 1 & \\
1 & -1 & 1 & -1 & \\
1 & 1 & -1 & -1 & \\
1 & -1 & -1 & 1 &
\end{array}$$

Furthermore, there is a famous theorem about Abelian finite groups which follows from the idempotent analysis in the preceding section. The theorem says: (1) Every finite Abelian group can be expressed as outer products of cyclic groups, and (2) $C_p \times C_q$ and C_{pq} are the same group if and only if integers p and q are relatively prime. This theorem allows one to name all the Abelian groups of an arbitrary finite order. For example, there is only one Abelian group of order 6, $C_3 \times C_2$, which is just the same as C_6. (We have already mentioned that $C_2 \times C_2$ is not the same as C_4.) For another example, all the groups below are different, and completely account for all Abelian groups of order $72 = 2^3 3^2$ (check Figure 2.2.2):

$$\begin{array}{rr}
C_2 \times C_2 \times C_2 \times C_3 \times C_3 & C_2 \times C_2 \times C_2 \times C_9 \\
C_4 \times C_2 \times C_3 \times C_3 & C_4 \times C_2 \times C_9 \\
C_8 \times C_3 \times C_3 & C_8 \times C_9 \sim C_{72}.
\end{array}$$

2.11 SOME ABELIAN POINT SYMMETRIES

A POINT SYMMETRY GROUP is a group of geometrical operations that keep at least one point fixed. These may include ROTATIONS around an axis through this point, or less familiar operations like REFLECTION or INVERSION. A CRYSTAL point symmetry group is a possible site symmetry at each lattice point in some infinite crystal lattice. Only onefold, two-fold (180°), threefold (120°), fourfold (90°), and sixfold (60°) axial symmetry can exist in a crystal. Hence the number of crystal point groups is restricted. It turns out there are just the 32 crystal point groups. These are named in Figure 2.11.1. Surprisingly, exactly half of them are Abelian. These 16

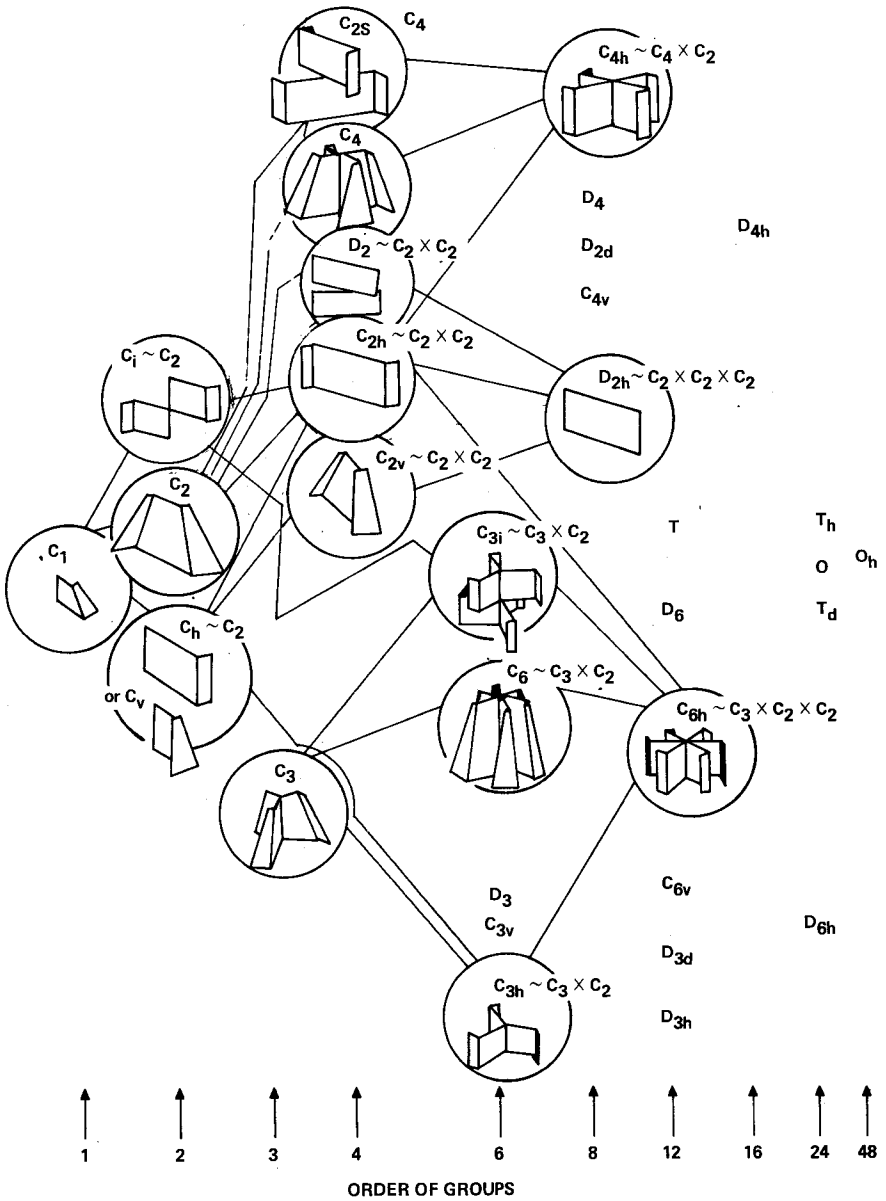

Figure 2.11.1 Abelian crystal point groups. Sixteen of the 32 crystal point groups are Abelian and are illustrated by models drawn in circles.

Abelian crystal point symmetries are indicated by drawings showing objects having the symmetry. (The 16 non-Abelian symmetries are drawn in Figure 3.1.1 at the beginning of Chapter 3.)

In Figure 2.11.1 the simplest objects having reflection symmetry are shown next to the symbols C_h or C_v. An h or v refers to a horizontal (xy) or vertical $((yz)$ or $(xz))$ mirror reflection plane which you can imagine bisecting the object. If you were to somehow map each point of the object into its mirror image point it would still look the same. The reflection operation is not as easily demonstrated as the rotation operation, but it is just as valid as a symmetry operator. For example, the horizontal reflection σ_{xy} through the (xy) plane changes a 3-vector (x, y, z) to $(x, y, -z)$. Similarly, vertical reflections σ_{xz} and σ_{yz} would change the same vector to $(x, -y, z)$ and $(-x, y, z)$, respectively. The representations of these reflections in the $\{x, y, z\}$ Cartesian vector basis are as follows:

$$\mathscr{V}(\sigma_{xy}) = \begin{pmatrix} 1 & 0 & 0 \\ 0 & 1 & 0 \\ 0 & 0 & -1 \end{pmatrix}, \qquad \mathscr{V}(\sigma_{xz}) = \begin{pmatrix} 1 & 0 & 0 \\ 0 & -1 & 0 \\ 0 & 0 & 1 \end{pmatrix},$$

$$\mathscr{V}(\sigma_{yz}) = \begin{pmatrix} -1 & 0 & 0 \\ 0 & 1 & 0 \\ 0 & 0 & 1 \end{pmatrix}. \tag{2.11.1}$$

Note that the symmetries C_{6h}, C_{4h}, D_{2h}, C_{3h}, C_{2h}, and C_h all have horizontal reflection symmetry. The symmetries C_{2v} and C_v have vertical reflection symmetry. The confusion between groups C_h and C_v comes about since no rotation axis serves to uniquely define "vertical." (Similarly, one could relabel D_{2h} to be D_{2v} just as well.)

The simplest object having inversion symmetry is shown by the symbol C_i in Figure 2.11.1. If each point of the object at $(\mathbf{r})$ is mapped through the origin at the centroid of the object, to the position $(-\mathbf{r})$, it will still look the same. This is another operation that we can only "do" mathematically. The inversion operator is usually labeled by I. The representation of I is

$$\mathscr{V}(I) = \begin{pmatrix} -1 & 0 & 0 \\ 0 & -1 & 0 \\ 0 & 0 & -1 \end{pmatrix} \tag{2.11.2}$$

in the $\{x, y, z\}$ basis. Other symmetries that include inversion are the groups C_{2h}, C_{3i}, C_{4h}, D_{2h}, and C_{6h}, which are connected by lines leading away from C_i. Any symmetry group A connected by a line in Figure 2.11.1 to a larger symmetry group B is contained in B. A is said to be a SUBGROUP of B $(A \subset B)$. You may read $(\subset)$ as "is less than" or, better, "is contained in."

The three symmetry groups C_i, C_2, and C_h are exactly the same as far as their mathematical properties are concerned. Their character tables or irreps look exactly the same. However, there are many conventional notations

which give different names to the same irreps depending on which symmetry is being labeled. Some examples are shown by the following:

	C_i		C_2		C_h	1	I	(inversion)
						1	R	(180° rotation)
						1	σ	(reflection)
0_2	A_g	(+)	A_1	A	A'	1	1	
	or		or					
1_2	A_u	(−)	A_2	B	A''	1	−1	

(2.11.3)

When different symmetry groups G and G' can be shown to share the same mathematical properties, they are said to be ISOMORPHIC symmetry groups. This is denoted by $G \sim G'$ in Figure 2.11.1. In the last example one has $C_i \sim C_h \sim C_2$. There are many different symmetries, but only a fraction of these are really different groups. For example, all the Abelian symmetries of order 6, namely, C_{3i}, C_6, and C_{3h}, are isomorphic to $C_3 \times C_2$, as explained in the preceding section. However, to define these symmetries more precisely one can write $C_{3i} = C_3 \times C_i$, $C_6 = C_3 \times C_2$, and $C_{3h} = C_3 \times C_h$.

Similarly, the symmetries $D_2 = C_2 \times C_2$, $C_{2h} = C_2 \times C_i$, and $C_{2v} = C_2 \times (C_v \sim C_h)$ are all isomorphic to $C_2 \times C_2$. To understand these groups a little better note that a product of inversion and a horizontal reflection is

$$\mathscr{V}(I)\mathscr{V}(\sigma_{xy}) = \begin{pmatrix} -1 & 0 & 0 \\ 0 & -1 & 0 \\ 0 & 0 & -1 \end{pmatrix}\begin{pmatrix} 1 & 0 & 0 \\ 0 & 1 & 0 \\ 0 & 0 & -1 \end{pmatrix} = \begin{pmatrix} -1 & 0 & 0 \\ 0 & -1 & 0 \\ 0 & 0 & 1 \end{pmatrix}$$
$$= \mathscr{V}(R_z(180°)), \tag{2.11.4}$$

which is a 180° rotation around the *vertical* z axis. Therefore, the elements $\{1, R_z, I, \sigma_{xy}\}$ make up C_{2h}. On the other hand, we have $C_{2v} = \{1, R_z, \sigma_{xy}, \sigma_{yz}\}$, since

$$\sigma_{xz} \cdot \sigma_{yz} = R_z. \tag{2.11.5}$$

Finally, note that C_{2s} is isomorphic to C_4. The former contains a 90° ROTATION-INVERSION operation in place of the simple 90° rotation operation of the latter. In other words, if the C_{2s} model is inverted before or after a 90° rotation, it will retain its original appearance. C_{2s} is often labeled C_{2i}.

In conclusion, one notes that the essential mathematical properties of all 16 Abelian crystal point groups are derived from those of three simple cyclic groups C_2, C_3, and C_4.

2.12 SYMMETRY ANALYSIS FOR QUANTUM MECHANICS

The mathematics of symmetry analysis for quantum mechanics is mostly the same as it was for the classical problems which were used to introduce it. This is especially true here, since we have made a point of using Dirac notation for classical problems. However, it is important to see how the physical interpretations of the similar mathematical solutions can be very different. We study below some of the simplest examples of quantum problems involving symmetry.

A. Bohr Levels and Bloch Waves: C_{12} Clocktane Orbitals

In this section we will consider an electron confined to orbit in a circular ring. The effects of 12 equivalent potential wells set around the ring at the 1 o'clock, 2 o'clock, ..., 11 o'clock, and 12 o'clock positions will be discussed using C_{12} symmetry analysis. Three cases will be treated, including (a) the Bohr-orbital case where no potential wells exist, (b) the nearly free electron case where very shallow or weak potential wells exist, and (c) the tight-binding or very hindered rotation case in which the potential wells are very deep. The potentials for cases (a), (b), and (c) are drawn at the top of Figures 2.12.1(a), 2.12.1(b), and 2.12.1(c), respectively.

This is a highly simplified model of the molecular orbitals of a 12-fold "clocktane" molecule. It will be the basis of quite a number of concepts developed in this book.

(a) Bohr Orbitals and Free Rotation If an electron orbits freely around a circular ring the time-dependent Schrödinger equation is

$$i\hbar\frac{\partial\psi}{\partial t} = H_0\psi = -(\hbar^2/2\mu)\frac{\partial^2\psi}{\partial x^2} = -(\hbar^2/2\mu r^2)\frac{\partial^2\psi}{\partial\phi^2}, \qquad (2.12.1)$$

where the independent variable may be azimuthal angle ϕ or else circumferential distance

$$x = r\phi \qquad (2.12.2)$$

around a ring of radius r. The solutions to the Schrödinger eigenvalue equation

$$H_0|m\rangle = \varepsilon_m|m\rangle \qquad (2.12.3)$$

are represented by the one-dimensional plane-wave functions,

$$\langle\phi|m\rangle = \frac{e^{im\phi}}{\sqrt{2\pi}} = \frac{e^{ikx}}{\sqrt{2\pi}} \equiv \langle x|k\rangle, \qquad (2.12.4)$$

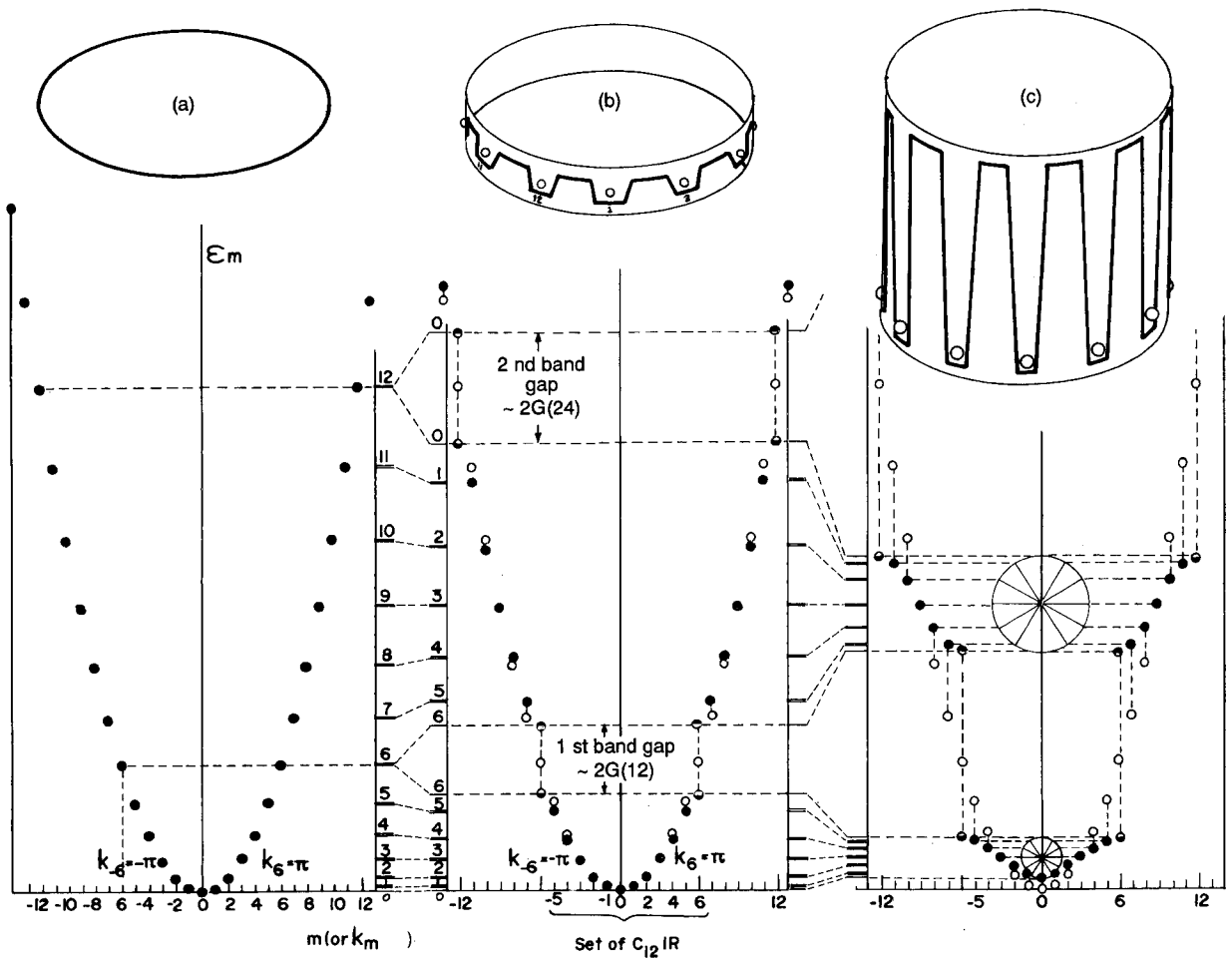

Figure 2.12.1 C_{12} "clocktane" potential wells and energy levels. (a) Zero potential gives Bohr orbital levels. (b) Weak potential gives small and-gap splittings at $(m) = 6, 12, \ldots$. (c) Strong potential gives tightly clustered bands and wide gaps. (Splitting of clusters is

having energy eigenvalues

$$\varepsilon_m = \frac{\hbar^2}{2\mu r^2} m^2 = \frac{\hbar^2}{2\mu} k^2, \tag{2.12.5}$$

where $m = 0, \pm 1, \pm 2, \ldots, +\infty$ is quantized by the circular boundary conditions $\langle \phi | m \rangle = \langle \phi + 2\pi | m \rangle$. Eigenstates may be labeled using either the angular-momentum quantum number m or else the plane-wave number

$$k = m/r. \tag{2.12.6}$$

The energy eigenvalues ε_m from Eq. (2.12.5) are plotted in Figure 2.12.1. Note that all energy levels except $m = 0$ are doubly degenerate. Moving-wave states $|m\rangle$ and $|-m\rangle$ move around the ring in opposite directions, since by Eqs. (2.12.1)–(2.12.4)

$$\langle \phi, t | \pm m \rangle = \frac{e^{i(\pm m\phi - \varepsilon_m t/\hbar)}}{\sqrt{2\pi}}; \tag{2.12.7}$$

however, the energy ε_m is the same for $(+m)$ and $(-m)$. Therefore, one may construct sine and cosine standing-wave states

$$\langle \phi | c_m \rangle = \frac{\langle \phi | m \rangle + \langle \phi | -m \rangle}{\sqrt{2}} = (\pi)^{-1/2} \cos m\phi, \tag{2.12.8a}$$

$$\langle \phi | s_m \rangle = \frac{\langle \phi | m \rangle - \langle \phi | -m \rangle}{i\sqrt{2}} = (\pi)^{-1/2} \sin m\phi, \tag{2.12.8b}$$

which have the same energy ε_m but stationary nodes and crests:

$$\langle \phi, t | c_m \rangle = (\pi)^{-1/2} e^{-i\varepsilon_m t/\hbar} \cos m\phi, \tag{2.12.9a}$$

$$\langle \phi, t | s_m \rangle = (\pi)^{-1/2} e^{-i\varepsilon_m t/\hbar} \sin m\phi. \tag{2.12.9b}$$

The position of the nodes makes no difference in the energy if the potential is constant.

(b) Weak C_{12} Potential and Nearly Free Rotations Consider the effect of a C_{12} symmetric perturbation V_{12} added to the Hamiltonian:

$$H = H_0 + V_{12}. \tag{2.12.10}$$

Let the perturbation consist of $(n = 12)$ identical potential wells separated by angle $(\Delta\phi = 2\pi/n = \pi/6)$ or by circumferential distance d, where

$$d = 2\pi r/n = \pi r/6, \tag{2.12.11}$$

as shown in the upper portion of Figure 2.12.1(b). The matrix elements $\langle m'|H|m\rangle$ of this new Hamiltonian must be zero unless states $|m\rangle$ and $|m'\rangle$ belong to the same irrep D^{k_n} of $C_n = C_{12}$. Using Eq. (2.12.4) one finds the matrix element to be

$$\begin{aligned}\langle m'|H|m\rangle &= \langle m'|H_0|m\rangle + \langle m'|V_{12}|m\rangle \\ &= \delta_{m'm}\varepsilon_m + \frac{1}{2\pi}\int d\phi\, e^{-im'\phi}V_{12}e^{im\phi} \\ &= \delta_{m'm}m^2E + \frac{1}{2\pi}\int d\phi\, e^{-i(m'-m)\phi}V_{12}, \qquad (2.12.12)\end{aligned}$$

where $E \equiv \hbar^2/2\mu r^2$. A portion of the H-matrix is displayed in Table 2.12.1 on p. 121 for $E = 1$. Note that all off-diagonal ($m' \neq m$) components are zero unless

$$\begin{aligned}|m' - m| &= n, 2n, 3n, \ldots \\ &= 12, 24, 36, \ldots, \qquad (2.12.13)\end{aligned}$$

or

$$m' = (m) \text{ modulo } (n).$$

Consider two ways to see this. First, the only nonzero Fourier components which a C_{12} symmetric potential V_{12} could have would be a 12th ($e^{\pm 12i\phi}$), 24th ($e^{\pm 24i\phi}$), etc. Note that the second term in Eq. (2.12.12) equals the $(m' - m)$th Fourier component

$$G(m' - m) = \frac{1}{2\pi}\int d\phi\, e^{-i(m'-m)\phi}V_{12} \qquad (2.12.14)$$

of V_{12}. Hence, Eq. (2.12.13) follows. For a second proof note that m and m' belong to the same irrep D^{k_n} of C_n if Eq. (2.7.7) holds. This implies Eq. (2.12.13). Note that the definition of wavevector k_n in Eq. (2.12.6) is

$$k_n = m/r = (2\pi m/nd) \qquad (2.12.15)$$

when Eq. (2.12.11) is used. This agrees with the original definition in Eq. (2.7.2) if the unit of distance is the lattice interval ($d = 1$).

The introduction of potential V_{12} may change the eigenstate $|m\rangle$ of H_0 into a new eigenstate $|e(m)\rangle$ of $(H_0 + V_{12})$, which is a combination:

$$\begin{aligned}|e(m)\rangle = \psi_m|m\rangle + \psi_{m-12}|m - 12\rangle + \psi_{m-24}|m - 24\rangle + \cdots \\ + \psi_{m+12}|m + 12\rangle + \psi_{m+24}|m + 24\rangle + \cdots \qquad (2.12.16)\end{aligned}$$

of all the states $|m - Nn\rangle$ labeled by the same irrep $D^{m_{12}}$ of C_{12}. Finding the perturbed eigensolutions ψ_j and the eigenvalues can be difficult in general.

However, if V_{12} is weak enough one may ignore all but two terms in Eq. (2.12.16), and consider only pairs of states with nearly equal unperturbed energies $\varepsilon_{m'} \sim \varepsilon_m = m^2E$. For example, $|5\rangle$ and $|-7\rangle$ only differ by $(7^2 - 5^2)E = 24E$, while the next possible contender in Eq. (2.12.16) is $|17\rangle$, which differs by $E(17^2 - 5^2) = 264E$. As long as $V_{12} \ll 264E$ we can ignore $|17\rangle$. The same is true for the pair $\{|7\rangle, |-5\rangle\}$. Approximate eigensolutions made from just these pairs are found by diagonalizing (2×2) H-submatrices derived from Equation (2.12.12) or extracted from Table 2.12.1:

$$\langle H\rangle_{5,-7} = \begin{array}{c} \begin{matrix} |5\rangle & |-7\rangle \end{matrix} \\ \begin{pmatrix} 25E & G(-12) \\ G(12) & 49E \end{pmatrix} \end{array}, \qquad \langle H\rangle_{-5,7} = \begin{array}{c} \begin{matrix} |-5\rangle & |7\rangle \end{matrix} \\ \begin{pmatrix} 25E & G(12) \\ G(-12) & 49E \end{pmatrix} \end{array}.$$

Note that the eigenvalues (ε) of these two matrices are identical:

$$\begin{aligned} \varepsilon(\pm 7) &= 37E + \left(144E^2 + |G(12)|^2\right)^{1/2} \cong 49E + |G(12)|^2/24E \\ \varepsilon(\pm 5) &= 37E - \left(144E^2 + |G(12)|^2\right)^{1/2} \cong 25E - |G(12)|^2/24E. \end{aligned} \tag{2.12.17}$$

So for small $|G(12)|^2$ the perturbation V_{12} shifts the $|\pm 7\rangle$ doublet level up slightly, and the $|\pm 5\rangle$ doublet level down by the same amount. This is shown between the (a) and (b) parts of Figure 2.12.1.

The splitting of the $|\pm 6\rangle$ doublet in the same part of Figure 2.12.1 deserves special attention. Now there is only one (2×2) matrix to diagonalize, and it is found at the center of Table 2.12.1:

$$\langle H\rangle_{\pm 6} = \begin{array}{c} \begin{matrix} |6\rangle & |-6\rangle \end{matrix} \\ \begin{pmatrix} 36E & G(-12) \\ G(12) & 36E \end{pmatrix} \end{array}.$$

Its eigenvectors and eigenvalues are the following:

$$\begin{aligned} |c_6\rangle &= \frac{|6\rangle + |-6\rangle}{\sqrt{2}}, \quad \text{with eigenvalues } \varepsilon(c_6) = 36E + G(12), \\ i|s_6\rangle &= \frac{|6\rangle - |-6\rangle}{\sqrt{2}}, \quad \text{with eigenvalue } \varepsilon(s_6) = 36E - G(12). \end{aligned} \tag{2.12.18}$$

Here it is assumed that $G(12) = G(-12) \leq 0$. This corresponds to picking origin $(x = 0 = \phi)$ in the center of an attractive $[V(0) < 0]$ symmetric $[V(x) = V(-x)]$ potential well. Once again (recall Figure 2.7.7) the $(m = \pm 6)$ doublet level is split by a C_{12} perturbation and standing-wave eigenstates

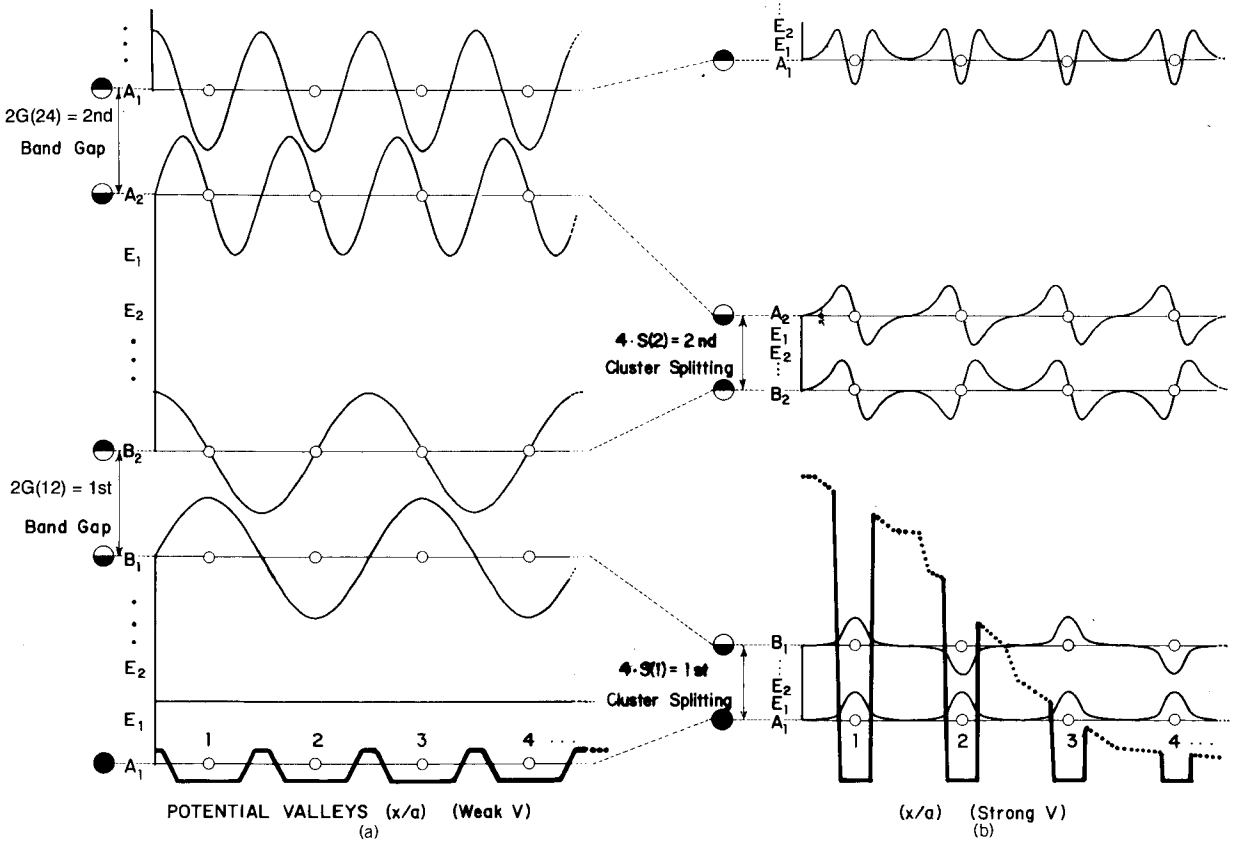

Figure 2.12.2 Standing-wave solutions to one-dimensional periodic potential (only band-gap boundary waves are drawn). (a) *Weak potential.* Energy differences are determined by potential energy to zeroth order. Waves which hover over the potential hills are higher in total energy. (b) *Strong potential.* Energy differences are determined by the number of zeros of nodes in the wave. Waves with more nodes are higher in total energy even if the nodes fall in the center of potential hills.

TABLE 2.12.1 H-matrix in plane wave basis for weak C_{12} potential $V(\phi) = V_{12} \ll 1$

$m=$	0	1	−1	2	−2	3	−3	4	−4	5	−5	6	−6	7	−7	8	−8	9	−9	10	−10	11	−11	12	−12	13
0	0	.	.	.	.	.	.	.	.	.	.	.	.	.	.	.	.	.	.	.	.	.	.	G	G*	.
1	.	1	.	.	.	.	.	.	.	.	.	.	.	.	.	.	.	.	.	.	.	.	G*	.	.	G
−1	.	.	1	.	.	.	.	.	.	.	.	.	.	.	.	.	.	.	.	.	.	G	.	.	.	.
2	.	.	.	4	.	.	.	.	.	.	.	.	.	.	.	.	.	.	.	.	G*	.	.	.	.	.
−2	.	.	.	.	4	.	.	.	.	.	.	.	.	.	.	.	.	.	.	G	.	.	.	.	.	.
3	.	.	.	.	.	9	.	.	.	.	.	.	.	.	.	.	.	.	G*	.	.	.	.	.	.	.
−3	.	.	.	.	.	.	9	.	.	.	.	.	.	.	.	.	.	G	.	.	.	.	.	.	.	.
4	.	.	.	.	.	.	.	16	.	.	.	.	.	.	.	.	G*	.	.	.	.	.	.	.	.	.
−4	.	.	.	.	.	.	.	.	16	.	.	.	.	.	.	G	.	.	.	.	.	.	.	.	.	.
5	.	.	.	.	.	.	.	.	.	25	.	.	.	.	G*	.	.	.	.	.	.	.	.	.	.	.
−5	.	.	.	.	.	.	.	.	.	.	25	.	.	G	.	.	.	.	.	.	.	.	.	.	.	.
6	.	.	.	.	.	.	.	.	.	.	.	36	G*	.	.	.	.	.	.	.	.	.	.	.	.	.
−6	.	.	.	.	.	.	.	.	.	.	.	G	36	.	.	.	.	.	.	.	.	.	.	.	.	.
7	.	.	.	.	.	.	.	.	.	.	G*	.	.	49	.	.	.	.	.	.	.	.	.	.	.	.
−7	.	.	.	.	.	.	.	.	.	G	.	.	.	.	49	.	.	.	.	.	.	.	.	.	.	.
8	.	.	.	.	.	.	.	.	G*	.	.	.	.	.	.	64	.	.	.	.	.	.	.	.	.	.
−8	.	.	.	.	.	.	.	G	.	.	.	.	.	.	.	.	64	.	.	.	.	.	.	.	.	.
9	.	.	.	.	.	.	G*	.	.	.	.	.	.	.	.	.	.	81	.	.	.	.	.	.	.	.
−9	.	.	.	.	.	G	.	.	.	.	.	.	.	.	.	.	.	.	81	.	.	.	.	.	.	.
10	.	.	.	.	G*	.	.	.	.	.	.	.	.	.	.	.	.	.	.	100	.	.	.	.	.	.
−10	.	.	.	G	.	.	.	.	.	.	.	.	.	.	.	.	.	.	.	.	100	.	.	.	.	.
11	.	.	G*	.	.	.	.	.	.	.	.	.	.	.	.	.	.	.	.	.	.	121	.	.	.	.
−11	.	G	.	.	.	.	.	.	.	.	.	.	.	.	.	.	.	.	.	.	.	.	121	.	.	H
12	G*	.	.	.	.	.	.	.	.	.	.	.	.	.	.	.	.	.	.	.	.	.	.	144	H*	.
−12	G	.	.	.	.	.	.	.	.	.	.	.	.	.	.	.	.	.	.	.	.	.	.	H	144	.
13	.	G*	.	.	.	.	.	.	.	.	.	.	.	.	.	.	.	.	.	.	.	.	H*	.	.	169

where: $G = \frac{1}{2\pi}\int d\phi e^{i12\phi}V(\phi)$, $G^* = \frac{1}{2\pi}\int d\phi e^{-i12\phi}V(\phi)$, $H = \frac{1}{2\pi}\int d\phi e^{i24\phi}V(\phi)$, $H^* = \frac{1}{2\pi}\int d\phi e^{-i24\phi}V(\phi)$, ⋯

= G(12) = G(−12) = G(24) = G(−24)

TABLE 2.12.2 H-matrix in local wave basis for strong C_{12} potential $V_{12} \gg 1$

	1	2	3	4	5	6	7	8	9	10	11	12	1'	2'	3'	4'	5'	6'	⋯
1	H	S	.	.	.	.	.	.	.	.	.	S							
2	S	H	S	.	.	.	.	.	.	.	.	.							
3	.	S	H	S	.	.	.	.	.	.	.	.							
4	.	.	S	H	S	.	.	.	.	.	.	.							
5	.	.	.	S	H	S	.	.	.	.	.	.							
6	.	.	.	.	S	H	S	.	.	.	.	.							
7	.	.	.	.	.	S	H	S	.	.	.	.							
8	.	.	.	.	.	.	S	H	S	.	.	.							
9	.	.	.	.	.	.	.	S	H	S	.	.							
10	.	.	.	.	.	.	.	.	S	H	S	.							
11	.	.	.	.	.	.	.	.	.	S	H	S							
12	S	.	.	.	.	.	.	.	.	.	S	H							
1'													H'	S'	.	.	.	.	.
2'													S'	H'	S'	.	.	.	.
3'													.	S'	H'	S'	.	.	.
4'													.	.	S'	H'	S'	.	.
5'													.	.	.	S'	H'	S'	.
6'													.	.	.	.	S'	H'	S'
⋮													.	.	.	.	.	S'	H'

where: H = 1st band center, H' = 2nd band center, ⋯

S = -S(1) = 1st band tunneling, S' = S(2) = 2nd band tunneling, ⋯

become mandatory. The cosine wave stands so its crests and troughs fall in the 12 attractive wells of the potential. The cosine wave is shown by the B_1 wave in Figure 2.12.2(a). It is drawn below the (B_2) sine wave of state $|s_6\rangle$. The sine wave has higher energy, since its crests fall in the high-potential regions, while its nodes stand in the low-potential wells. The energy difference between $|c_6\rangle$ and $|s_6\rangle$ states is called the first BAND GAP. It equals twice the 12th Fourier component of V_{12}:

$$\varepsilon(c_6) - \varepsilon(s_6) = 2G(12). \tag{2.12.19}$$

When moving-wave orbitals are forced to combine to make standing-wave eigenstates, one generally says that the orbital momentum has been QUENCHED. The same thing happens to the ($m = \pm 12$) pair of states. The cosine state $|c_{12}\rangle$ is labeled A_1 in Figure 2.12.2(a) and drawn above the sine wave state $|s_{12}\rangle$, which is labeled A_2. The splitting of this second band gap depends on the 24th Fourier coefficient of V_{12}; that is,

$$\varepsilon(c_{12}) - \varepsilon(s_{12}) = 2G(24), \tag{2.12.20}$$

in the approximation which assumed V_{12} is weak. We have assumed $G(24)$ is positive in the figure, but it is easy to make a potential which gives the opposite sign. However, the energy level structure is the same for either sign.

The m-levels within the bands where m is not divisible by ($n/2 = 6$) may belong to moving-wave states. From these states one may construct waves which move around the ring or else make standing waves which stand anywhere on the ring. However, even moving waves with energies near a band edge or m-values approaching $n/2$, n, $3n/2$, etc., may exhibit very sluggish motion. A measure of a wave state's ability to move is derived from the wave ENERGY DISPERSION RELATION $\varepsilon(k_m)$. This is determined (approximately) by the eigenvalues of the Hamiltonian (sub)matrix

$$\langle H\rangle_{m,m-n} = \begin{array}{c} \\ |m\rangle \\ |m-n\rangle \end{array} \begin{array}{c} \begin{array}{cc} |m\rangle & |m-n\rangle \end{array} \\ \begin{pmatrix} m^2E & G(n) \\ G(n) & (m-n)^2E \end{pmatrix} \end{array}$$

for small potentials. A good measure of wave motion is found by computing the wave GROUP VELOCITY

$$v_g = \frac{d\omega}{dk} = (\hbar)^{-1}\frac{d\varepsilon(k_n)}{dk_n}. \tag{2.12.21}$$

It is important not to confuse v_g with the PHASE VELOCITY $v_p = \omega/k$; V_g is proportional to the slope of the energy eigenvalue function plotted versus k_m or m as in Figure 2.12.1. Note how the slopes of the curves which would

connect the dark circles in the figure tend toward zero near the band gaps or Brillouin boundaries. As the number (n) of potential wells increases each band becomes a quasicontinuum of energy levels. Then the wave states vary continuously from moving waves to standing waves as the energy approaches a band edge.

(c) Very Hindered Rotation: Bloch Waves and Tunneling For energy eigenstates that lie deep in strong C_n symmetric potentials, many higher terms in Eq. (2.12.16) may be significant. In general the wave function for this state assumes the form of a BLOCH wave:

$$\begin{aligned}\langle \phi | e(m) \rangle &= \sum_{N=-\infty}^{\infty} \psi_{m+Nn} \langle \phi | m + Nn \rangle \\ &= e^{im\phi} u_e(\phi) \equiv e^{ik_n x} u_e(x),\end{aligned} \tag{2.12.22}$$

where $u(\phi)$ is a local or BLOCH FUNCTION:

$$u_e(\phi) = \sum_{N=-\infty}^{\infty} \psi_{m+Nn} e^{iNn\phi} = u_e(\phi + 2\pi/n), \tag{2.12.23}$$

which has the C_n symmetry of the periodic potential. (This result is also called FLOQUET'S THEOREM.)

For deeply bound eigenfunctions it is useful to make another approximation for the Bloch solution. With high barriers between each of the n potential wells it makes sense to use the eigenfunctions of each individual well as a basis. Let $|1\rangle$ be an eigenstate for the first well obtained by assuming that it is the only well on the ring. (One can imagine filling in all the other wells with a constant potential equal to the maximum of the potential hills.) Then let the basis $\{|1\rangle, |2\rangle, |3\rangle, \ldots, |n\rangle\}$ of states be defined each by a C_n group operation on the first one; i.e., $|1\rangle = \mathbf{1}|1\rangle$, $|2\rangle = r|1\rangle$ (see Figure 2.12.3), $|3\rangle = r^2|1\rangle, \ldots, |n\rangle = r^{n-1}|1\rangle$. Finally, let the Schrödinger eigenvalue equation $H|\psi\rangle = \varepsilon|\psi\rangle$ be represented in the $\{|1\rangle, |2\rangle, \ldots, |n\rangle\}$ basis by

$$\begin{pmatrix} H & -S & 0 & \cdots & -S \\ -S & H & -S & \cdots & 0 \\ 0 & -S & H & \cdots & 0 \\ \vdots & \vdots & \vdots & & \vdots \\ -S & 0 & 0 & & H \end{pmatrix} \begin{pmatrix} \langle 1|\psi\rangle \\ \langle 2|\psi\rangle \\ \langle 3|\psi\rangle \\ \vdots \\ \langle n|\psi\rangle \end{pmatrix} = \varepsilon \begin{pmatrix} \langle 1|\psi\rangle \\ \langle 2|\psi\rangle \\ \langle 3|\psi\rangle \\ \vdots \\ \langle n|\psi\rangle \end{pmatrix}, \tag{2.12.23}$$

There is one such submatrix for each band as shown in Table 2.12.2.

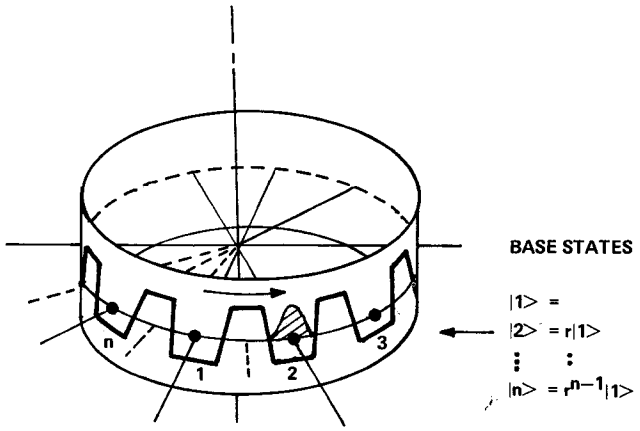

Figure 2.12.3 C_n symmetric ring potential and localized base state $|2\rangle = r|1\rangle$.

where H is the single-well energy, and $-S$ is the tunneling amplitude between nearest neighboring wells in the n-well problem. Amplitude S is proportional to the rate at which a particle originally in well (j) may "sneak" next door to well $(j + 1)$ or $(j - 1)$. Remember, $|j\rangle$ is an eigenstate only if neighboring wells are unavailable to accept the electron; i.e., if $S = 0$.

Except for a change in notation, the matrix in Eq. (2.12.23) is identical to the acceleration matrix in Eq. (2.7.1). The C_n projectors P^{k_n} applied to $|1\rangle$ give moving-wave eigenvectors:

$$|k_n\rangle = P^{k_n}|1\rangle\sqrt{n} = (|1\rangle + e^{-ik_n}|2\rangle + e^{-2ik_n}|3\rangle + \cdots)/\sqrt{n}, \quad (2.12.24)$$

which have eigenvalues

$$\varepsilon_n = H - 2S\cos k_n, \quad (2.12.25)$$

where the distance between potential wells is set equal to unity $(d = 1)$. The latter equation gives the well-known cosine dispersion function $\varepsilon_n(k_n)$ for bands of tightly bound electrons. This result is indicated by the 12-fold polygonal projections which are drawn next to the energy levels in Figure 2.12.1(c). The bandwidth $(4S)$ between the band edge states $|k_1\rangle$ and $|k_6\rangle$ is schematically exaggerated for the two bands in the figure. In the limit of strong potentials the bandwidths should be a tiny fraction of the band gaps. When propagation is reduced to a slow "oozing" or tunneling at rate S and this corresponds to a small group velocity and nearly zero slopes along $\varepsilon(k_n)$.

As in the treatment of pendulum waves the sine ($|s_n\rangle$) and cosine ($|c_n\rangle$) wave states are easier to picture:

$$|c_n^k\rangle = (|k_n\rangle + |-k_n\rangle)/\sqrt{2} = (|1\rangle + \cos k_n|2\rangle + \cdots)(2/n)^{1/2},$$
$$|s_n^k\rangle = -i(|k_n\rangle - |-k_n\rangle)/\sqrt{2} = (\sin k_n|2\rangle + \cdots)(2/n)^{1/2}.$$

Examples for $n = 3$ and 4 are shown in Figure 2.12.4. These are the analog of the pendulum standing waves depicted in Figure 2.7.3. Figure 2.12.4 is an attempt to display simple molecular orbitals. However, the "blob" wave functions drawn there cannot tell one much about the local potential well wave functions $\{\langle x|1\rangle, \langle x|2\rangle, \ldots, \langle x|n\rangle\}$. The waves in the figure depict the $e^{ik_n x}$ (or $\cos k_n x$) part of the Bloch wave [Eq. (2.12.22)], not the local $[u_e(x) = \langle x|1\rangle]$ part. The former varies from state to state within a given band, while the latter varies from band to band.

A more detailed picture of Bloch waves is shown in Figure 2.12.2(b). Note that the local Bloch function $[u(x) = \langle x|1\rangle]$ has the same shape in all wells for all states within a given band. It consists of zero, one, two,... rapid oscillations within each well for the first, second, and third bands, respectively. The local functions are modulated by a more or less slowly varying envelope function ($e^{ik_n x}$ or $\cos k_n x$) to give each Bloch wave.

The node structure of Bloch waves is an important consideration. According to an elementary theorem of quantum mechanics, a one-dimensional wave with more nodes always has more total energy. (This was proved by

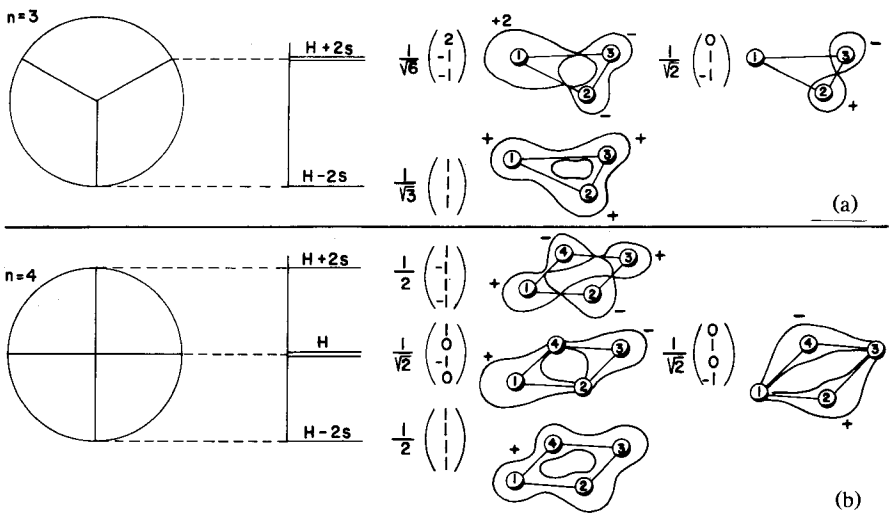

Figure 2.12.4 Sketches of molecular orbital wave functions and tunneling spectra for homocyclic potentials. (a) C_3 symmetry, (b) C_4 symmetry.

Schrödinger). Therefore the B_1 wave ($m = n/2$) in Figure 2.12.2(b), which has n nodes, must be higher in energy than all the states with lesser $m = 0, 1, 2, \ldots$, which have zero, two, four, ... nodes, respectively. The A_1 wave ($m = 0$), which has no nodes, is lowest in energy. This is paradoxical, since the A_1 wave has nonzero amplitudes in the centers of the high-potential regions where the B_1 wave is zero. (Schrödinger's theorem is *not* a trivial result.) Therefore the negative sign of $(-S)$ in Eq. (2.12.25) is right for the lowest band, since then the ($k = 0$) or A_1 wave is the lowest state.

In the second band, however, (S) changes sign as well as magnitude. The B_2 wave belongs to the ($m = n/2$) irrep of C_n, as does the B_1 wave on top of the first band. (B can stand for Brillouin or band boundary.) Starting with the B_2 wave, which has n nodes, one proceeds upward in energy with $n + 2, n + 4, \ldots, 2n - 2$, and finally $2n$ nodes while the m label *decreases*: $m = n/2 - 1, n/2 - 2, \ldots, 1$, and finally $m = 0$ for the A_2 wave on top of the second band. Notice that adding one more node inside each potential well increases the energy by roughly one whole band gap. Increasing the number of nodes between wells may increase the energy by only one bandwidth at the most.

(d) Intermediate Potentials: Exact Solutions It is instructive to study exact solutions to the Schrödinger eigenvalue equation,

$$\frac{d^2\psi}{d\phi^2} + (2\mu r^2/\hbar^2)(\varepsilon - V(\phi))\psi = 0, \tag{2.12.26}$$

for a mass μ particle on a ring of radius r subject to a C_n symmetric potential $V(\phi) = V(\phi + 2\pi/n)$. Two cases that have been analyzed are the cosine potential,

$$V(\phi) = -V\cos(n\phi), \tag{2.12.27}$$

and the n-square-well potential

$$V(\phi) = U(n\phi), \tag{2.12.28}$$

where,

$$U(\theta) = \begin{cases} 0, & -\pi/2 < \theta < \pi/2, \\ U, & \pi/2 < \theta < 3\pi/2. \end{cases}$$

These two cases represent two opposite extremes. The cosine potential has only one nonzero Fourier coefficient, namely, $G(n)$, since it is, after all, just one cosine wave. The n-square well, on the other hand, has the most

slowly converging Fourier series of any n-well potential of finite depth; i.e., $G[(2N+1)n] = (-1)^N 4\pi/(2N+1)$ $\{N = 0, 1, 2, \ldots\}$.

For the cosine potential the Schrödinger equation (2.12.26) becomes MATHIEU'S equation

$$\frac{d^2\psi}{dt^2} + A[\varepsilon + V\cos(2t)]\psi = 0, \tag{2.12.29}$$

where $t \equiv \phi n/2$ and

$$A = 8\mu r^2/n^2\hbar^2.$$

Mathieu's equation is treated in most standard texts on mathematical physics. The eigenvalues ε of the A and B standing-wave solutions are plotted in Figure 2.12.5 for a range of well depth V. Recall that the A levels belong to m-values for which $m = 0$ modulo n; the B levels belong to $m = n/2$ modulo n. (No B levels exist for odd n.) A and B levels are the boundaries between bands and gaps. Notice that the first, second, third, and Nth gaps originate at $\varepsilon = 1, 4, 9, \ldots$ and N^2, respectively, in the units $[2m^2\hbar^2/n^2\mu r^2]$ of the figure axis for $V = 0$. [This corresponds to our case (a)]. Notice that only the first gap is open for small V [case (b)]. This is because $G(Nn)$ is zero except for $N = 1$. Notice that the A and B levels run together and the bandwidths shrink rapidly for levels $E = \varepsilon$ that are much less than V. This corresponds to our case (c), which was treated in the preceding section. Each band between the A and B curves in Figure 2.12.5 contains $(n/2 - 1)[(n/2 - 1/2)]$ doubly degenerate moving-wave levels for n even (odd). These are not drawn, since they depend upon your choice for n.

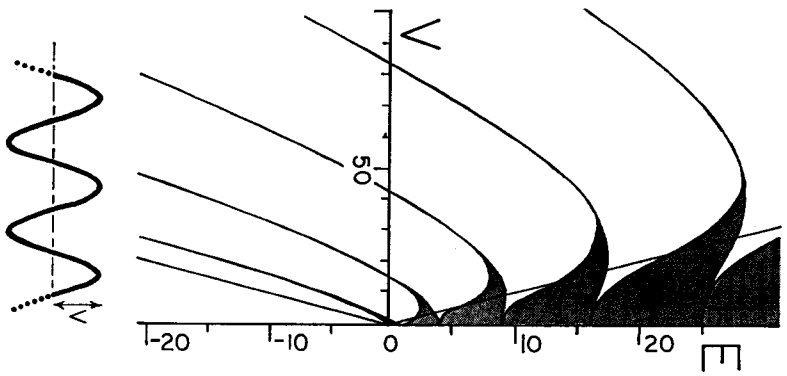

Figure 2.12.5 Energy versus V plots for band-gap edges for sinusoidal potential (Mathieu equation).

The solutions for the n-square-well potential are the well-known KRONIG-PENNEY bands. The A- and B-band boundary levels are plotted in Figure 2.12.6 using Kronig-Penney equations which are given in many quantum mechanics and solid state texts. The energy E is measured from the bottom of the wells instead of from a point halfway up, as it was in the preceding figure. In this way it is easy to see that the case (c) "tight bands" approach asymptotes at $E = 4, 16, 36, \ldots$. These correspond to the infinite-square-well energies.

Aside from this, the main thing which distinguishes the square-well solutions is the remarkable crossing of A and B levels on the case (b) or nearly free side of the spectrum where $E > U$. This comes about whenever the energy E and the potential U are adjusted so that an integral number n_w of half-waves fit into each well while another integral number n_p of half-waves

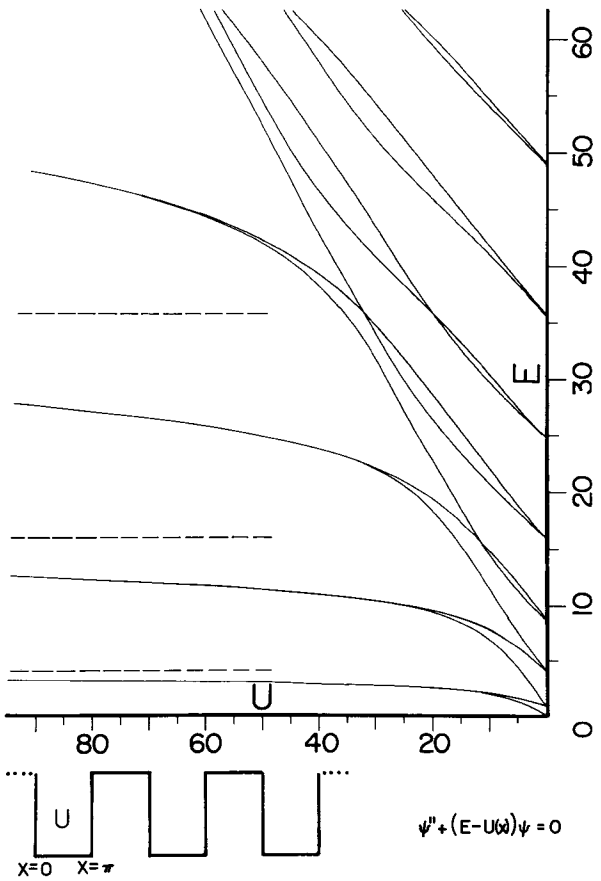

Figure 2.12.6 Energy versus U plots for band-gap edges for square-well potential (Kronig-Penney equation).

fit on the plateau between wells. For example, with $n_w = 3$ and $n_p = 2$ there is a crossing at $E = (2n_w)^2 = 36$ and $U = (2n_w)^2 - (2n_p)^2 = 20$ in Figure 2.12.6. The double degeneracy at this point corresponds to sine and cosine waves with the same energy.

(e) Comparison: When Is Parameter Fitting Useless? The approximate modeling of subsection (c) treats each band subspace as though it was all alone. It provides no information about where a given band is or how wide it is. Location and width depend on the "unknown" parameters H and S, respectively. Furthermore, the approximate theory fails to account for the mixing of states in one band with those belonging to other bands. One effect of this mixing would be the alteration of the cosine level spacing predicted by Eq. (2.12.25).

However, an approximate modelist could say, "But, wait... I have some other parameters besides H and S, namely, T, for next-nearest-neighbor tunneling, and U for next-next... ." Then he could give you a formula that would "explain" the modified spacing (see Problem 2.12.3). Eventually you can pull out as many parameters as there are level spaces; however, this is no more useful than a 52-parameter theory for weekly rainfall averages of 1927.

The approximate tunneling models are quite valid when V/E is large or when the energy gap between subspaces is large. The signal for impending failure is the need for too many parameters to reproduce the correct energy level spacing.

A more detailed formulation of the S parameter in the very hindered case is given in Section 2.12.D using semiclassical WKBJ formulas.

B. C_2 Symmetry and the Two-Level System

The C_2-like groups only have two irreps corresponding to even [A or $(+)$] and odd [B or (-1)]. Hence all the energy levels $\varepsilon^{(A,B)}$ in the four lowest spectral bands of a two-well potential of depth ($0 < V < 100$) are given by the curves in Figures 2.12.5 and 2.12.6 for cosine and square wells, respectively. In either figure the lower-lying spectrum for large V consists of pairs of nearly degenerate levels. This corresponds to case (c) [recall Section 2.12.A(c)] in which the two wells are nearly isolated from each other by large barriers of height U or V.

In this limit let each pair of states be described by a Schrödinger equation:

$$i\hbar \frac{\partial}{\partial t}|\psi\rangle = H|\psi\rangle, \tag{2.12.30a}$$

represented by

$$i\hbar \frac{\partial}{\partial t}\begin{pmatrix} \langle 1|\psi\rangle \\ \langle 2|\psi\rangle \end{pmatrix} = \begin{pmatrix} H & -S \\ -S & H \end{pmatrix}\begin{pmatrix} \langle 1|\psi\rangle \\ \langle 2|\psi\rangle \end{pmatrix} \tag{2.12.30b}$$

in the basis $|1\rangle$ and $|2\rangle$ for which the particle is localized in wells 1 and 2, respectively. The Schoŕdinger eigenequation,

$$H|\psi\rangle = \varepsilon|\psi\rangle, \tag{2.12.31a}$$

$$\begin{pmatrix} H & -S \\ -S & H \end{pmatrix}\begin{pmatrix} \langle 1|\psi\rangle \\ \langle 2|\psi\rangle \end{pmatrix} = \varepsilon\begin{pmatrix} \langle 1|\psi\rangle \\ \langle 2|\psi\rangle \end{pmatrix} \tag{2.12.31b}$$

is a special case of Eq. (2.12.23). The eigensolutions may be obtained using C_2 projectors $P^+ = P^A$ and $P^- = P^B$:

$$\begin{aligned} |\psi^{(+)}\rangle &= P^+|1\rangle\sqrt{2} = (|1\rangle + |2\rangle)/\sqrt{2}, \qquad \text{eigenvalue } \varepsilon^{(+)} = H - S, \\ |\psi^{(-)}\rangle &= P^-|1\rangle\sqrt{2} = (|1\rangle - |2\rangle)/\sqrt{2}, \qquad \text{eigenvalue } \varepsilon^{(-)} = H + S. \end{aligned} \tag{2.12.32}$$

The time behavior of eigenstate $|\psi^{(+)}\rangle$ and $|\psi^{(-)}\rangle$ according to Eq. (2.12.30) is simple harmonic phase oscillation at angular eigenfrequency $(H - S)/\hbar$ and $(H + S)/\hbar$, respectively,

$$\begin{aligned} |\psi^{(+)}(t)\rangle &= e^{(H-S)t/i\hbar}|\psi^{(+)}(0)\rangle, \\ |\psi^{(-)}(t)\rangle &= e^{(H+S)t/i\hbar}|\psi^{(-)}(0)\rangle. \end{aligned}$$

This is analogous to the behavior of the (+) and (−) resonant modes of the two-pendulum system described in Section 2.3.

One of the most well-known applications of these solutions involves the ammonia (NH_3) inversion doublet levels. The base states are imagined to be $|1\rangle = |\text{up}\rangle$ and $|2\rangle = |\text{dn}\rangle$ for which the N atom lies in a potential well above and below the H_3 plane, respectively, as shown in Figure 2.12.7. If the N atom can tunnel between $|\text{up}\rangle$ and $|\text{dn}\rangle$ there is an energy splitting between eigenstates $|(+)\rangle$ and $|(-)\rangle$. The splitting is equal to $2S$, and the tunneling frequency is the difference frequency $\omega = 2S/\hbar$. Tunneling is analogous to "beat trading" between two pendulums in Figure 2.3.2.

Consider what happens to the ammonia doublet states when an electric field is applied along the direction of (N)-atom motion. The field breaks the C_2 symmetry (to be precise the reflection symmetry of NH_3 is called C_h) symmetry according to Section 2.11 and makes the up-field state $|\text{up}\rangle$ energetically less favorable than the down-field state $|\text{dn}\rangle$. The Hamiltonian matrix becomes

$$\begin{pmatrix} \langle \text{up}|H|\text{up}\rangle & \langle \text{up}|H|\text{dn}\rangle \\ \langle \text{dn}|H|\text{up}\rangle & \langle \text{dn}|H|\text{dn}\rangle \end{pmatrix} = \begin{pmatrix} H - pE & -S \\ -S & H + pE \end{pmatrix}, \tag{2.12.33}$$

where E is the field strength and p is the dipole moment of the N atom. The effect of the E field on the energy eigenvalues is to make them go further

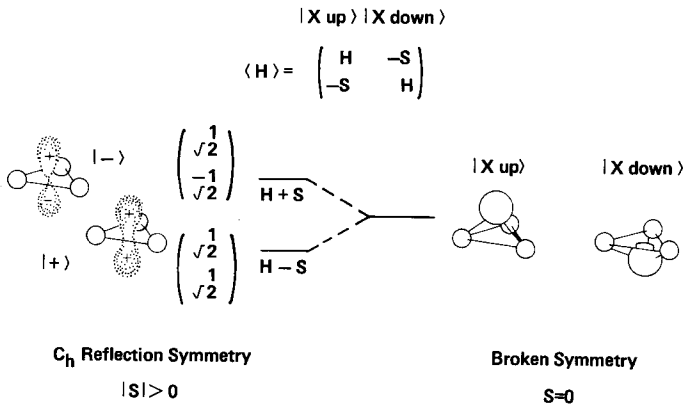

Figure 2.12.7 Two-state model for ammonia (NH_3) inversion. The case ($S = 0$) corresponds to internal or "spontaneous" symmetry breaking.

apart, as shown in Figure 2.12.8. The figure shows a plot of the eigenvalues ε:

$$\varepsilon = H \pm \left[S^2 + p^2E^2\right]^{1/2}. \tag{2.12.34}$$

For small E field ($pE \ll S$) ε is given by

$$\varepsilon = H \pm \left[S + p^2E^2/(2S)\right],$$

while for large E field ($pE \gg S$) ε is linear in E:

$$\varepsilon = H \pm pE.$$

The large E field eigenstates are $|\text{up}\rangle$ and $|\text{dn}\rangle$, the original base states. This is indicated by the drawings next to the energy trajectories in Figure 2.12.8.

The hyperbola in the figure is the simplest example of what spectroscopists call an "avoided level crossing." One can imagine that the straight-line trajectory for $|\text{up}\rangle$ is crossing that of $|\text{dn}\rangle$. If $S = 0$ that is exactly what would occur. However, with nonzero tunneling $|\text{up}\rangle$ and $|\text{dn}\rangle$ get mixed up to make $|\psi^{(+)}\rangle$ and $|\psi^{(-)}\rangle$ at $E = 0$. What starts out being the $|\text{dn}\rangle$ trajectory curves around at ($E = 0$) and goes out on the $|\text{up}\rangle$ trajectory, and vice versa. It can be shown that if you vary E slowly ($\dot{E} \ll S$) from large positive to large negative values then state $|\text{dn}\rangle$ does indeed turn into state $|\text{up}\rangle$ and vice versa. This is called ADIABATIC FOLLOWING. However, if you make the same change suddenly ($\dot{E} \gg S$) the initial state $|\text{up}\rangle$ or $|\text{dn}\rangle$ will not have time to change. The effect will be to jump the curves and cross over to the other branch of the hyperbola. In this way the field will change the energy of the system. Two-state dynamics are discussed in Sections 7.5 and 8.5.

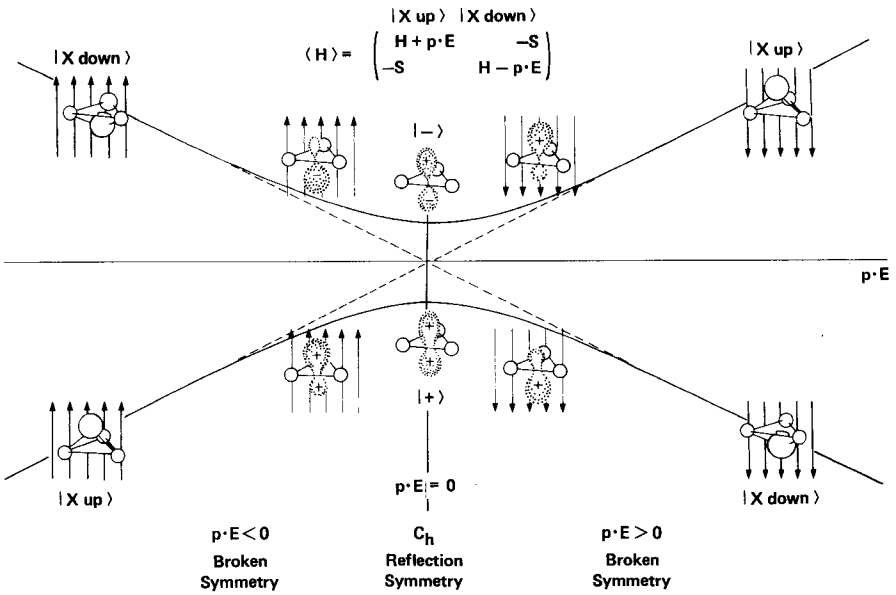

Figure 2.12.8 Effect of axial electric field on ammonia two-state eigensolutions. Cases with nonzero field ($p \cdot E \neq 0$) correspond to external or applied symmetry breaking.

C. C_2 Symmetry Analysis and Scattering Theory

Consider the scattering wave functions ψ_1 and ψ_2 for a single particle outside of a square-well potential as indicated by Figure 2.12.9:

$$\psi_1(x) = I_1 e^{ikx} + O_1 e^{-ikx}, \qquad (x < -a)$$
$$\psi_2(x) = I_2 e^{-ikx} + O_2 e^{ikx} \qquad (x > a). \tag{2.12.35}$$

The outside or scattering waves must match the "inside" wave

$$\psi_\omega = Ae^{ilx} + Be^{-ilx} \qquad (-a < x < a), \tag{2.12.36}$$

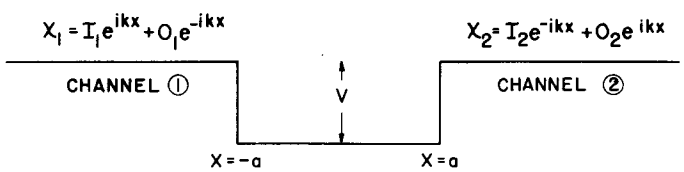

Figure 2.12.9 C_2 symmetric scattering potential.

where their respective wave vectors are given by

$$l = \sqrt{2mE/h}\,, \qquad k = \sqrt{2m(E - V)}\,h. \tag{2.12.37}$$

The match is made through boundary conditions:

$$\psi_1(-a) = \psi_\omega(-a), \qquad \psi_\omega(a) = \psi_2(a),$$
$$\psi_1'(-a) = \psi_\omega'(-a), \qquad \psi_\omega'(a) = \psi_2'(a),$$

on either side of the well. Substituting these conditions and eliminating constants A and B yields a linear "S-matrix" relation between the ingoing amplitudes I_j in channels $j = 1$ and 2, and the corresponding outgoing amplitudes O_j as follows:

$$\begin{pmatrix} O_1 \\ O_2 \end{pmatrix} = \begin{pmatrix} (i/D)(l^2 - k^2)\sin 2la & 2lk/D \\ 2lk/D & (i/D)(l^2 - k^2)\sin 2la \end{pmatrix} \begin{pmatrix} I_1 \\ I_2 \end{pmatrix}, \tag{2.12.38a}$$

where

$$D \equiv -e^{2ika}\left(2lk\cos 2la - i(l^2 + k^2)\sin 2la\right). \tag{2.12.38b}$$

In general the presence of any penetrable potential well would yield an S-matrix relation

$$\begin{pmatrix} O_1 \\ O_2 \end{pmatrix} = \begin{pmatrix} S_{11} & S_{12} \\ S_{21} & S_{22} \end{pmatrix} \begin{pmatrix} I_1 \\ I_2 \end{pmatrix}, \tag{2.12.39}$$

where the components S_{ij} are complicated functions of energy E and the potential. As explained in Section 2.1.3A, the S matrix is unitary if the particles are not destroyed or created by the well.

Without looking at the explicit form of the S matrix, we can tell from the left-to-right (C_2) symmetry analysis [following Section 2.3, Eq. (2.3.4)] that the following vectors must be the eigenvectors of this matrix:

$$\mathscr{X}^+ = \begin{pmatrix} 1/\sqrt{2} \\ 1/\sqrt{2} \end{pmatrix}, \qquad \mathscr{X}^- = \begin{pmatrix} 1/\sqrt{2} \\ -1/\sqrt{2} \end{pmatrix}. \tag{2.12.40}$$

Furthermore, since the S matrix is unitary [recall Eq. (1.3.4)] we know that the eigenvalues will be of the form $e^{i\mu_+}$ and $e^{i\mu_-}$. Just this much information by itself can simplify the visualization of the scattering process. Suppose the

incoming amplitudes are proportional to the components of $\mathscr{X}^+$ as follows:

$$\begin{pmatrix} I_1 \\ I_2 \end{pmatrix} = A\mathscr{X}^+ = \begin{pmatrix} A/\sqrt{2} \\ A/\sqrt{2} \end{pmatrix}. \tag{2.12.41}$$

Then the following must be the resulting outgoing amplitudes:

$$\begin{pmatrix} O_1 \\ O_2 \end{pmatrix} = e^{i\mu_+} \begin{pmatrix} A/\sqrt{2} \\ A/\sqrt{2} \end{pmatrix}. \tag{2.12.42}$$

The resulting waves in channels 1 and 2 are then given by

$$\begin{aligned} \begin{pmatrix} \psi_1 \\ \psi_2 \end{pmatrix} &= \begin{pmatrix} I_1 e^{ikx} + O_1 e^{-ikx} \\ I_2 e^{-ikx} + O_2 e^{ikx} \end{pmatrix} = \frac{A}{\sqrt{2}} \begin{pmatrix} e^{ikx} + e^{-i(kx-\mu_+)} \\ e^{-ikx} + e^{i(kx+\mu_+)} \end{pmatrix} \\ &= \sqrt{2}\, A e^{i(\mu_+/2)} \begin{pmatrix} \cos\left(kx - \dfrac{\mu_+}{2}\right) \\ \cos\left(kx + \dfrac{\mu_+}{2}\right) \end{pmatrix}. \end{aligned} \tag{2.12.43}$$

This represents the (+) or EVEN STANDING-WAVE scattering solution. Similarly, the choice of the ingoing amplitudes given by

$$\begin{pmatrix} I_1 \\ I_2 \end{pmatrix} = B\mathscr{X}^- = \begin{pmatrix} B/\sqrt{2} \\ -B/\sqrt{2} \end{pmatrix}$$

yields the (−) or ODD STANDING-WAVE scattering solution:

$$\begin{pmatrix} \psi_1 \\ \psi_2 \end{pmatrix} = \begin{pmatrix} I_1 e^{ikx} + O_1 e^{-ikx} \\ I_2 e^{-ikx} + O_2 e^{ikx} \end{pmatrix} = \sqrt{2}\, B e^{i(\mu_-/2)} \begin{pmatrix} \cos\left(kx - \dfrac{\mu_-}{2}\right) \\ -\cos\left(kx + \dfrac{\mu_-}{2}\right) \end{pmatrix}. \tag{2.12.44}$$

Equations (2.12.43) and (2.12.44) give the form of the waves for what are called EIGENCHANNEL SCATTERING STATES or PARTIAL WAVES of even (+) and odd (−) symmetry, respectively.

In Figure 2.12.10 these waves are sketched to show how the two types evolve with a steady increase of V. Note that the behavior of either type is related to the behavior of its EIGENPHASE SHIFT $\delta_\alpha \equiv \mu_\alpha/2$. Notice that phase shift δ_+, for example, is fairly constant, while V varies until one

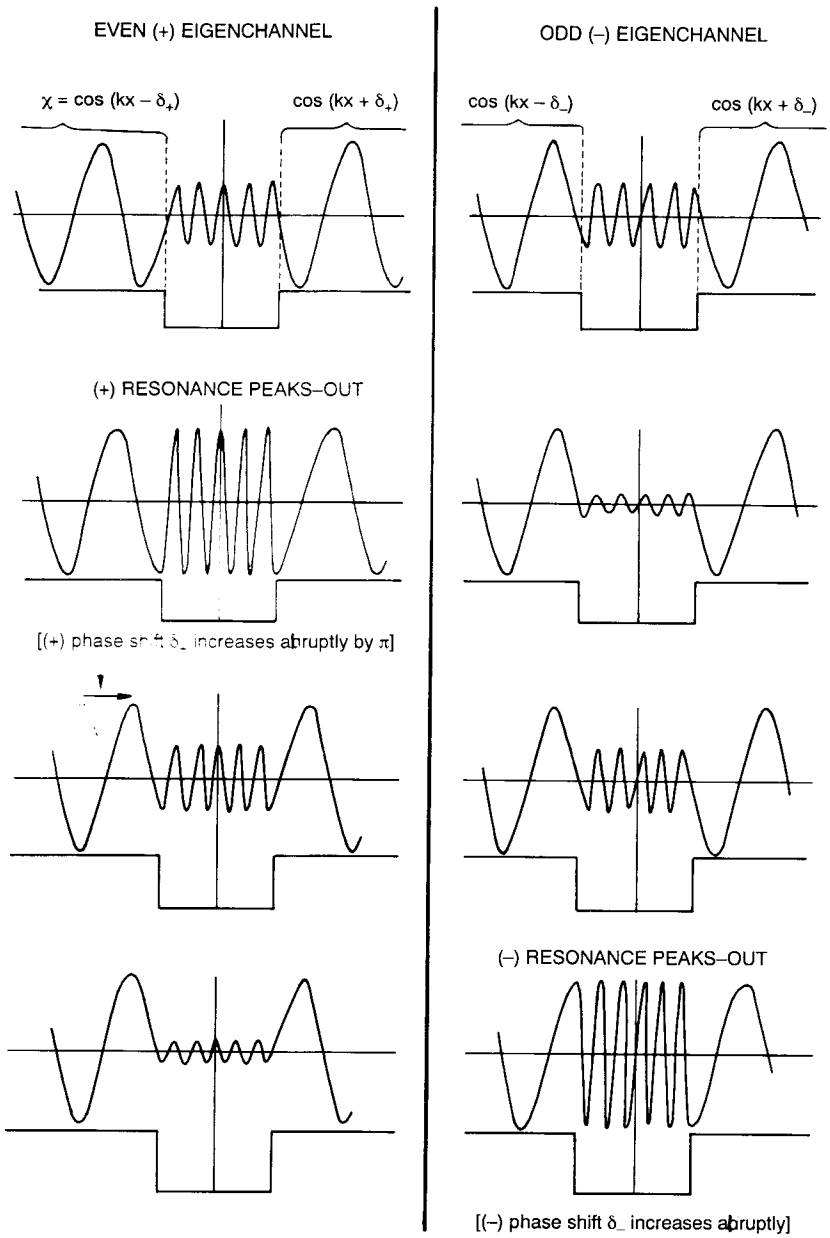

Figure 2.12.10 Scattering eigensolutions for C_2 symmetric square-well potential.

approaches a scattering RESONANCE of type (+). This occurs when an integral number of wavelengths fit in the well. In passing the (+) resonance the shift δ_+ quickly jumps by about π as another crest is more or less abruptly swallowed by the well. The same applies to (−) resonances except that they occur when a half-integral number of waves fit in the well.

Now ordinary transmission-reflection scattering can be expressed in terms of the (+) and (−) standing waves since they are a complete basis set. The most general scattering function can be represented by

$$\Psi = A^+\mathscr{X}^+ + A^-\mathscr{X}^- \tag{2.12.45}$$

using a combination of standing-wave solutions:

$$\begin{aligned} x^- &= \mathscr{X}^+ \cos(kr + \delta_+), \qquad x^- = \mathscr{X}^- \cos(kr + \delta_-) \\ &= \begin{pmatrix} 1/\sqrt{2} \\ 1/\sqrt{2} \end{pmatrix} \cos(kr + \delta_+), \quad = \begin{pmatrix} 1/\sqrt{2} \\ -1/\sqrt{2} \end{pmatrix} \cos(kr + \delta_-) \end{aligned} \tag{2.12.46}$$

and complex coefficients A^+ and A^-. Note that the "radial factors" $\cos(kr + \delta_\alpha)$ are functions of r, where $r = x$ for $x > a$ and $r = -x$ for $x < -a$.

The two components of the "angular factors" or vectors ($\mathscr{X}$) refer to channel (1) (left) or (2) (right), respectively. For example, a scattering state that had only outgoing particles in channel (2) would be represented by the following wave function:

$$\begin{aligned} \Psi &= A^+\mathscr{X}^+ \cos(kr + \delta_+) + A^-\mathscr{X}^- \cos(kr + \delta_-) \\ &= \begin{pmatrix} A^+ \cos(kr + \delta_+) + A^- \cos(kr + \delta_-) \\ A^+ \cos(kr + \delta_+) - A^- \cos(kr + \delta_-) \end{pmatrix} 1/\sqrt{2} = \begin{pmatrix} ? = \psi_1 \\ \alpha e^{ikr} \end{pmatrix}. \end{aligned} \tag{2.12.47}$$

The last equation gives the boundary condition, which yields a relation between A^+ and A^-:

$$\left(\frac{A^+e^{i\delta_+} - A^-e^{i\delta_-}}{2\sqrt{2}}\right)e^{ikr} + \left(\frac{A^+e^{-i\delta_+} - A^-e^{-i\delta_-}}{2\sqrt{2}}\right)e^{-ikr} = \alpha e^{ikr},$$

$$A^+ = A^-e^{i(\delta_+ - \delta_-)}. \tag{2.12.48}$$

Substituting Eq. (2.12.48) into the first component of Eq. (2.12.47) gives the

following:

$$\psi_1 = 2A^-\left[\cos(\delta_+ - \delta_-)e^{ikr}e^{i\delta_+} + e^{-ikr}e^{-i\delta_-}\right]. \qquad (2.12.49)$$

This shows that the reflected wave e^{ikr} in channel (1) will vanish when $\delta_+ - \delta_- = n\pi/2$. This corresponds to the perfect transmission that occurs at a resonance and is called the RAMSAUER-TOWNSEND effect in the theory of scattering.

D. Crossing Matrices and One-Dimensional Tunneling

The boundary conditions in piecewise constant potential provide relations between the amplitudes of right-hand and left-hand moving-wave solutions. If x_{12} is at the boundary between two different regions then continuity of the wave function ψ and its derivative $\psi' = d\psi/dx$ gives

$$R_1 e^{g_1 x_{12}} + L_1 e^{-g_1 x_{12}} = R_2 e^{g_2 x_{12}} + L_2 e^{-g_2 x_{12}},$$
$$R_1 g_1 e^{g_1 x_{12}} - L_1 g_1 e^{-g_1 x_{12}} = R_2 g_2 e^{g_2 x_{12}} - L_2 g_2 e^{-g_2 x_{12}},$$

where the exponential factors corresponding to the two sides are

$$g_1 = \left[\frac{2m}{\hbar}(V_1 - E)\right]^{1/2}, \qquad g_2 = \left[\frac{2m}{\hbar}(V_2 - E)\right]^{1/2}.$$

These factors are real (for $V_j > E$) or imaginary (for $V_j < E$). These relations may be solved to give the *crossing-matrix* relation

$$\begin{pmatrix} R_1 \\ L_1 \end{pmatrix} = \begin{pmatrix} C_{11} & C_{12} \\ C_{21} & C_{22} \end{pmatrix} \begin{pmatrix} R_2 \\ L_2 \end{pmatrix}, \qquad (2.12.50a)$$

where the C-matrix components are the following:

$$C_{11} = e^{-(g_1 - g_2)x_{12}}\left(\frac{g_1 + g_2}{2g_1}\right), \qquad C_{12} = e^{-(g_1 + g_2)x_{12}}\left(\frac{g_1 - g_2}{2g_1}\right),$$
$$C_{21} = e^{(g_1 + g_2)x_{12}}\left(\frac{g_1 - g_2}{2g_1}\right), \qquad C_{22} = e^{(g_1 - g_2)x_{12}}\left(\frac{g_1 + g_2}{2g_1}\right). \qquad (2.12.50b)$$

The crossing matrix for two or more boundaries is simply the matrix product of the C matrices for each boundary in the order in which they occur. For the square-well example in Figure 2.12.9 the crossing matrix

relation is

$$\begin{pmatrix} I_1 \\ O_1 \end{pmatrix} = \begin{pmatrix} C_{11} & C_{12} \\ C_{21} & C_{22} \end{pmatrix} \begin{pmatrix} O_2 \\ I_2 \end{pmatrix}$$

where:

$$C_{11} = e^{i2ka}\left[\cos 2la - i\frac{l^2 + k^2}{2kl}\sin 2la\right], \qquad C_{12} = -i\frac{l^2 - k^2}{2kl}\sin 2la$$

$$C_{21} = i\frac{(l^2 - k^2)}{2kl}\sin 2la, \qquad C_{22} = e^{-i2ka}\left[\cos 2la + i\frac{l^2 + k^2}{2kl}\sin 2la\right]. \tag{2.12.51}$$

Note that the identification of amplitudes $O_2 = R_2$ and $I_2 = L_2$, which is consistent with Eq. (2.12.35).

For an arbitrary one-dimensional potential system the C matrix and S matrix may be related by solving their respective relations (2.12.50) and (2.12.39):

$$\begin{pmatrix} S_{11} & S_{12} \\ S_{21} & S_{22} \end{pmatrix} = \begin{pmatrix} C_{21}/C_{12} & \det C/C_{11} \\ 1/C_{11} & -C_{12}/C_{11} \end{pmatrix} \tag{2.12.52a}$$

$$\begin{pmatrix} C_{11} & C_{12} \\ C_{21} & C_{22} \end{pmatrix} = \begin{pmatrix} -\det S^*/S_{21}^* & S_{11}^*/S_{21}^* \\ S_{11}/S_{21} & -\det S/S_{21} \end{pmatrix}. \tag{2.12.52b}$$

Note that it is generally true that $\det C = 1$, and the S matrix is unitary.

The crossing-matrix methods can be extended to treat WKBJ approximate solutions of the form

$$\psi = (Re^{\theta} + Le^{-\theta})/N^{1/2}, \tag{2.12.53a}$$

where the exponents

$$\theta = \int k(x)\,dx \tag{2.12.53b}$$

and normalization

$$N = \frac{2\pi\hbar^2}{m}k(x) \tag{2.12.53c}$$

depend on the potential through the wave vector

$$k(x) = \left[\frac{2m}{\hbar^2}(E - V(x))\right]^{1/2}, \tag{2.12.53d}$$

which may be real or imaginary. The WKBJ approximations are most accurate when the potential varies slowly compared to wave function. The crossing matrices are used to connect the amplitudes at neighboring classical turning points where the wave function reaches an inflection point and the WKBJ solution fails.

For example, the crossing matrix which relates the amplitudes across a potential barrier from points a to b in Figure 2.12.11 is approximately given by

$$C_{\text{barrier}} = \begin{pmatrix} [1+\theta^2]^{1/2} & i\theta \\ -i\theta & [1+\theta^2]^{1/2} \end{pmatrix}, \tag{2.12.54a}$$

where

$$\theta = e^{\int_a^b |k(x)|\,dx}. \tag{2.12.54b}$$

There are discrepancies between various texts and papers concerning the form of C_{barrier}. However, these become unimportant for high barriers ($\theta \gg 1$). For crossing the valley in Figure 2.12.11 the C matrix is

$$C_{\text{valley}} = \begin{pmatrix} e^{i\alpha} & 0 \\ 0 & e^{-i\alpha} \end{pmatrix}, \tag{2.12.55a}$$

where

$$\alpha = \int_b^c k(x)\,dx. \tag{2.12.55b}$$

Combinations of these matrices can be used to describe the entire C_n symmetric potential system in Figure 2.12.11. The product of the $2n$ C-matrix factors must yield the identity matrix in order to satisfy C_n symmetric periodic boundary conditions. We have

$$\left[C_{\text{barrier}} \quad C_{\text{valley}}\right]^n = \mathbf{1}$$

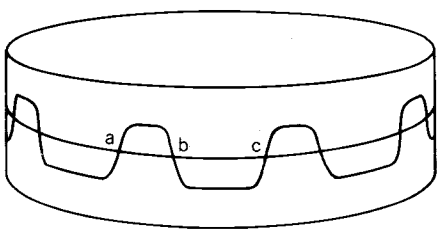

Figure 2.12.11 General C_n symmetric potential function.

or

$$\begin{pmatrix} [1+\theta^2]^{1/2}e^{i\alpha} & i\theta e^{-i\alpha} \\ -i\theta e^{-i\alpha} & [1+\theta^2]^{1/2}e^{-i\alpha} \end{pmatrix}^n = \begin{pmatrix} 1 & 0 \\ 0 & 1 \end{pmatrix}. \quad (2.12.56)$$

This requires that the eigenvalues of $C = C_{\text{barrier}}C_{\text{valley}}$ be conjugate pairs of the nth roots of the unity ($e^{\pm i2\pi m/n}$, where $m = 0, 1, 2, \ldots, n-1$). This leads to the following trace relation:

$$[1+\theta^2]^{1/2}\cos\alpha = \cos\left(\frac{2\pi m}{n}\right). \quad (2.12.57)$$

We know that if each valley existed by itself it would have a series of energy levels ($E_0, E_1, E_2, \ldots, E_j, \ldots$). For a single isolated potential valley the jth energy level would satisfy a quantization condition of the form

$$\alpha(E_j) = \int_b^c k(x)\,dx = \left(j + \tfrac{1}{2}\right)\pi \qquad (j = 0, 1, 2, \ldots). \quad (2.12.58)$$

This amounts to a phase change across the valley of $(j + 1/2)\pi$ corresponding $(j + 1)$ half-waves minus a fraction of a half-wave which would protrude beyond the valley turning points if the wave could continue on either side. It is remarkable that this protruding fraction is approximately one quarter of a half-wave, that is, a $\pi/4$ phase decrement on either side. This WKBJ approximation holds for a wide range of potential slopes. The square well, on the other hand, has a protruding phase shift δ that varies continuously with the barrier height. (See Problem 2.12.2.) The $\pi/4$ phase shift is found in the standard WKBJ analysis and the resulting zero-point quantum term $\frac{1}{2}$ is called a Maslov constant.

All this assumes the absence of tunneling. With n valleys there will be a cluster of n levels around each single valley level E_j. A Taylor expansion around each level E_j gives the phase as a function of nearby energy E:

$$\begin{aligned} \alpha(E) &= \alpha(E_j) + \frac{\partial\alpha}{\partial E}(E - E_j) \\ &= \left(j + \frac{1}{2}\right)\pi + \left(\frac{\pi}{\hbar\omega_{\text{classical}}}\right)(E - E_j). \end{aligned} \quad (2.12.59)$$

Here we used a relation between the action S and the phase shift $\alpha = S/2\hbar$ and the classical angular frequency,

$$\frac{\partial S}{\partial E} = \frac{2\pi}{\omega_{\text{classical}}}.$$

A general proof of this relation is given in Section 8.1 [Eq. (8.1.31)]. An elementary derivation is easily made, also. Substituting the approximation (2.12.59) into the boundary condition (2.12.57) yields

$$\begin{aligned}\frac{\cos(2\pi m/n)}{[1+\theta^2]^{1/2}} = \cos\alpha &= \cos\left[\left(j+\frac{1}{2}\right)\pi + \left(\frac{\pi}{\hbar\omega_{\text{classical}}}\right)(E-E_j)\right] \\ &= \cos\left(j\pi+\frac{\pi}{2}\right)\cos\left[\frac{\pi}{\hbar\omega_{\text{classical}}}(E-E_j)\right] \\ &\quad - \sin\left(j\pi+\frac{\pi}{2}\right)\sin\left[\frac{\pi}{\hbar\omega_{\text{classical}}}(E-E_j)\right] \\ &\cong -(-1)^j\frac{\pi}{\hbar\omega_{\text{classical}}}(E-E_j).\end{aligned}$$

This leads to an energy-level cluster splitting formula for the (m)th level in the (j)th cluster:

$$E = E_j - (-1)^j\frac{\hbar\omega_{\text{classical}}}{\pi}[1+\theta^2]^{-1/2}\cos k_m\left(k_m = \frac{2\pi m}{n}\right). \quad (2.12.60)$$

This corresponds to an approximate formula for the tunnelling or "sneak" factor S in Eq. (2.12.25), where $2S$ is the magnitude of the *intra*cluster splitting.

$$S = (-1)^j\frac{\hbar\omega_{\text{classical}}}{2\pi}\theta^{-1} = (-1)^j\hbar\nu_{\text{classical}}e^{-\int_a^b|(2m/\hbar^2)(V-E)|^{1/2}\,dx}.$$

Note that the S amplitude depends on two factors. The first is the classical frequency $\nu_{\text{classical}}$ which is the number of times the particle "knocks at the door" of the barrier each second. (The energy $h\nu_{\text{classical}}$ is the *inter*cluster splitting.) The other factor is the exponential of the tunneling integral. The tunneling factor decreases rapidly with the height $(V-E)$ of the barrier above the energy level. The sign of the amplitude alternates from cluster to cluster according to $(-i)^j$. This is consistent with the observation that bands in Figure 2.12.2 would have A-type waves on the lower boundary and B-type waves on the upper boundary for even j and vice versa for odd j.

ADDITIONAL READING

For a discussion of wave motion and Fourier analysis it is hard to beat two of the original texts by Leon Brillouin

Leon Brillouin, *Wave Propagation and Group Velocity* (Academic, New York, 1960); *Wave Propagation in Periodic Structures*, 2nd ed. (Dover, New York, 1953).

An excellent modern book on Fourier theory with lots of interesting mathematics, examples of physical effects, and historical notes on engineering applications is by Körner.

T. W. Körner, *Fourier Analysis* (Cambridge University Press, Cambridge, 1988).

A good introduction to oscillation and wave mechanics is available from the Berkeley Course volume by Frank S. Crawford.

F. S. Crawford, *Waves*, Berkeley Physics Course, Vol. 3, (McGraw-Hill, New York, 1968).

A wonderful application to boat wakes by the same author is in the *American Journal of Physics*.

F. S. Crawford, "Elementary derivation of the wake pattern of a boat," *Am. J. Phys.*, **52**, 782 (1984).

An article on the two-Fourier-component waves and their galloping motion is the following:

W. G. Harter, J. Evans, R. Vega, and S. Wilson, "Galloping waves and their relativistic properties," *Am. J. Phys.*, **53**, 671 (1985).

The problem of scattering and tunneling in potential wells has been treated arduously if not clearly. The supposedly definitive work on WKB approximations is by Froman and Froman.

N. Froman and P. O. Froman, *JWKB Approximation, Contributions to the Theory* (North-Holland, Amsterdam, 1965).

They find a number of problems with tunneling amplitudes found in quantum mechanics texts such as the text by Merzbacher.

E. Merzbacher, *Quantum Mechanics* (Wiley, New York, 1970) p. 126.

Despite this the Merzbacher text has one of the clearer introductions to crossing and scattering matrices.

The most widely used barrier tunneling factors come from an article by Miller and Good, *Phys. Rev.*, **91**, 174 (1953).

The semiclassical description of barrier tunneling chemical physics is described quite clearly by William H. Miller.

W. H. Miller, *J. Phys. Chem.*, **83**, 960 (1979).

This has been applied extensively. For a modern application see the following and references contained therein.

J. M. Robbins, S. C. Creagh, and R. G. Littlejohn, *Phys. Rev. A* **39**, 2838 (1989).

An earlier description of barrier tunneling and reflection is found in the following reference:

M. S. Child, *J. Mol. Spectrose*, **53**, 280 (1974).

This contains a graphical description of quantum mechanics of multiple potentials with barriers and valleys connected with a variety of topologies. See also

M. S. Child, in *Nonadiabatic Transitions, Atom-Molecule Collision Theory*, R. B. Bernstein (ed.), (Plenum, New York, 1979).

R. P. Bell, *The Tunnel Effect in Chemistry* (Chapman and Hall, London, 1980).

PROBLEMS

Section 2.3

2.3.1 Use group postulates 1 to 4 to answer or prove: If $ab = c$ for a, b, and c in a group G, can $ad = c$, too, where $d \neq b$? How many times can a group element appear in a given row or a given column of a group table?

2.3.2 If a set $\delta = \{a, b, c, \ldots, g, .\}$ of operators satisfying postulates 1 and 2 has a "left identity" 1_L (such that $1_L g = g$) for all g, and a "left inverse" g_L^{-1} for each g (such that $g_L^{-1} g = 1_L$), can you prove that the set is a group; i.e., rules 3 and 4 are satisfied?

2.3.3 Consider the oscillator Hamiltonian

$$H = \frac{A}{2}(p_1^2 + q_1^2) + \frac{D}{2}(p_2^2 + q_2^2) + B(q_1 q_2 + p_1 p_2) + C(q_1 p_2 - q_2 p_1).$$

(a) Write out Hamilton's equations of motion which give time derivatives of p_1, p_2, q_1, and q_2 in terms of A, B, C, D.

(b) For $C = 0$ determine the acceleration matrix $\langle \mathbf{a} \rangle$ in Newton's equations of motion.

(c) What (if any) constraints on A, B, and D are needed to yield a C_2 symmetric system?

(d) Give a simple formula for the normal mode angular frequencies $\omega\uparrow$ and $\omega\downarrow$ in the C_2 symmetric case.

Assume $A = 1.0$, $B = 0.3$, $C = 0$, $D = 1.0$ [units of (radian) H_z] in the following problems.

(e) Compute the time period between beat maxima (in seconds!) How many wiggles per beat?

(f) Compute the time period between perfect recurrences of all variables (Poincaré period). How many beats per recurrence?

2.3.4 If the two-pendulum C_2 symmetric system is acted upon by a periodic driving force, suppose the force on pendulum 1 is equal to $f_1 \cos(\omega t)$ and the force on pendulum 2 is equal to $f_2 \cos(\omega t)$. Suppose also that there are frictional forces. Let the operator equation of motion be

$$|\ddot{x}\rangle + \mathbf{d}|\dot{x}\rangle + \mathbf{a}|x\rangle = |f\rangle,$$

$$\text{where } |x\rangle = \begin{pmatrix} x_1 \\ x_2 \end{pmatrix}, \quad |f\rangle = \begin{pmatrix} f_1 \cos(\omega t) \\ f_2 \cos(\omega t) \end{pmatrix},$$

$$\text{and } \mathbf{d} = \begin{pmatrix} d & e \\ e & d \end{pmatrix}, \quad \mathbf{a} = \begin{pmatrix} a & b \\ b & a \end{pmatrix}.$$

(a) Derive and plot the pendulum steady-state response amplitude as a function of the stimulus frequency ω for $a = 3.0$, $b = 10.$, $d = 0.1 = e$, $f_1 = 1.0$, and $f_2 = 0.0$.

(b) Do the same for $a = 3.0$, $b = 1.0$, $d = 0.1 = e$, $f_1 = 1.0$, and $f_2 = 1.0$.

(c) Do the same for $a = 3.0$, $b = 1.0$, $d = 0.1 = e$, $f_1 = 1.0$, and $f_2 = -1.0$.

Section 2.6

2.6.1 Let $\{|1\rangle, |2\rangle = R|1\rangle\}$ be the basis in which the representation of a general C_2 symmetric Hamiltonian is $\langle H_2\rangle = \begin{pmatrix} a & b \\ c & d \end{pmatrix}$. Let $\{|1\rangle, |2\rangle = r|1\rangle, |3\rangle = r^2|1\rangle\}$ be the basis in which the representation of a general C_3 symmetric Hamiltonian is

$$\langle H_3\rangle = \begin{pmatrix} A & B & C \\ D & E & F \\ G & H & I \end{pmatrix}.$$

(a) Derive equations relating a, b, c, and d.

(b) Derive equations relating A, B, C, ... and I.

Can any of these quantities be complex if $H^\dagger = H$?

2.6.2 Could an unsymmetrical system such as is shown in the diagram ever behave something like a C_2 symmetric system? (Suppose we're allowed to assign different scale factors to different coordinates.)

Suppose that $m_1 = 10m_2$, $k_1 = 20$, and $k_{12} = 1$. What (if any) value of k_2 mimics C_2 behavior?

Suppose, instead that $m_1 = 10m_2$, $k_1 = 8$, and $k_{12} = 1$. Is the C_2 symmetry physically possible? What, if any, restrictions are there for the constants?

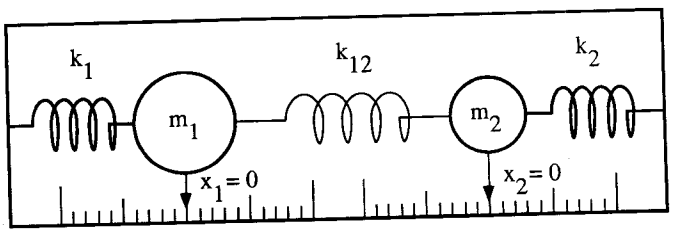

2.7.1 Consider C_n symmetric coupled pendulum systems described by Eq. (2.7.1). Give a detailed account of the eigensolutions for $n = 4$, 5, and 8, as follows.

(a) Label the coordinates with C_n group operators.

(b) Write the C_n character table and projection operators.

(c) Sketch the moving-wave modes of vibration using phasors. (Label them with C_n group representation labels.)

(d) Sketch the standing-wave modes of vibration using phasors and sine or cosine curves.

(e) Calculate the eigenfrequencies for $a = 1.0$ and $b = 0.0$.

(f) Discuss the effect of nonzero constant ($b \neq 0$) on the dispersion function. How does the phase and group velocity change for low wave number? Draw the dispersion function and indicate the first Brillouin zone.

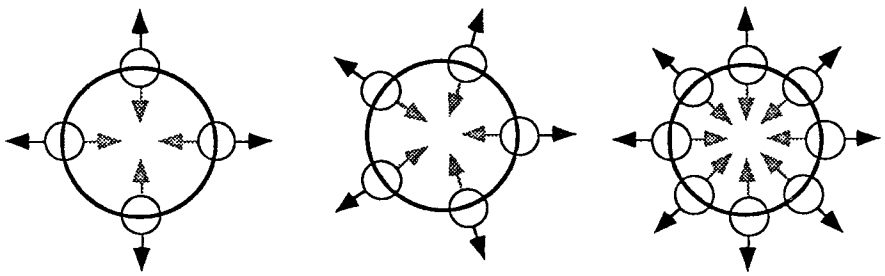

2.7.2 Derive the wave speed for a nondispersive wave given by Eq. (2.7.12) in terms of its phase velocity $c = \omega/k$, time t, the incident amplitude I, and reflected amplitude R. Give maximum and minimum speed in terms of the SWR quantity $\Delta = (I - R)/(I + R)$.

2.7.3 Consider the C_8 symmetric coupled pendulum system (use results of Problem 2.7.1) when the coupling strengths alternate between $\bar{a} > a$ and $\underline{a} < a$ as described around Eq. (2.7.8).

(a) Derive the eigenfrequencies for $\bar{a} = 1.2$ and $\underline{a} = 0.8$, and sketch the modes of vibration. Pay particular attention to the frequency doublet levels (or level) which split(s) when $\bar{a} \neq \underline{a}$.

2.7.4 Use a "higher symmetry embedding" technique to find the normal modes of the four-pendulum ($m = 4$) system shown in the top and side views of the figure. What higher C_n ($m > n$) symmetry ring would have the same motions for a subset of its pendulums with the walls in

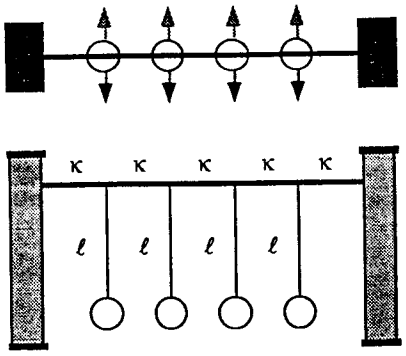

the figure corresponding to nodal pendulums? Use this system to give formulas for the mode frequencies in terms of torsional spring constants (κ) and lengths (l) indicated in the figure. Generalize this for $5, 6, \ldots, m$ pendulums between walls.

2.7.5 Consider a set of oscillators that have C_3 symmetry but only C_3 symmetry and no higher symmetry. Suppose there is some kind of amplifier by which oscillator x_1 can perturb oscillator x_2, and oscillator x_2 can perturb oscillator x_3, and oscillator x_3 can perturb oscillator x_1 more than vice versa. In other words, let us suspend Newton's third law and make the action and reaction forces unequal. This corresponds to the following equation of motion, in which the coupling constants s and t are unequal:

$$\begin{pmatrix} \ddot{x}_1 \\ \ddot{x}_2 \\ \ddot{x}_3 \end{pmatrix} = \begin{pmatrix} a & s & t \\ t & a & s \\ s & t & a \end{pmatrix} \begin{pmatrix} x_1 \\ x_2 \\ x_3 \end{pmatrix}$$

Discuss this system. Does it really have C_3 symmetry? What are its mode solutions? Which are stable?

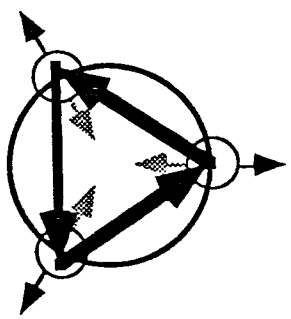

Double Trouble

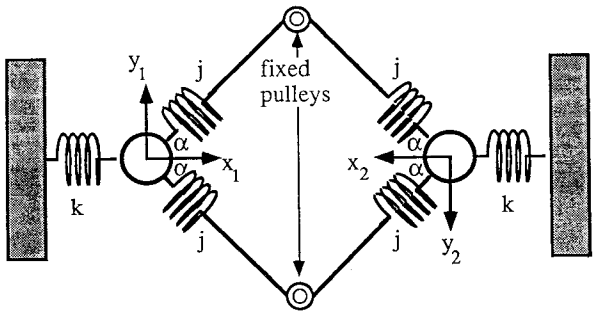

2.8.1 **(a)** Describe and label a symmetry group that would be appropriate and adequate to help solve the equations of motion for the four-freedom oscillator system shown. Label the base states using group operators and derive a representation R of this group. (Show that it obeys your group table.)

(b) Write the Lagrangian and acceleration matrix in terms of x_1, x_2, y_1, y_2, mass m, and spring constants j, k for small oscillations. (Treat angle α as a constant.) Write the equations of motion.

(c) Reduce the representation R and the acceleration matrix using symmetry projectors of the group. Sketch and describe the normal modes and their frequencies for each type of projection or irrep for the case $j = 1.0$, $k = 2.0$, and $\alpha = 45°$.

(d) Suppose each mass could move in *three* directions ($x_{1,2}$, $y_{1,2}$, and $z_{1,2}$) and the symmetry was bilateral in the z direction, as well. What symmetry group or groups would be appropriate? [Give the answer in terms of ($C_p \times C_q \times \cdots$, etc.) for some $p, q, \ldots$.]

(e) Give the character table of the largest group you found in answer (d) and tell which irreps would be used to label normal modes of the three-dimensional double-mass oscillator.

2.8.2 Calculate the number of nonisomorphic Abelian groups of order n and express them in terms of outer products of cyclic groups of prime order for the following values of n.

(a) $n = 8$.

(b) $n = 9$.

(c) $n = 12$.

(d) $n = 16$.

(e) $n = 24$.

Write out character tables for $n = 8$ Abelian groups.

2.8.3 The Fourier series for an infinite one-dimensional square wave $S(x)$ has the form

$$S(x) = 4/\pi[\cos(x) - \tfrac{1}{3}\cos(3x) + \tfrac{1}{5}\cos(5x) - \tfrac{1}{7}\cos(7x) + \cdots],$$

where $S(s) = +1$ if $\cos(x) > 0$ and $S(x) = -1$ otherwise. (Derive this series.) Consider a 12-mass ring of C_{12} symmetry subject to square standing-wave initial conditions as shown in the diagram. Calculate the coefficients of a *finite* series of C_{12}-defined modes that would give these initial conditions and compare them to the first few coefficients just given.

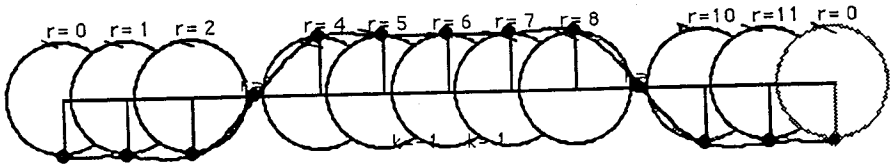

What is needed to make a square *moving* wave?

2.12.1 The Kronig-Penney bands in Figure 2.12.6 exhibit "accidental" degeneracies for three nonzero values of the potential barrier height V with energy $E < 50$. [Bohr units $= \hbar^2\pi^2/2\mu(a+b)^2$, where μ is mass, a is well width, and b is barrier width. here let $a = b$.]

(a) What are these special values of V and E in Bohr units? Sketch the wave functions for each of the three accidental cases and explain the degeneracies.

(b) List the other cases (if any) for $a = b$ and $E < 75$ Bohr units. What degeneracies occur just above the top of Figure 2.12.6?

(c) Give a formula for finding these degeneracies for general a and b values.

2.12.2 Prove the straight-line-sine (k, δ)-space geometric solution in the diagram for the one-dimensional square well. The diagram uses special values of the mass ($m = \frac{1}{2}$), well width ($x = 2$), and Planck's constant ($\hbar = 1$). Show how this construction gives information about the eigenfunctions as well as the eigenvalues. Derive it for general

width ($x = 2a$), particle mass (m), and Planck's constant. Check it against Figure 2.12.6 for $V = 25$. (Explain *why* you can check it against Figure 2.12.6.)

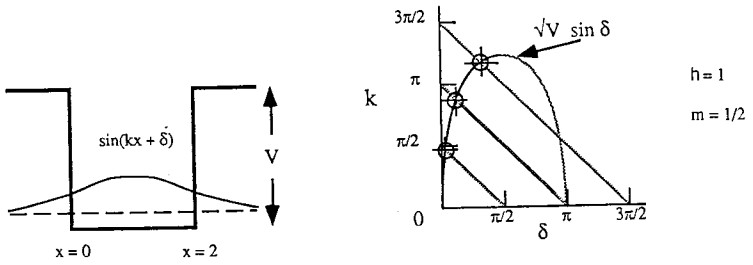

2.12.3 Draw to scale the approximate (use Figure 2.12.6 again) E spectrum ($0 < E < 80$) for the following potential wells. (Schrödinger equation $\psi'' + (E - U(x))\psi = 0$):

(a) C_4 symmetric square wells. [See diagram (a).]

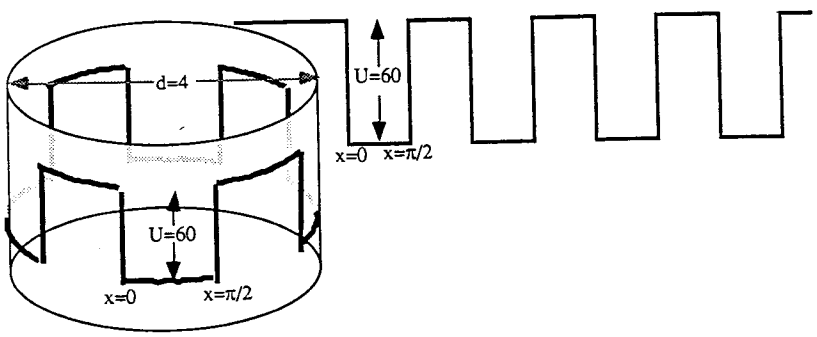

(*a*) Four equilvalent wells on a circle

(*b*) Four equivalent wells in a straight line

(b) Four equivalent square wells in a straight line. [See diagram (b)].

(c) Give a detailed magnified view and approximate accounting of the lowest two bands or "clusters" of fine structure levels and a rough sketch of the eigenfunction in each case.

2.12.4 (Discussion). The spectrum of $1, 2, 3, \ldots$ or n square potential wells on an infinite one-dimensional line is usually thought to be a *discrete* portion of energy below the top of the barriers, followed by a *continuum* for energy above the wells. However, for $n = \infty$ it is well known that the continuum breaks into bands and gaps above *and* below the top of the wells. Do these gaps suddenly appear at $n = \infty$? Discuss and find a way to reconcile this apparent discrepancy in the spectral properties.